Technical Report

528

Millstone Hill Thomson Scatter Results for 1971

J. V. Evans

B. A. Emery

J. M. Holt

24 March 1978

Prepared for the National Science Foundation
under NSF Grant No. ATM 7522193

Lincoln Laboratory

MASSACHUSETTS INSTITUTE OF TECHNOLOGY

LEXINGTON, MASSACHUSETTS

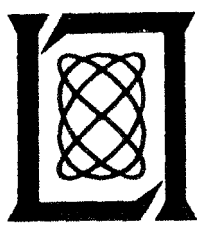

ABSTRACT

During 1971, the incoherent scatter radar at Millstone Hill (42.6°N, 71, 5°W) was employed to measure the electron density, electron and ion temperatures, and the vertical velocity of the O^+ ions in the F-region over periods of 24 hours on 20 days. The observations spanned the height interval 200 to 900 km, approximately, and achieved a time resolution of about 30 minutes. This report presents these results, after smoothing as a set of machine-drawn contour plots.

The report discusses the behavior observed in 1971 in light of that seen in previous years. A significant number of days appear to have been disturbed by large traveling ionospheric disturbances. Results for the average exospheric temperature, the mean meridional, and zonal winds for 1970 and 1971 derived from these incoherent scatter measurements in a separate study by B.A. Emery* are summarized here for completeness. The results appear to confirm the mean wind behavior that would be predicted by the recent Mass-Spectrometer, Incoherent-Scatter (MSIS) global model for the thermosphere and support the view that interhemispheric transport of light neutral constituents (e.g., atomic oxygen) gives rise to the anomalous seasonal behavior of the ionosphere at midlatitudes.

*Presently at Centre de Recherches en Physique de L'Environment Terrestre et Planetaire, CNET/RST France.

CONTENTS

MILLSTONE HILL THOMSON SCATTER RESULTS FOR 1971

I. INTRODUCTION

Since 1963, incoherent (Thomson) scatter radar measurements of F-region electron densities, and electron and ion temperatures have been conducted at Millstone Hill, Westford, Massachusetts (42.6°N, 71.5°W) (Refs. 1 to 8). This paper is the ninth in a series of annual reports, and presents the results gathered in this program during the calendar year 1971. The observations reported were made for periods of 24 hours, approximately twice a month. The results obtained in earlier years have been published in the articles listed in Table I, and have been transmitted to the World Data Center A, Boulder, Colorado.

In addition to the measurements reported here of F-region electron densities, electron and ion temperatures, and vertical velocity, a number of measurements were conducted in 1971 of

TABLE I

PUBLICATIONS CONCERNING THE MILLSTONE HILL UHF (68-cm Wavelength) THOMSON SCATTER RESULTS

Year	Months Covered	Publication
1963	February 1963 to January 1964	Ref. 1
	March, July, August, September	Ref. 9
	April, July, November	Ref. 10
1964	January through December	Ref. 2
	April, July, November	Ref. 11
1965	January through December	Ref. 3
	January, April, August	Ref. 12
	June	Ref. 13
	June, August, September	Ref. 14
1966	January through December	Ref. 4
	January, March, July, September	Ref. 15
1967	January through December	Ref. 5
	February, June, October, December	Ref. 15
1968	January through December	Ref. 6
	October	Ref. 16
1969	January through December	Ref. 7
	February, April, July	Ref. 17
	September, October	Ref. 17
1970	January through December	Ref. 8

the electron density, and electron and ion temperatures in the lower ionosphere employing a digital filter to subtract coherent echoes from distant hills at the same range.[18] These measurements spanned the height interval 100 to 500 km, approximately, and were the first at Millstone that permitted electron and ion temperatures in the E-region to be determined with good height resolution.[19] To achieve this fine height resolution as well as subtract the unwanted clutter echoes, the site digital computer (XDS 9300) was employed to calculate the autocorrelation function of the signals instead of measuring their frequency spectra with a bank of filters – the method used for the results reported here.

The measurements of the echo autocorrelation function were accomplished by transmitting pairs of short pulses and calculating in the digital computer the correlation between samples of the echoes taken with the same spacing. This method of operation allows the height and frequency resolution of the measurements to be set independently of one another, while in the measurements reported here, the length of the single long pulse used establishes both parameters. The new method became known as the "double-pulse" experiment to distinguish it from the earlier single-pulse measurement method.

Routine measurements using the double-pulse method commenced in 1971 and have been used extensively to study the propagation of thermal tides from the mesosphere into the lower thermosphere.[20-22] These measurements also permit the determination of the neutral density in the lower thermosphere (in the region where ion-neutral collisions become important) and the ion composition in the F1-region;[23] a complete reduction of these data for this purpose is in process.

As time progressed, increasing emphasis was devoted to the two-pulse measurements with the result that it became somewhat difficult to schedule two 24-hour single-pulse runs each month and only 16 such runs were attempted in 1971. However, additional data were gathered during satellite tracking operations, and four of these were of sufficient length to warrant inclusion in this report.

During the spring of 1971, a number of days were devoted to the study of the incoherent scatter plasma lines. These observations were made by R. J. Cicerone (University of Michigan). They extended earlier measurements by him[24] and I. J. Gastman[25] and were reported in Ref. 26.

Another effort continued from prior years entailed attempting to operate the radar during occurrences of an overhead stable auroral (red) arc. Under this effort, the radar would be brought into operation upon notification of auroral activity as seen at the Blue Hills Observatory by J. F. Noxon. These alerts resulted in useful data being gathered during two low-latitude auroras.[27] Although the radar was recalled twice in 1971 (on 16 February and 2 June), little activity seems to have developed within the overhead beam of the radar.

In this report, we present only the results of the measurements made with single long pulses during regularly scheduled operations. These covered the altitude interval 200 to 900 km, approximately, with a height resolution (for the measurements of temperature) of 75 km. These data can be used to deduce the temperature of the exosphere from thermal balance arguments,[28] and results obtained in this way for the period March 1969 through March 1971 already have been reported.[20] However, as part of an effort to determine the thermospheric winds over Millstone from the data,[29] the values for T_∞ in 1970 and 1971 were redetermined, and the revised values are presented here.

Section II summarizes the equipment, observing, and data-analysis procedures. The experimental results are presented and discussed in Sec. III. Section IV provides a summary of

the study of the thermospheric temperature and winds over Millstone performed using the results of Sec. III as well as those gathered in 1970.[8]

II. EQUIPMENT, OBSERVING, AND DATA-ANALYSIS PROCEDURES

A. Equipment

The UHF* incoherent scatter equipment has been described.[1] During 1968, the spectrum analyzer portion of the receiver was replaced by one of newer design that was interfaced directly into the XDS 9300 computer. These changes are documented fully in Ref. 30 and discussed further in Ref. 7. As mentioned above, the principal changes made during 1970 were the development of the double-pulse modes for operating the equipment.[8] A brief description of one of these (the F-mode) has been given elsewhere[22] and a full account of the complete system is reserved for a separate report.

No major changes were made to the incoherent scatter equipment in 1971. During this year, the major program at the Field Station entailed tracking artificial earth satellites in an effort to determine the magnitude of any anomalous refraction effects that may exist along rays traversing the aurora.[31] The desire to verify the accuracy of the measurements by means of ray-tracing calculations prompted a need for accurate ionospheric electron density profiles. Thus, it was considered important to try to operate the incoherent scatter radar to measure the ionospheric electron density profiles between passes of the satellites being tracked (at intervals of approximately one hour). These operations became known as STATS (Satellite Tracking and Thomson Scatter). In order to facilitate this, it was necessary to reduce the amount of time it required to change between the L-band† (tracking) and UHF (incoherent scatter) radars. Most of the delay was introduced by the time required to changeover between high-power transmitters and, commencing late in 1970, efforts were begun to reduce this. A surplus, three-phase, 208-volt inductrol and distribution system was installed to permit simultaneous operation of the magnets, filaments, and air coolers in both the UHF and L-band transmitters. A surplus driver power supply also was installed to permit simultaneous operation of both driver stages. However, major problems were encountered in implementing rapid changeover of the power amplifier cooling system and the high-voltage power supply. (Only a single water cooling system and power supply are available at Millstone.) The cooling circuits for the dummy loads were combined successfully by connecting both loads in parallel and making minor adjustments to bypass valves. The cooling circuits for the klystron final amplifiers, however, require a flow rate of 125 gallons/minute for each transmitter and could not be combined without increasing the output pressure of the pumps by 10 lb/in.^{2} Unfortunately, this would have required two additional pumps and motors. The major restriction to coolant flow, aside from the klystrons themselves, was the heat exchanger. By placing an adjustable bypass around the heat exchanger and using both the normal and spare pumps, it was possible to combine the power amplifier cooling systems of both transmitters and satisfy the flow rate requirement. Fortunately, the original cooling system was rated conservatively enough for the airflow through the heat exchanger to be adequate for the increased input coolant temperature.

The other major problem was in switching the high voltage applied to the klystrons via the modulators. Both the L-band modulator and the UHF modulator take high voltage from a switch room where one or the other normally is connected to a "supply" bushing. By connecting both

* UHF = 440 MHz.

† L-band = 1295 MHz.

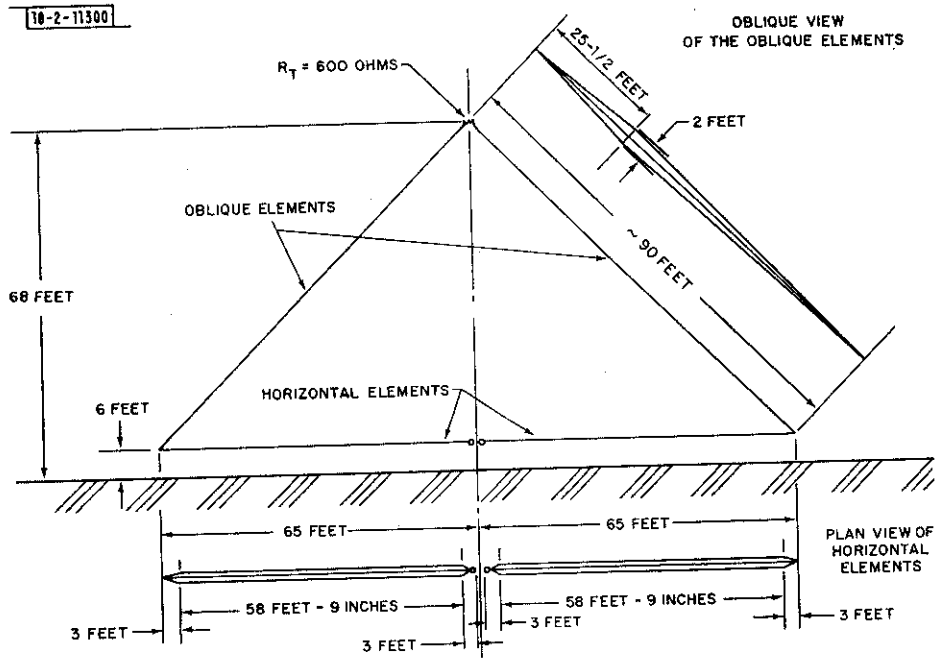

Fig. 1. Diagram showing the dimensions of one of the two delta aerials employed the C-4 sounder. These were supported by a 90-foot wood utility pole and arranged at right angles to one another.

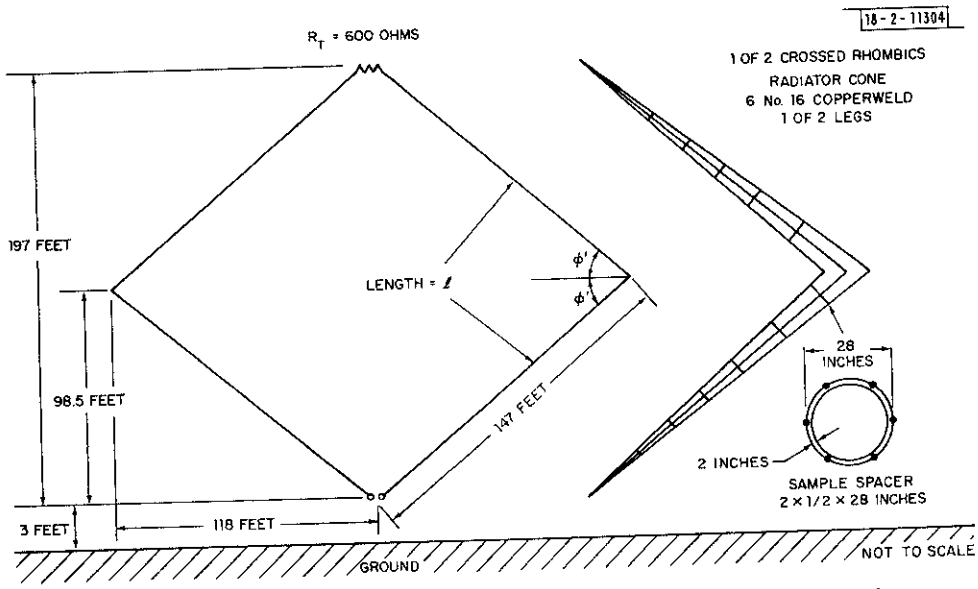

Fig. 2. Diagram showing the dimensions of one of the two nonresonant rhombic aerials constructed in 1971 to replace the delta antenna (Fig. 1). These are supported by a 200-foot metal tower (Fig. 3) and arranged at right angles to one another.

leads to this supply bushing and separately controlling each modulator so that only one was energized at a time, it became possible to switch transmitters on a pulse-by-pulse basis (<5 msec). However, normal operations never exploited this pulse-by-pulse switching capability.

During July 1971, the rapid changeover capability was used for the first time for a two-frequency Thomson scatter experiment in which the L-band and UHF transmitters were alternated at 15-minute intervals. Although this operation was successful, later STATS operations suffered from severe transmitter "arc overs." Some of these resulted in severe damage to the L-band and UHF modulators. The cause of these failures was never established fully, although it was thought that the trouble lay with operating one of the modulators at full voltage without drawing any current. The STATS operations entail reloading computer programs between satellite tracking and Thomson scatter segments and this takes at least two minutes; thus, there was time to permit mechanical switching of the high voltage. Accordingly, an electromechanical switch was installed that disconnected the high-voltage line of the transmitter not in use from the high-voltage supply bushing. This switch is controlled by a changeover switch in the control room. When operated in the "dual mode," it now takes approximately one minute to switch between transmitters and no further "arc overs" have since been encountered.

The rapid changeover between the transmitters has remained a useful capability that has been exploited considerably in subsequent years. It permits three components of the plasma drift to be measured using the UHF and L-band radars, alternately.

Another significant event in 1971 was the improvement of the operation of the C-4 ionosonde. Since its installation (in about 1961), the C-4 ionosonde was operated with separate aerials for transmitting and receiving, as this obviated the need for a transmit/receive switch. The aerials used were identical "delta" antennas constructed according to the design shown in Fig. 1. The two aerials were oriented at right angles to one another and supported by a 90-foot wooden utility pole. The elements were fed by 600-ohm open-wire lines. This design is intended to operate essentially as a rhombic by virtue of an image produced by reflection from the ground. Our antenna, however, appeared quite sensitive to the nature of the ground cover and appeared to be degraded seriously whenever there was snow beneath the antenna with a depth of a couple of feet.

A pair of crossed vertical, nonresonant, rhombic aerials was constructed to replace the original delta antenna. These elements may be thought of as a terminated transmission line whose wires have been separated and hence made to radiate. Thus, the nonresonant rhombic is a traveling-wave antenna, and when directed vertically should not be very sensitive to the presence of the ground.

Figure 2 shows the dimensions of the elements employed at Millstone. The length of the sides of the rhombus together with the included angle φ (Fig. 2) determine the input impedance and gain of the antenna at a given wavelength λ. Since it is impractical to change the height of the tower, some ionosonde antennas have been constructed using as many as four vertical rhombics, supported by the same tower, each of which is used over an octave portion of the frequency band (e.g., 1 to 2, 2 to 4, 4 to 8, 8 to 16 MHz). Such a scheme necessitates switching between elements, and this in turn requires turning off the transmitter when the switching takes place. To avoid this complication, in some installations, a pair of transmitting and receiving antennas are used that have different sizes. These are chosen to yield an approximately constant overall gain over the required frequency band.

For the aerial constructed at Millstone, it was decided to make the transmitter and receiving elements of equal size, so that they might be connected to permit circular polarization to be used. Successful application of such a scheme would permit the extraordinary echoes to be suppressed, rendering the ionograms easier to interpret and thereby facilitating their reduction by computer. Unfortunately, a wideband, high-power element that will provide the quarter-wavelength phase shift needed to produce circular polarization using two aerials has not yet been found. Thus, the two rhombics currently are being employed as separate transmitting and receiving aerials.

Fig. 3. The new nonresonant rhombic aerial system. To the right of the picture is the building that houses the C-4 sounder. To the left of the building is the original delta antenna (Fig. 1).

The new antenna is shown in Fig. 3. Sections of surplus steel tower were used to support the two rhombics. The center tower is 200 feet high and those supporting the corners are 100 feet high. Each tower is guyed by steel cables whose length is broken by electrical insulators. The currents induced in the central tower from the four legs of each rhombic are thought to be equal and opposite, and hence should cancel. That is, the metal center tower should not distort seriously the radiation pattern. The same argument should not apply to the other four towers, and as a precaution, the sections of these were electrically insulated one from another, so that they could not form long continuous radiators.

The 600-ohm terminations for the antennas are of special noninductive construction and are mounted in weatherproof fiberglass boxes at the top of the center tower. In contrast to earlier practice, the circular spacers between the wires in each of the antenna legs (Fig. 2 and 3) were made of metal (aluminum), since no good reason could be found why they should be nonconducting. The spacers at the corners were, however, made of insulating rods.

The transmitter antenna is fed by twin-wire 600-ohm line, while the receiving rhombic is connected to a balance-to-unbalance transformer which drives an RG-9 coaxial cable that conveys the received signals to the building (Fig. 3). Within the building, a receiver preamplifier is employed to drive the C-4 receiver.

The new antenna was brought into operation in October 1971. Figure 4 contrasts ionograms obtained, within about a one-hour period, with the delta antenna (shown in the background in Fig. 3) and the rhombic. Both ionograms were made with the C-4 sounder. A clear improvement

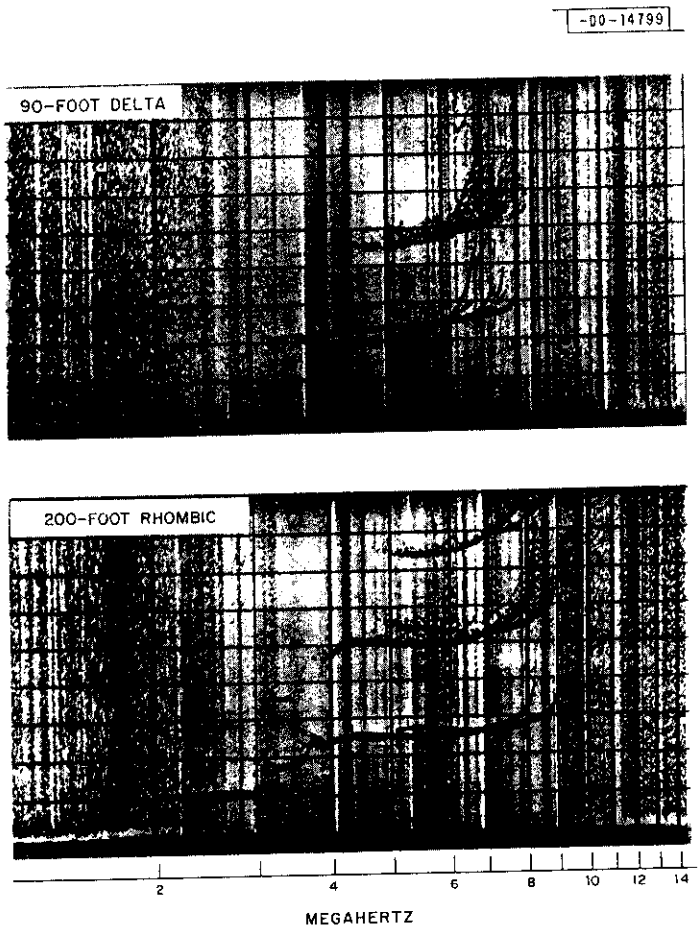

Fig. 4. Comparison of ionograms obtained using the C-4 sounder with the delta aerial (top) and rhombic aerial (bottom) about an hour apart.

in the intensity of the returns is evident at frequencies below 5 MHz. In addition, the "3rd hop" echo now is visible above 5 MHz indicating improved sensitivity in this portion of the frequency band also. A further indication of the increased directivity is the total absence of oblique echoes in the lower panel in contrast to the number seen in the upper panel.

B. Observing Procedure

During 1971, we attempted to make F-region observations twice per month for periods of 24 hours. As already noted, however, press of other work precluded this in some months.

TABLE II

THE NORMAL "ONE-PULSE" EXPERIMENT MODE SEQUENCE

Mode	Pulse Length (μsec)	Height Resolution (km)	Sample Spacing (km)	Altitude Coverage (km)	Measured Parameters	
					Direct	Deduced
A	100	15	7.5	100-1000	Power	N_e
B	500	75	30	150-1500	Power	N_e
			75	225-675	Power spectrum	T_e, T_i, V_z
C	1000	150	30	300-2000	Power	N_e
			75	450-1125	Power spectrum	T_i, T_i, V_z

The observations reported here normally were carried out using the single long-pulse experiments A to C described previously,[30] which provide the coverage indicated in Table II. However, on two occasions, measurements also were made using 2-msec pulses (D-mode)[30] in an effort to extend the observations to altitudes where H^+ ions predominate. As these did not seem to be successful, they were not pursued.

Three types of experiment were conducted. The normal procedure was to cycle through the three modes every 30 minutes, thereby yielding about 50 profiles of electron density, and electron and ion temperature during a 24-hour run; these operations were termed "regular." Joint STATS operations were conducted in which a single cycle of incoherent scatter measurements would be made between passes of the Navy Navigation Series Satellites, i.e., approximately every hour. As these operations usually were conducted for only short periods (e.g., 8 hours), only the results from four of the longer ones are included here. Finally, observations were conducted on some days in which the C-mode measurements were repeated once, before the next cycle commenced; these were termed "drifts." As it was recognized that the vertical velocity at altitudes below 450 km also is of interest (e.g., in determining neutral winds), emphasis ceased to be given to repeated C-mode observations (and hence "drifts" operations) during 1971.

As in previous years,[6-8] measurements of f_oF2 were attempted both in real time and from film records using the C-4 ionosonde. These were combined with values obtained at Ottawa and Wallops Island to secure a curve of diurnal variation of f_oF2 that was used to establish the values of N_{max} F2 for the electron density profiles measured with the incoherent scatter radar.

C. Observations

The dates for which we have been able successfully to reduce to regular, drifts, and STATS data gathered in 1971 are listed in Table III. As noted above, additional single measurements were made in 1971 over short periods as part of the STATS operations and in an effort to observe a stable auroral red (SAR)-arc. The results from these shorter periods did not appear to be unusual and have not been included here. The two-pulse measurements made in 1971 will be published in a separate report.

TABLE III

INCOHERENT SCATTER OBSERVATIONS – 1971

Begin			End			Mean		
Date	C*	EST	Date	C*	EST	Kp	Obs†	Comment
11 January		1620	12 January	QQ	1630	1	Reg	Problems with tape errors
20 January	D	1235	21 January		1235	3–	Drift	
18 February		1930	19 February		1950	3–	Reg	
8 March	D	1600	9 March		1600	2–	Reg	
30 March		1600	31 March	D	1600	4	Reg	Includes D-mode
27 April	Q	1540	28 April		2100	3+	Reg	
27 May	QQ	1530	28 May	QQ	1530	1–	Reg	Includes D-mode
18 June		0815	19 June	QQ	1300	1	Reg	
14 July		1600	15 July		2030	2	Reg	
19 July		1900	20 July		1930	2–	Drift	
28 July	Q	1100	29 July		1000	1–	Reg	
19 August	Q	1450	20 August	QQ	1450	1–	Reg	
31 August	D	1740	1 September		1420	3–	STATS	
3 September	QQ	0930	4 September		0530	1+	STATS	Velocity data not reliable
7 September	D	1600	8 September		1630	3–	Reg	
10 September	Q	0840	11 September	Q	0445	1+	STATS	Velocity data not reliable
23 September	QQ	1240	24 September	Q	0530	0	STATS	Velocity data not reliable
26 October	QQ	1100	27 October	QQ	0100	1+	Reg	
2 November	Q	1515	3 November	QQ	1530	1–	Reg	
22 December	D	1500	23 December		1500	3	Reg	

*Condition:

QQ One of five quietest days in month.

Q One of ten quietest days in month.

D One of five most disturbed days in month.

† Observations:

Data gathered and analyzed as described in Lincoln Laboratory Technical Report 477 (Ref. 30).

Reg = Regular; Drift = Drift Measurement; STATS = Satellite Tracking and Thomson Scatter.

It is clear from Table III that the days of observation in 1971 included many that were either very quiet (mean Kp $\leq$ 1+ on 7 days) or mildly disturbed (mean Kp $\geq$ 3 – on 8 days). No observations appear to have been made during the course of a very large magnetic storm. However, many of the disturbed days appear to exhibit effects due to very large Traveling Ionospheric Disturbances (TIDs).

D. Data Analysis

The results gathered in 1971 were analyzed in the manner described for those of 1970.[8] This entailed using each cycle of measurements to construct a single electron density profile vs altitude and secure values of T_e, T_i, and V_z at each altitude for which spectrum measurements were made. The computer program (called ANALYSIS) that performs this has been described in Ref. 30. As part of this process, attempts were made to correct the temperatures gathered in the B-mode to compensate for an instrumental error introduced by the imperfect match of the filters to the spectrum of the pulse.[30] The correction scheme was derived by J. E. Salah from comparing results from the B- and C-modes in the region where they overlap, and has been described in Ref. 7.

The values of electron density, electron and ion temperatures, and vertical drift velocity were next smoothed with respect to height and time by fitting to them a two-dimensional polynomial surface in a least-mean square sense.[8] The program that performs this step (known as INSCON) usually must be run more than once before acceptable results are obtained. Following the first attempted fit, hand-editing of the input data is undertaken to remove obviously bad points that lie far from the surface fitted to the data set. A second attempt then is made with the INSCON program to obtain a fit to the data that does not exhibit any nonphysical peculiarities (such as regions of increasing electron density at altitudes above h_{max} F2). Next the fits to N_e, T_e, and T_i are treated by the program DERQ that obtains height derivatives; from this corrections for the difference between the nominal height of the pulse and its effective center (i.e., that weighted by the altitude variation of the signal-to-noise ratio) can be computed.[8] The data points for T_e, T_i, and V_z then can be reassigned to their effective center heights and INSCON again employed to obtain a final height-corrected fit.[8]

In the process of using the 1970 and 1971 results to calculate the exospheric temperature, B. A. Emery encountered step changes at night that appeared artificial. Upon inspection, these were traced to the scheme for correcting the B-mode temperature values mentioned above. In this scheme[7] corrections are applied to the B-mode temperatures derived from spectra measured at 2.0- and 2.5-msec delay (300- and 375-km nominal heights) wherever the temperature ratios obtained from the B- and C-modes at 525 km differ by more than 0.1 or if the ion temperatures derived from the two pulses differ by more than 100°K.

These empirical corrections removed the worst features of the discrepancies, but introduced step changes in the ion temperature values (of as much as 200°K) during the nighttime. This in turn caused the exospheric temperature derived from these data also to exhibit point-to-point fluctuations at some times, and these served to enhance the amplitude of the highest frequency Fourier component (6- or 8-hour) fitted to the results.

To remedy this defect, a new correction procedure was devised by B. A. Emery[29] using 63 days of data spanning the three-year period of 1970 through 1972. Values for the temperature obtained from spectra measured at three delays along the radar time base in each of the two modes were examined. These were delay times of 3.0, 3.5, and 4.0 msec, corresponding

to the nominal heights of 450, 525, and 600 km. (Measurements made at the 4.5-msec delay time with the B-mode were considered to be too unreliable to be used.)

By employing three delays, it was possible to remove any altitude-dependent features of the comparison. Because of the different height resolutions provided by the two modes, a proper comparison of their results requires knowledge of their equivalent or effective center heights.

Table IV shows the range of equivalent heights found for the B- and C-modes for delays of 3.0, 3.5, and 4.0 msec. The true heights for the C-mode are lower than the corresponding ones for the B-mode because of its longer pulse length.

TABLE IV

VARIATIONS IN THE TRUE HEIGHTS FOR VARIOUS DELAY TIMES IN THE B- AND C-MODES

Mode	True Height (km)		
	Delay Time 3.0 msec Nominal Height 450 km	Delay Time 3.5 msec Nominal Height 525 km	Delay Time 4.0 msec Nominal Height 600 km
B	437-441	512-517	586-593
C	398-428	479-488	551-568

Besides adjusting the results for differences in their effective center heights, it also was decided to remove a correction applied to the electron temperature to compensate for the effect on the signal spectrum of the changing Debye length.[30] This correction was

$$T_e = T'_e/(1 - 1.62\ T'_e/N_e) \quad (1)$$

where T_e and T'_e are the corrected and uncorrected electron temperatures, and N is the electron density given in units of electrons/cubic centimeter. As the purpose of the exercise was to compare the interpretations of spectra gathered at the same altitudes by the two modes, it was considered prudent to remove this correction to the results, although at the altitudes under consideration, its effect generally was small.

A straight line interpolation of the T_e and T_i values at the three true heights corresponding to the three delays examined was used to find T_e and T_i at true heights of 450 and 525 km. The individual values next were sorted into groups of B-mode ion temperatures (TIB) vs B-mode temperature ratios T_e/T_i (TRB) in intervals of spanning 100°K in TIB over the range 600 to 1700°K and intervals of 0.2 in TRB from 0.9 to 3.1. Next, all the points in each of these groups were averaged.

The corresponding C-mode temperature ratios (TRC) then were averaged to give what were taken to be accurate or "true" values for each "box." The averages originally were kept separately for the two heights (450 and 525 km), but later were combined into one to obtain a more extensive data base. Provided all height-dependent features of the data are removed, the corrections found with the data at 450 km should be the same as those found with data at 525 km. The averaged values of the C-mode ion temperatures (TIC) are plotted for each TIB box vs TRB in Fig. 5, and the TRC values for each TRB box are plotted against TIB in Fig. 6.

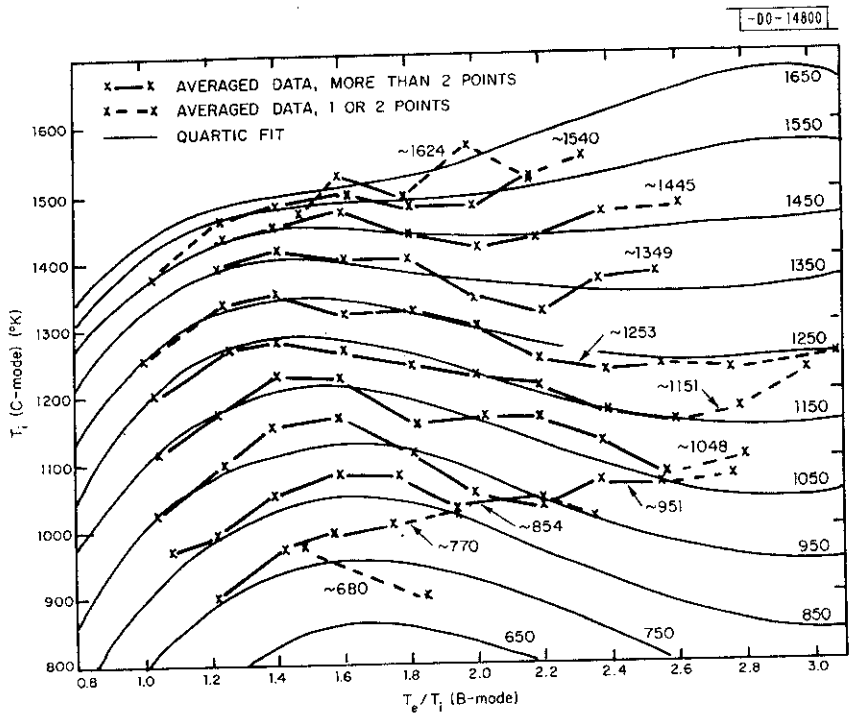

Fig. 5. Average values of ion temperature (crosses) obtained from C-mode measurements corresponding to B-mode for estimates organized into bins 100°K high by 0.2 in T_e/T_i (B-mode) wide. Also shown are the smooth quartic fits (continuous lines); these are labeled at the right.

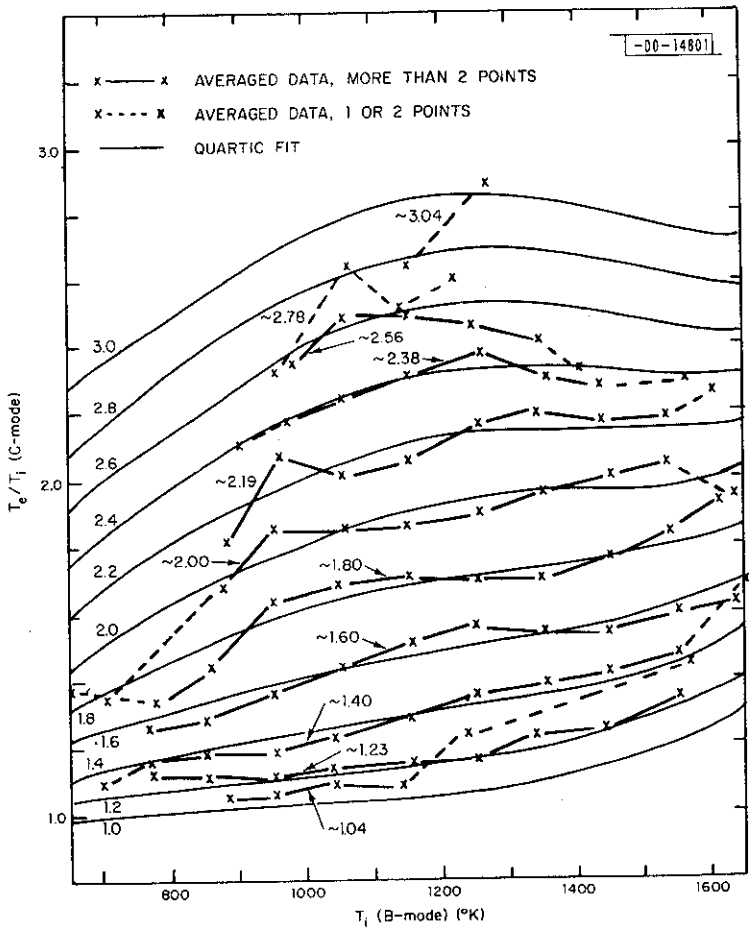

Fig. 6. Average values of temperature ratio T_e/T_i (crosses) obtained from C-mode measurements corresponding to B-mode estimates organized into bins 0.2 high by 100°K in T_i (B-mode) wide. Also shown are the smooth quartic fits (continuous lines); these are labeled at the right.

To obtain a smoothly varying correction for TIB and TRB, appropriate boundary conditions were placed around the edges of these matrices and quartic surfaces were fitted to the points for TIC and TRC of the form

$$\text{TIC (or TRC)} = \sum_{i=1}^{5} (a_{1i} + a_{2i}\text{TIB} + a_{3i}\text{TIB}^2 + a_{4i}\text{TIB}^3 + a_{5i}\text{TIB}^4)\,\text{TRB}^{(i-1)} \quad . \qquad (2)$$

There were 86 nonzero boxes and 48 exterior ones. The boundary points and most of the interior points of the matrix were given an equal weight of 50 in the fitting procedure. Exceptions were interior boxes containing only one or two data points; these were weighted one or two, respectively. The interior boxes with the lowest B-mode temperature ratios were weighted 200 if they contained more than two data points. The coefficients that were derived by this procedure are listed in Table V. Figures 5 and 6 show the resulting fits plotted against the averaged data.

TABLE V

COMPUTER LISTING OF QUARTIC COEFFICIENTS FOR THE FITS TO T_i AND T_e/T_i C-MODE USED IN EQUATION (2)

T_i C-Mode					
i	a_{1i}	a_{2i}	a_{3i}	a_{4i}	a_{5i}
1	−.796867E-01	−.367180E-01	.482273E-02	−.196736E-05	.243638E-09
2	.173999E-01	.622118E-01	−.382242E-02	.652307E-06	.457058E-10
3	.106960E-00	−.205804E-01	−.500643E-03	.939378E-06	−.264987E-09
4	−.324305E-00	.146370E-00	.551828E-03	−.318412E-06	.766356E-10
5	.206308E-01	.605626E-03	−.384643E-04	−.223650E-08	.565875E-13
T_e/T_i C-Mode					
i	a_{1i}	a_{2i}	a_{3i}	a_{4i}	a_{5i}
1	−.464355E-00	.786786E-02	−.953145E-05	.537837E-08	−.111904E-11
2	.149215E-01	−.110487E-01	.111261E-04	−.617450E-08	.145316E-11
3	.130935E-00	.350796E-02	−.690789E-06	−.226501E-09	.255717E-13
4	−.257652E-00	−.611208E-03	.144244E-07	.106388E-09	−.408892E-13
5	.644512E-01	.271592E-04	−.354883E-07	.273383E-10	−.156774E-14

The results from this analysis were found to be very similar to those found by Salah,[7] except that a strong dependence on T_i was found as well as the dependence on T_e/T_i. For B-mode temperatures of about 1450°K, little correction to T_i is made. For temperatures above this, the correction to TIB for B-mode temperature ratios less than about 2.6 is negative and is approximately −139°K for TIB = 1650°K and TRB = 1.6. For B-mode temperatures less than 1450°K, the correction to TIB is positive and approaches 200°K for TIB = 950°K and TRB = 1.6. For B-mode temperature ratios above about 1.2, the largest corrections to TRB are at the

lowest ion temperatures, the correction to TRB = 2.0 at TIB = 750°K being about −0.4. For TIB = 1150°K, the correction is only about −0.1. The new corrections were applied to all the B-mode data.

The new correction scheme still depends upon the assumption that the C-mode results are accurate and hence fails to remove any bias errors that may exist in the C-mode results. It does, however, force the B- and C-mode results to connect smoothly in altitude better than the previous scheme, and has the advantage that it does not introduce jumps in the corrected temperatures since the correction is selected from a smoothly varying surface and always is applied regardless of the initial B-mode temperature estimates.

The new correction scheme also was applied to most of the data gathered in 1970 and revised in INSCON fits obtained for these results. For the most part, the changes to the reported results[8] are small, and hence the revised plots will not be published. They are, however, available upon request. The filter bank spectral analysis scheme upon which the results reported here depend was replaced in 1976 with a digital correlator that eliminated these inherent defects.

III. RESULTS

A. General

The smoothed INSCON contour diagrams of $\log_{10} N_e$, T_e, T_i, and V_z vs height and time for the days listed in Table III are presented in Figs. 7(a-d) through 26(a-d). These plots together with the INSCON tapes containing the coefficients of the fits have been furnished to the World Data Center A (Boulder, Colorado). The tapes together with the "recover" program RCVR (listed in Ref. 8, and also available from the World Data Center) permit the numerical values of any of the parameters to be obtained as functions of height or of time during any of the observation periods. Appendix A provides a copy of the listing of the INSCON fits, and gives the start and end times of the fit, the test value that allows the program to be checked, as well as the identification number (KDAT) of the type of fit and "fit number."[8]

The KDAT number identifies the parameter plotted by the first numeral (N_e = 1, T_e = 2, T_i = 3, V_z = 10). The second numeral indicates whether the results have been corrected for the difference between nominal and effective height (corrected = 9, not corrected = 0). Note, however, that the electron density results are secured in a way that requires no correction and hence only the "uncorrected" plots are available. The "fit number" is a six-digit number, the first two digits of which give the year the data were collected. The last four digits are used to identify the final edited fit obtained for each particular day.

B. Magnetically Quiet Summer Behavior

We have discussed in previous reports[4-8] the characteristic behavior of the F-layer over Millstone. A clear variation of the behavior between summer and winter is evident with a rapid transition near equinox. Additional characteristic changes occur that are associated with magnetically disturbed conditions, and these also have been discussed previously.

Examples of quiet summer daytime behavior are provided by 27-28 May, 18-19 June, 19-20 July, 19-20 August, and 3-4 September (Figs. 13, 14, 16, 18, and 20). On these days there was little diurnal variation in electron density. The F2-region peak density usually was a maximum around sunset, and there often would be a slight minimum near noon. By contrast, the electron temperature rose rapidly at sunrise and fell again at sunset, with only small variations at any height between these times.

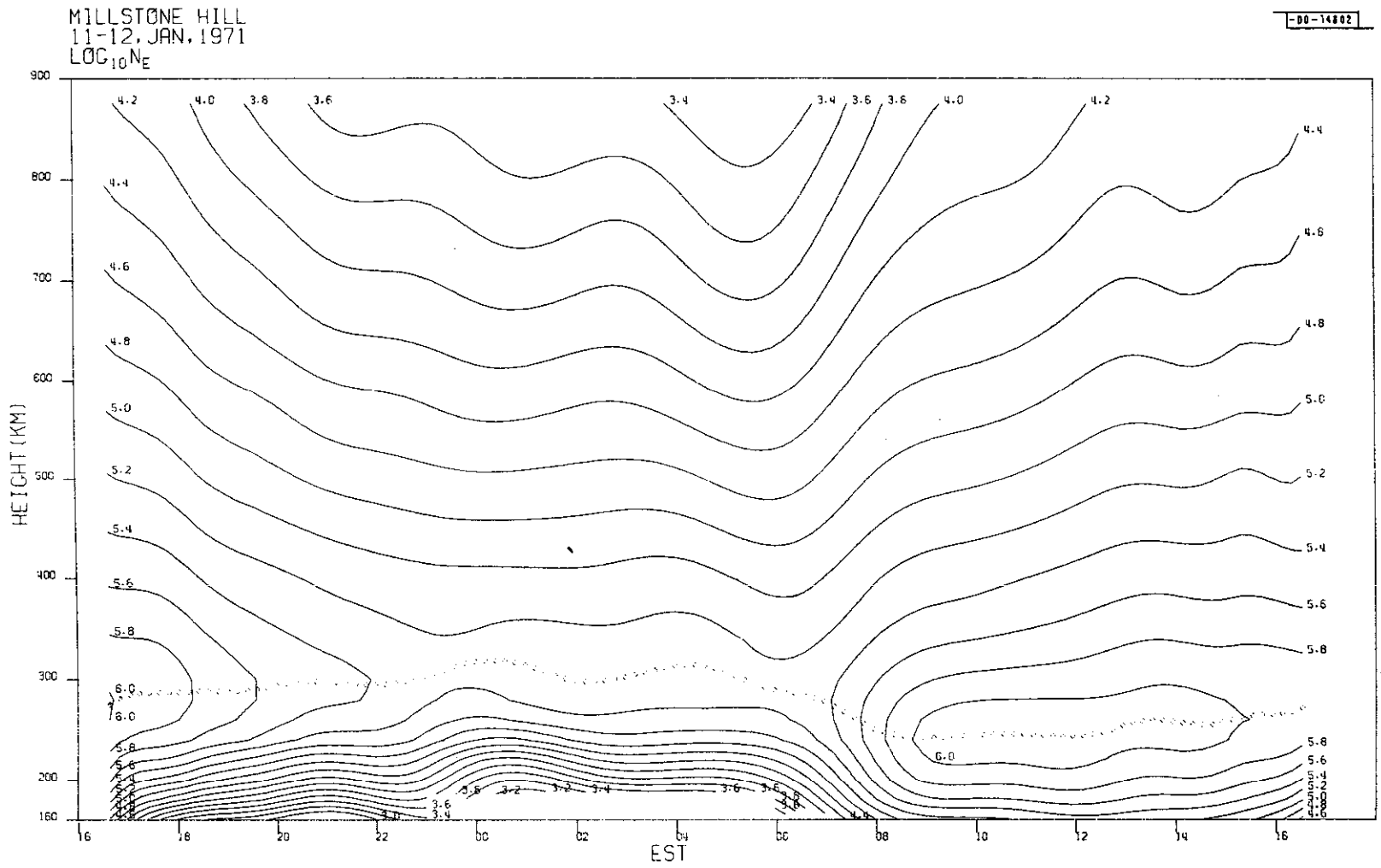

(a) $\text{Log}_{10} N_e$.

Fig. 7(a-d). Contours of density, temperature, and vertical velocity for 11-12 January 1971.

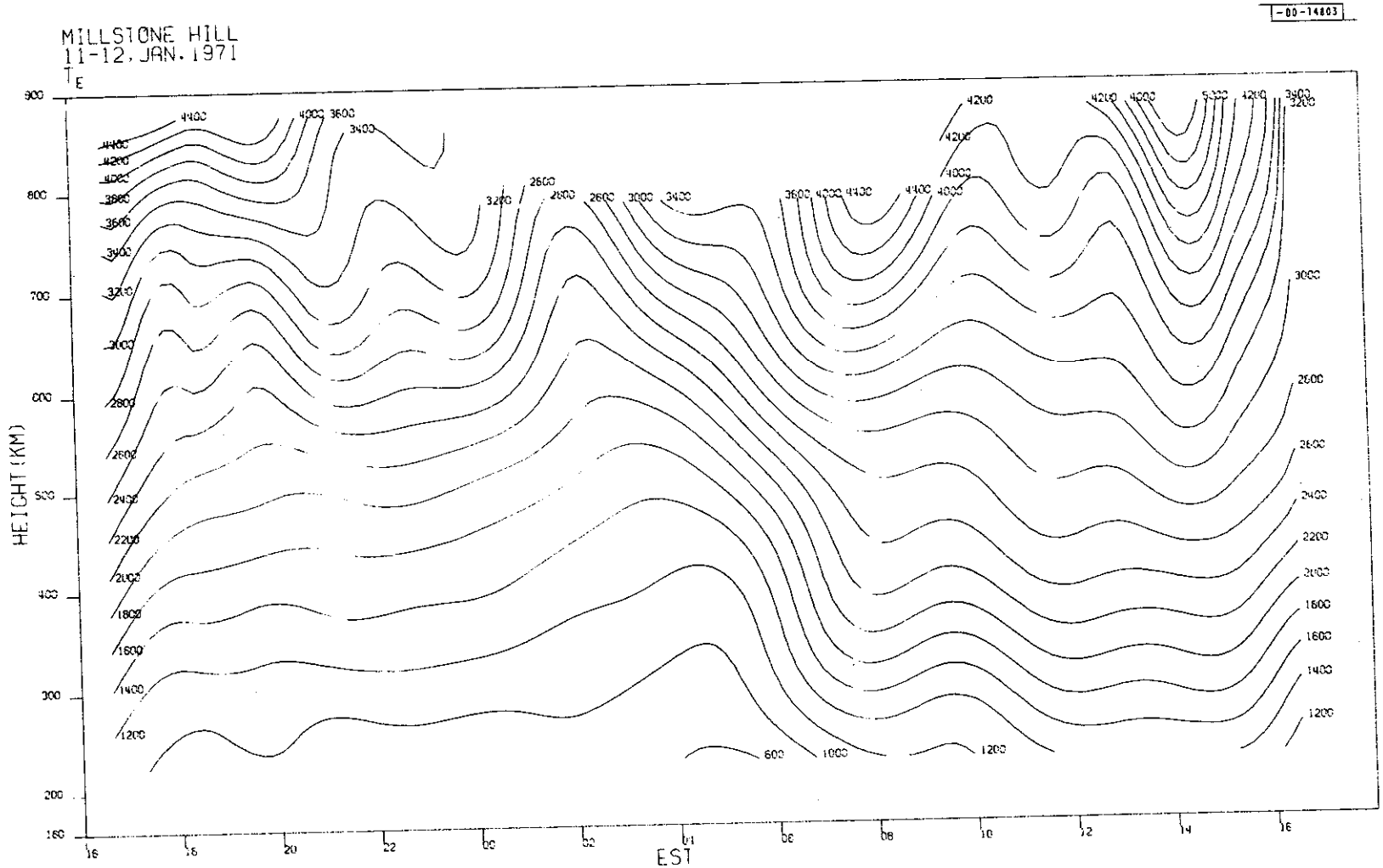

(b) T_e.

Fig. 7(a-d). Continued.

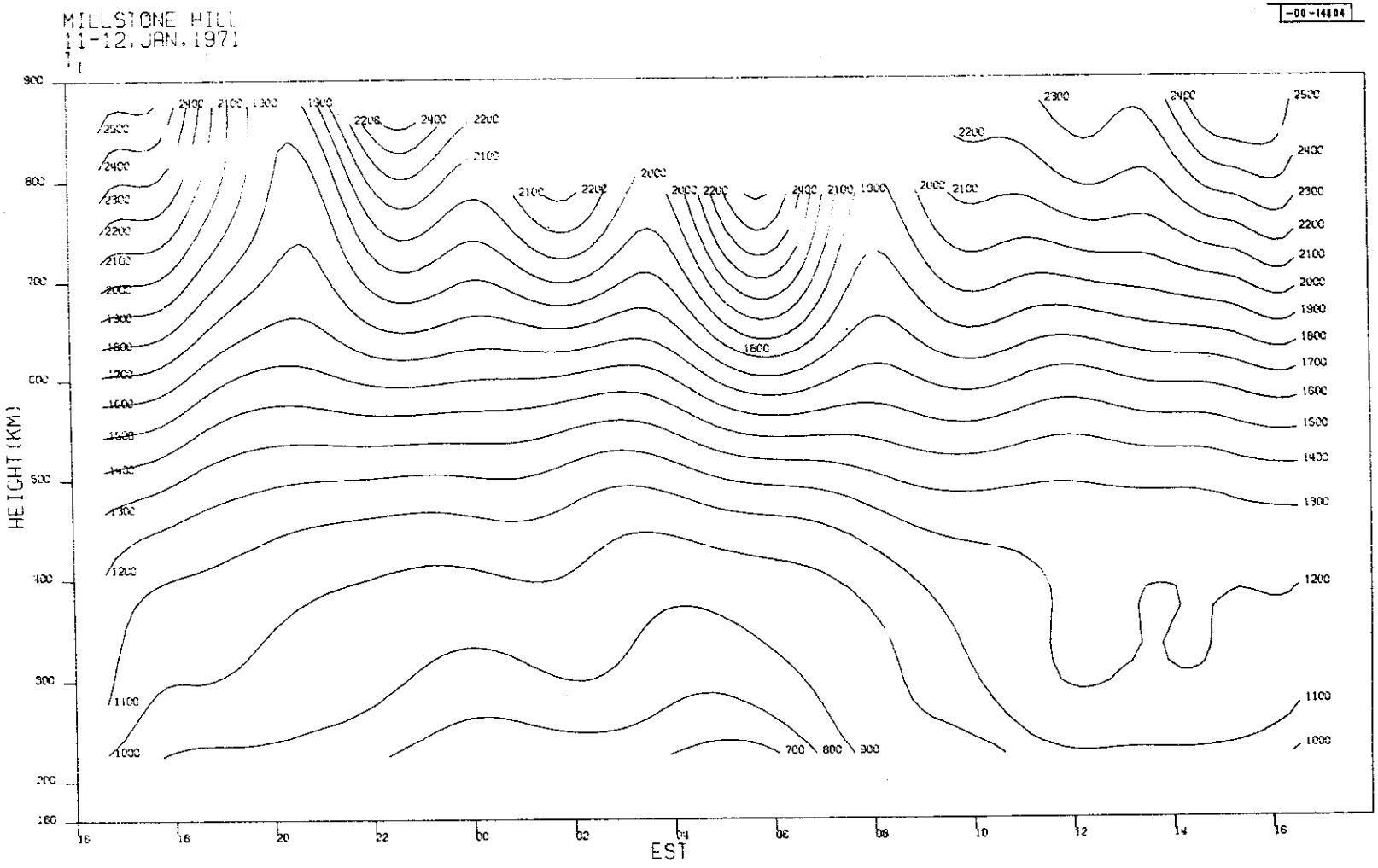

(c) T_i.

Fig. 7(a-d). Continued.

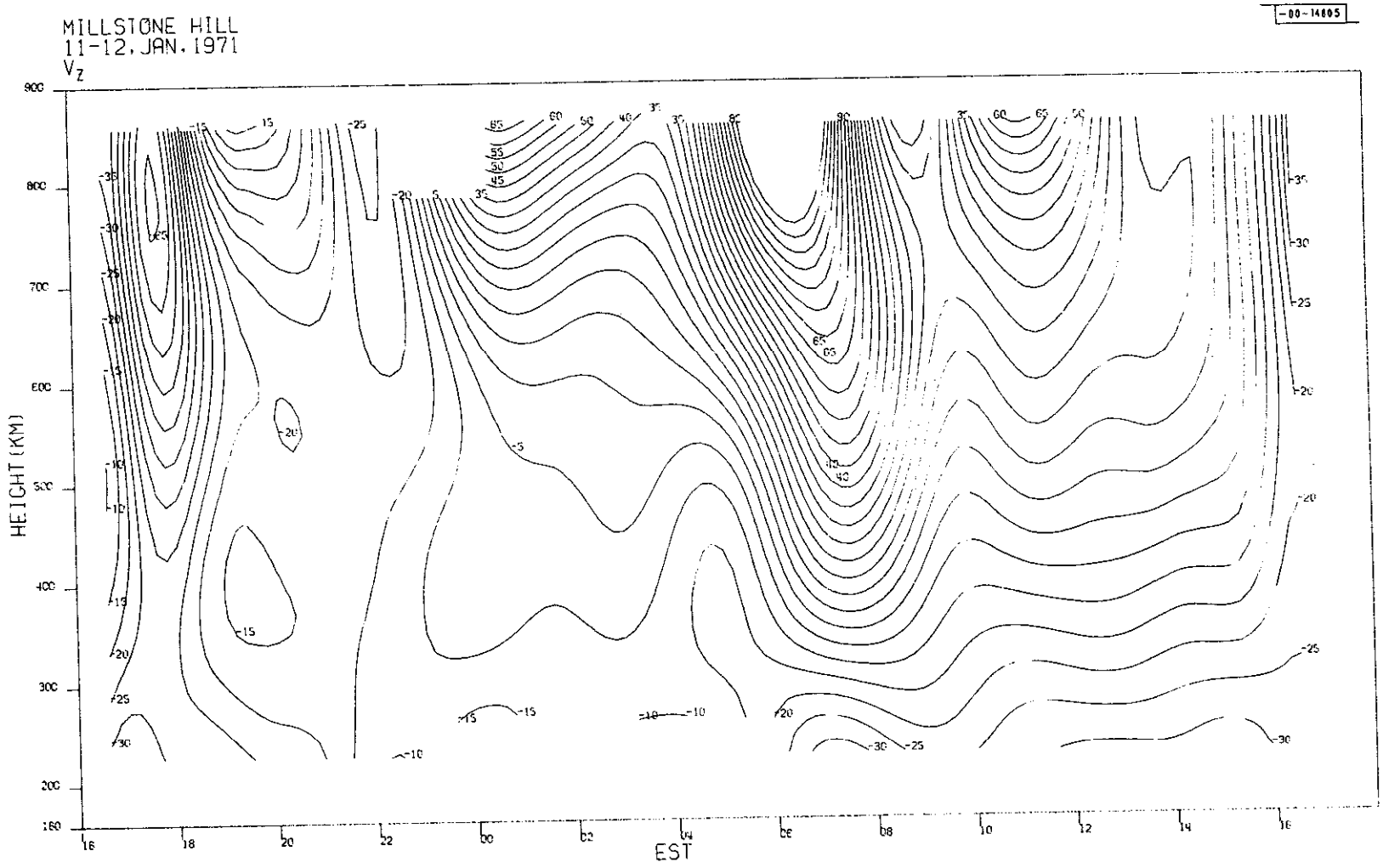

(d) V_z.

Fig. 7(a-d). Continued.

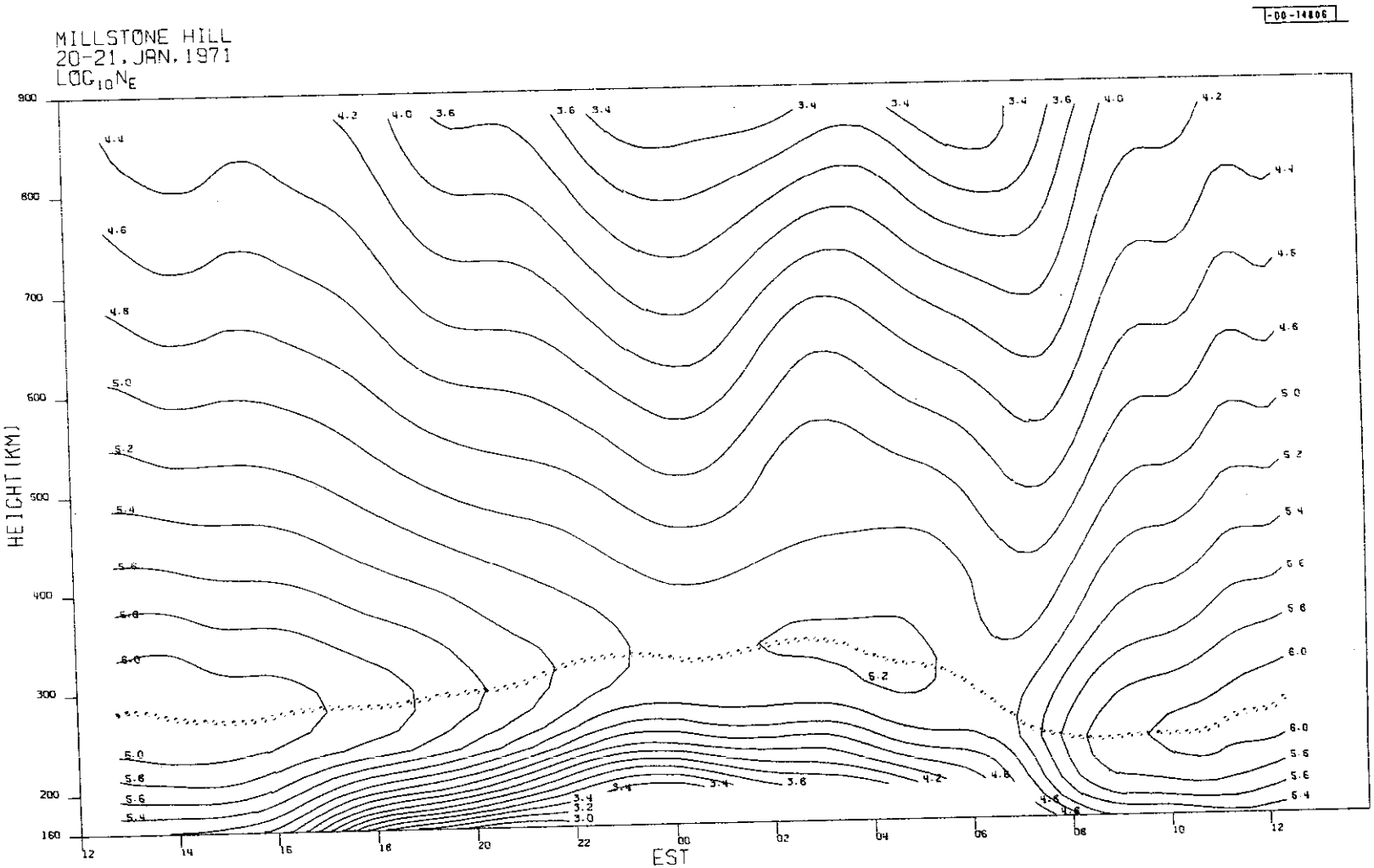

(a) $\text{Log}_{10}\ ^{N}e$.

Fig. 8(a-d). Contours of density, temperature, and vertical velocity for 20-21 January 1971.

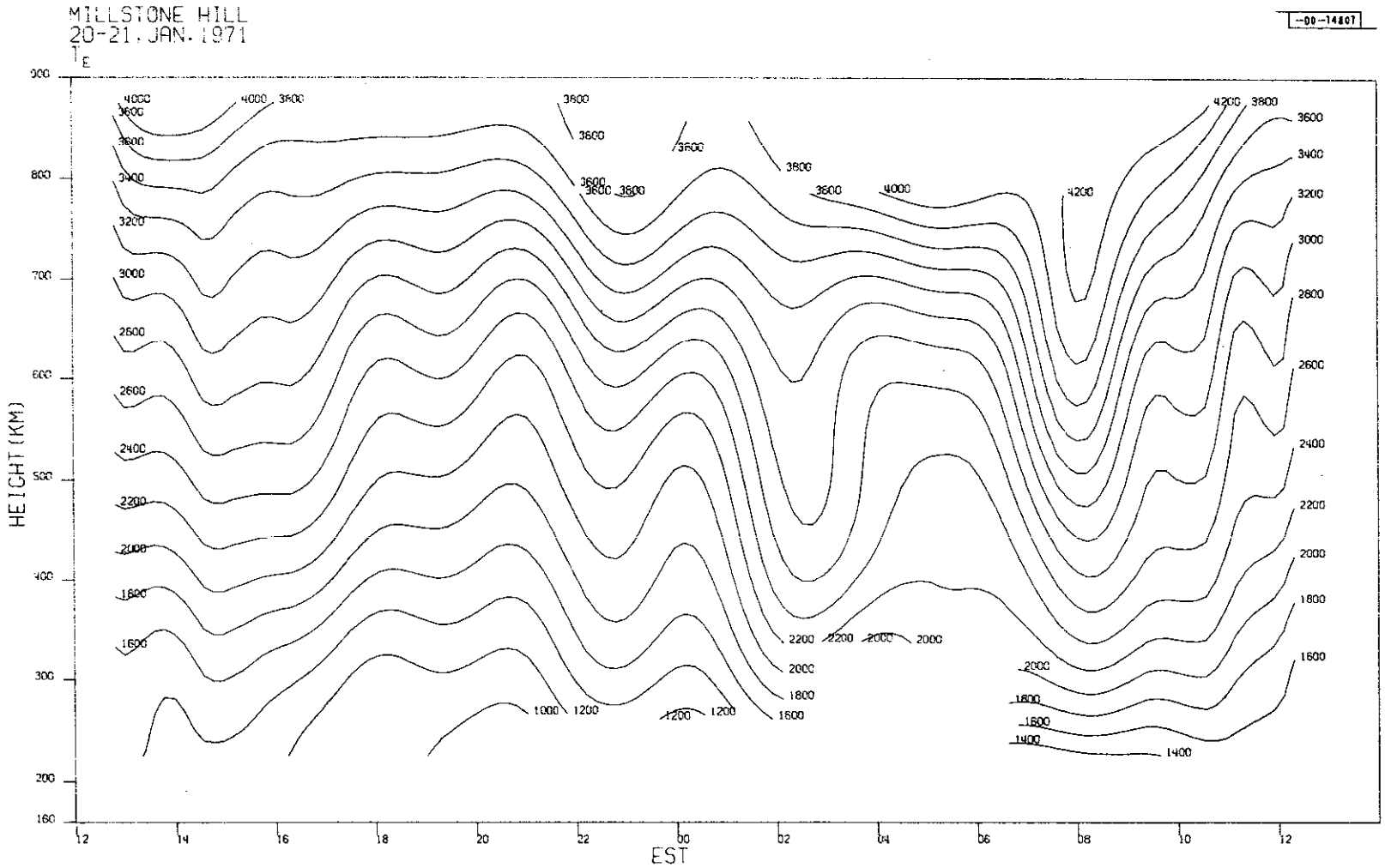

(b) T_e.

Fig. 8(a-d). Continued.

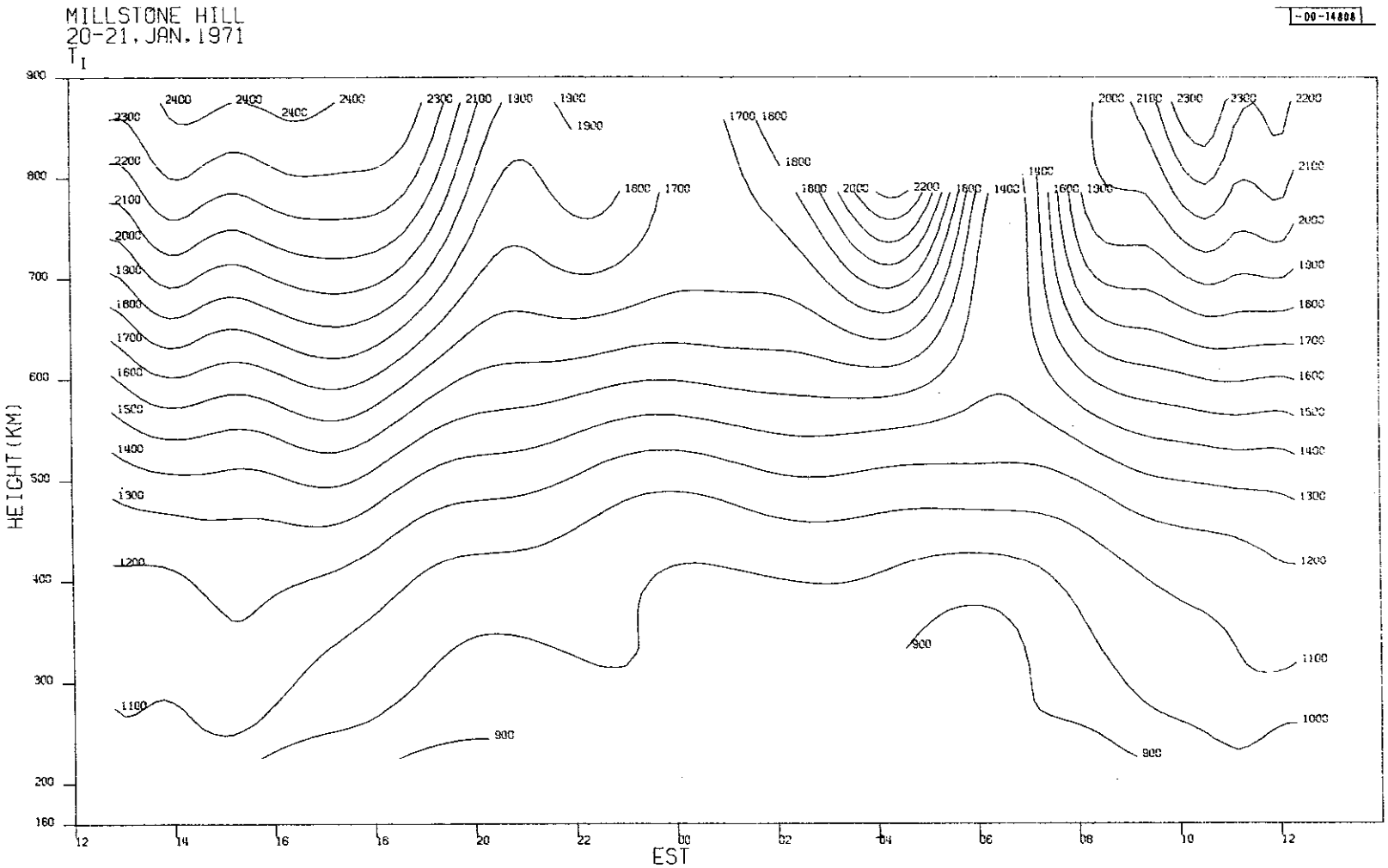

(c) T_i.

Fig. 8(a-d). Continued.

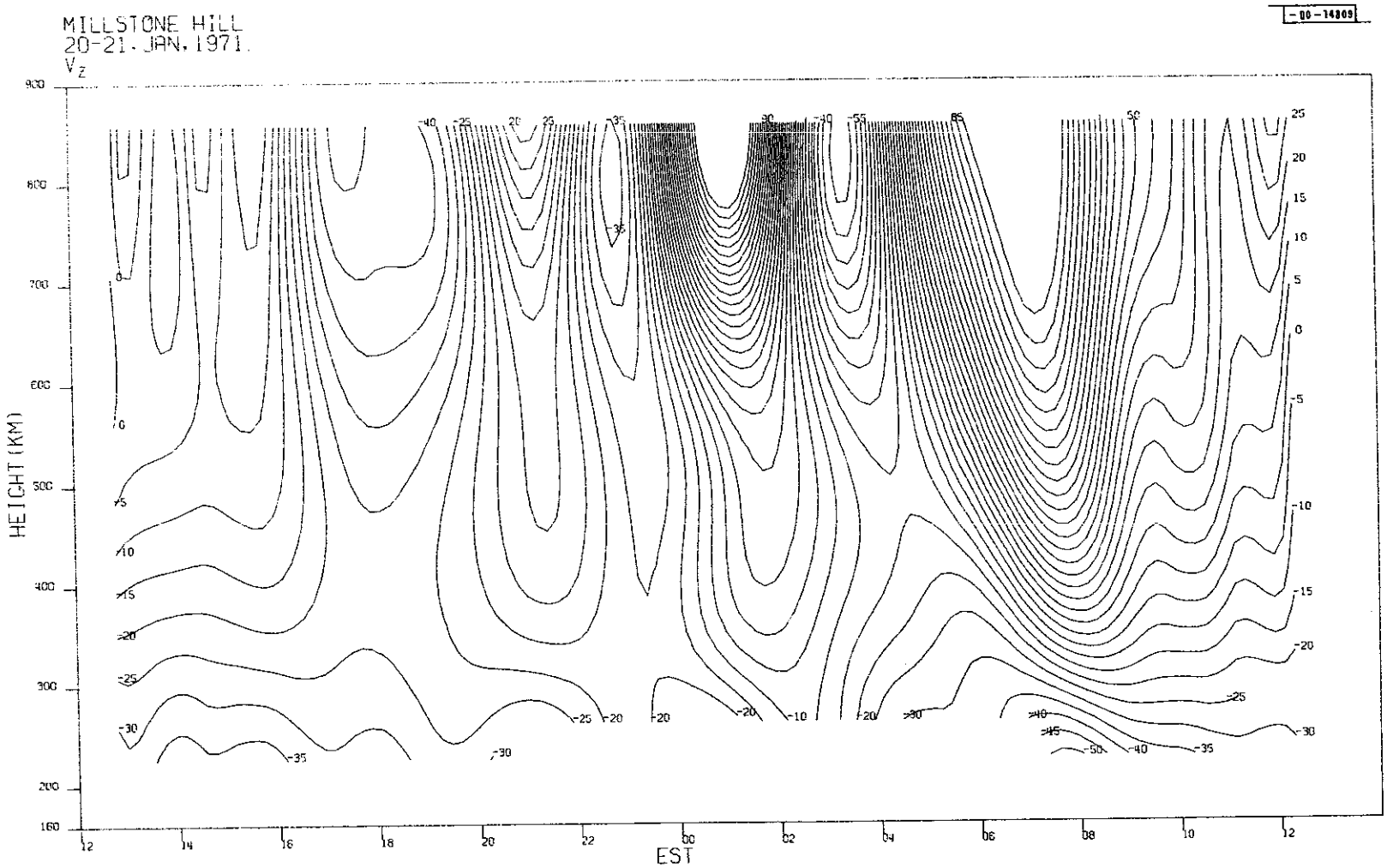

(d) V_z.

Fig. 8(a-d). Continued.

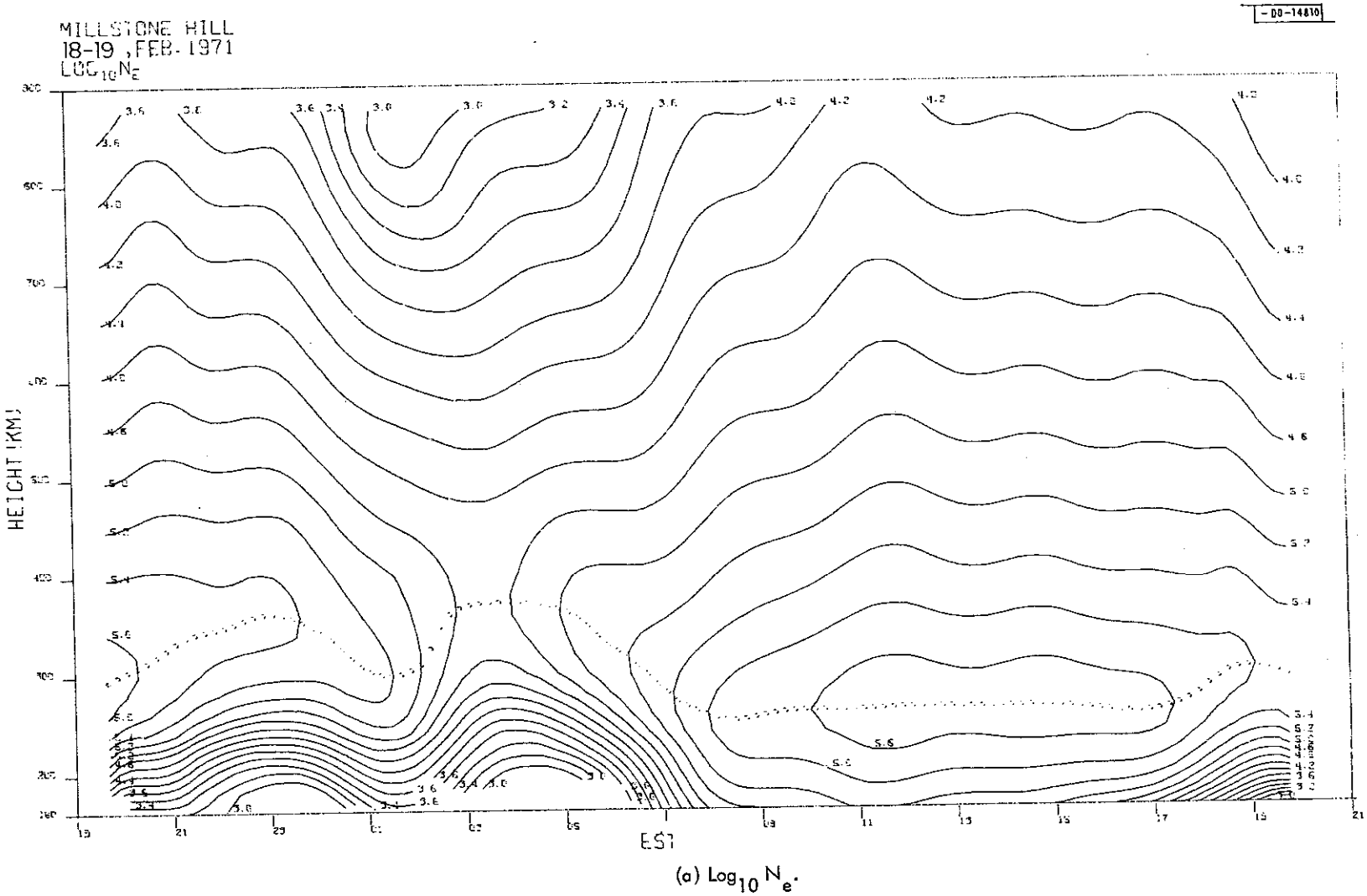

Fig. 9(a-d). Contours of density, temperature, and vertical velocity for 18-19 February 1971.

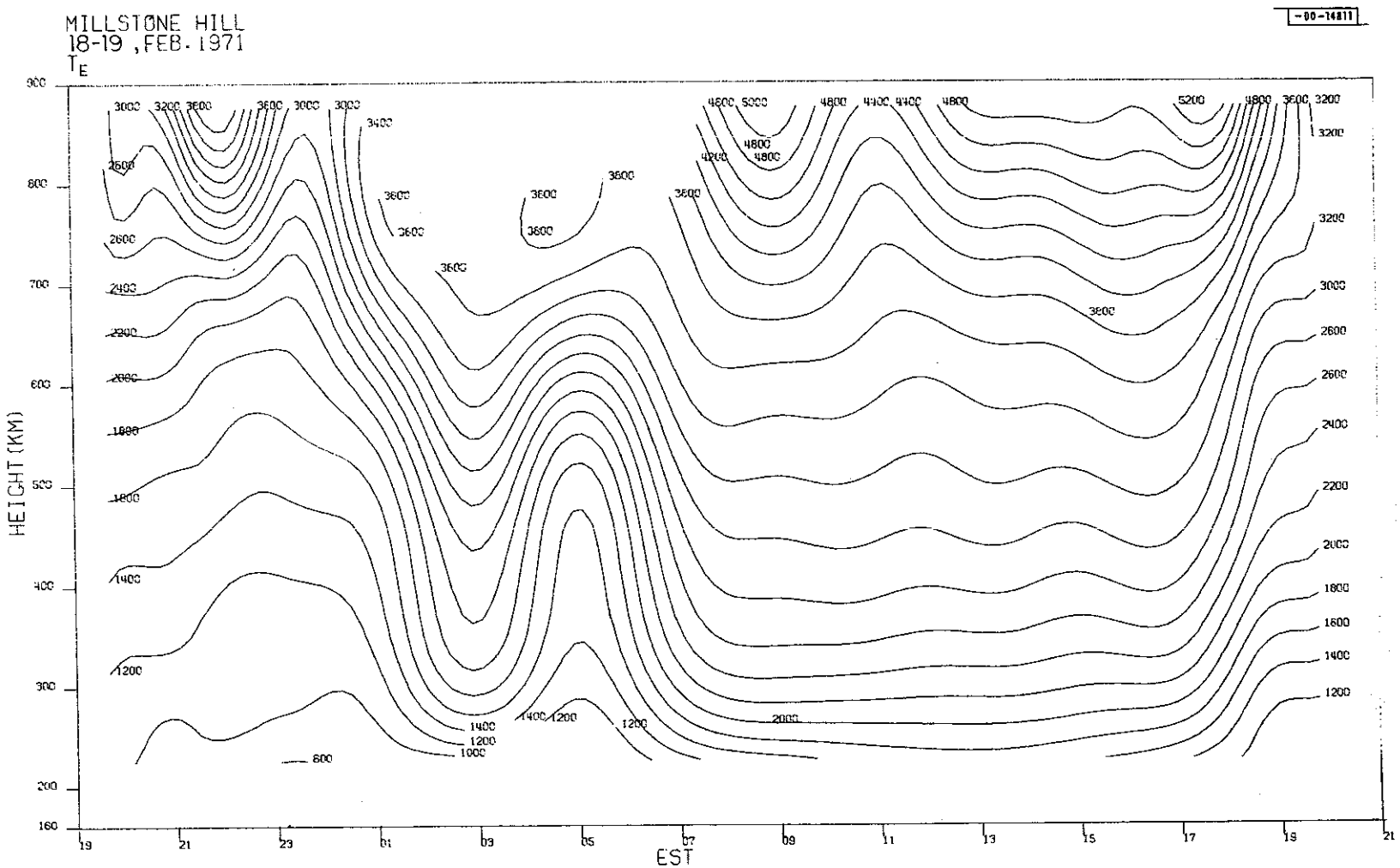

(b) T_e.

Fig. 9(a-d). Continued.

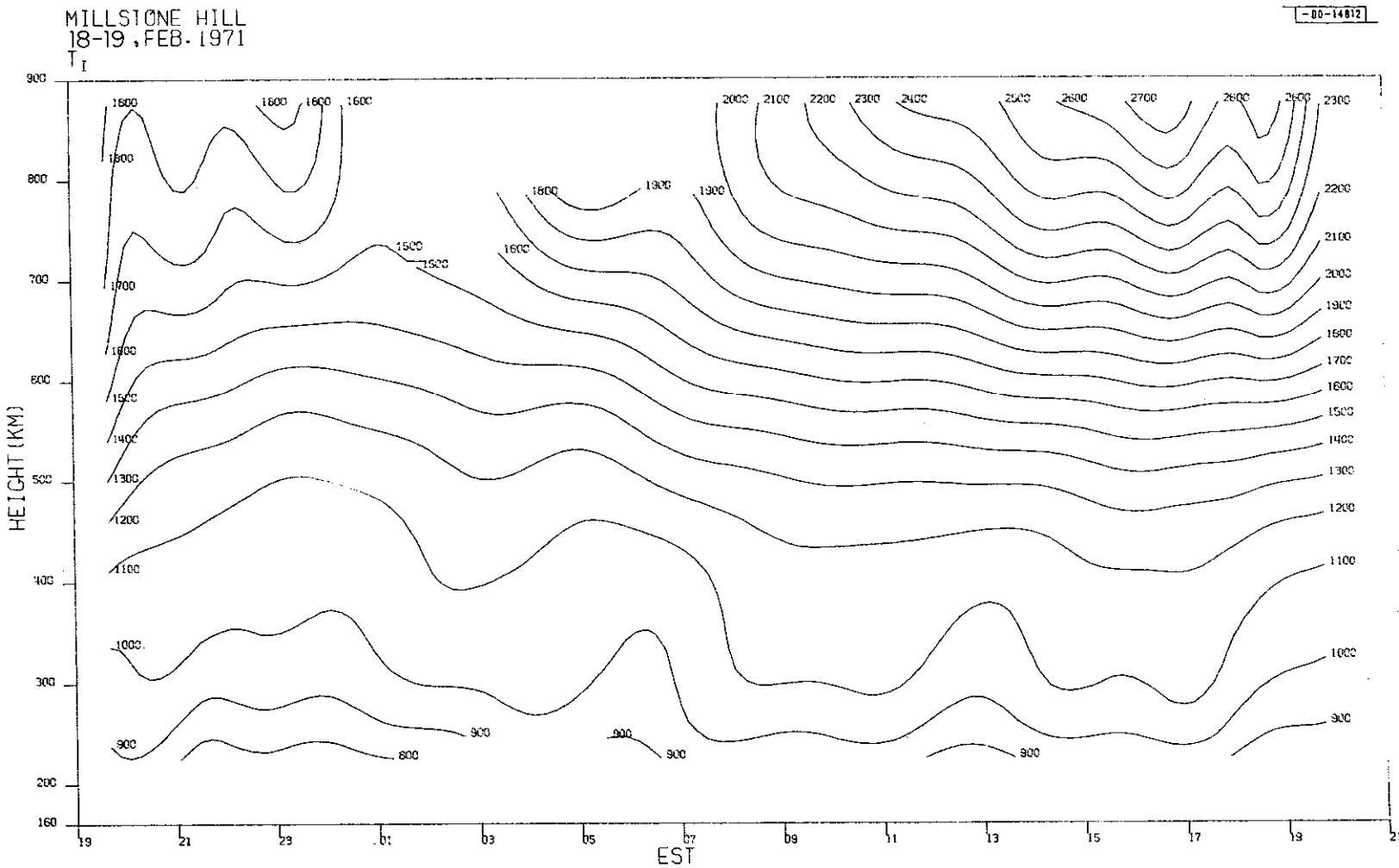

(c) T_i.

Fig. 9(a-d). Continued.

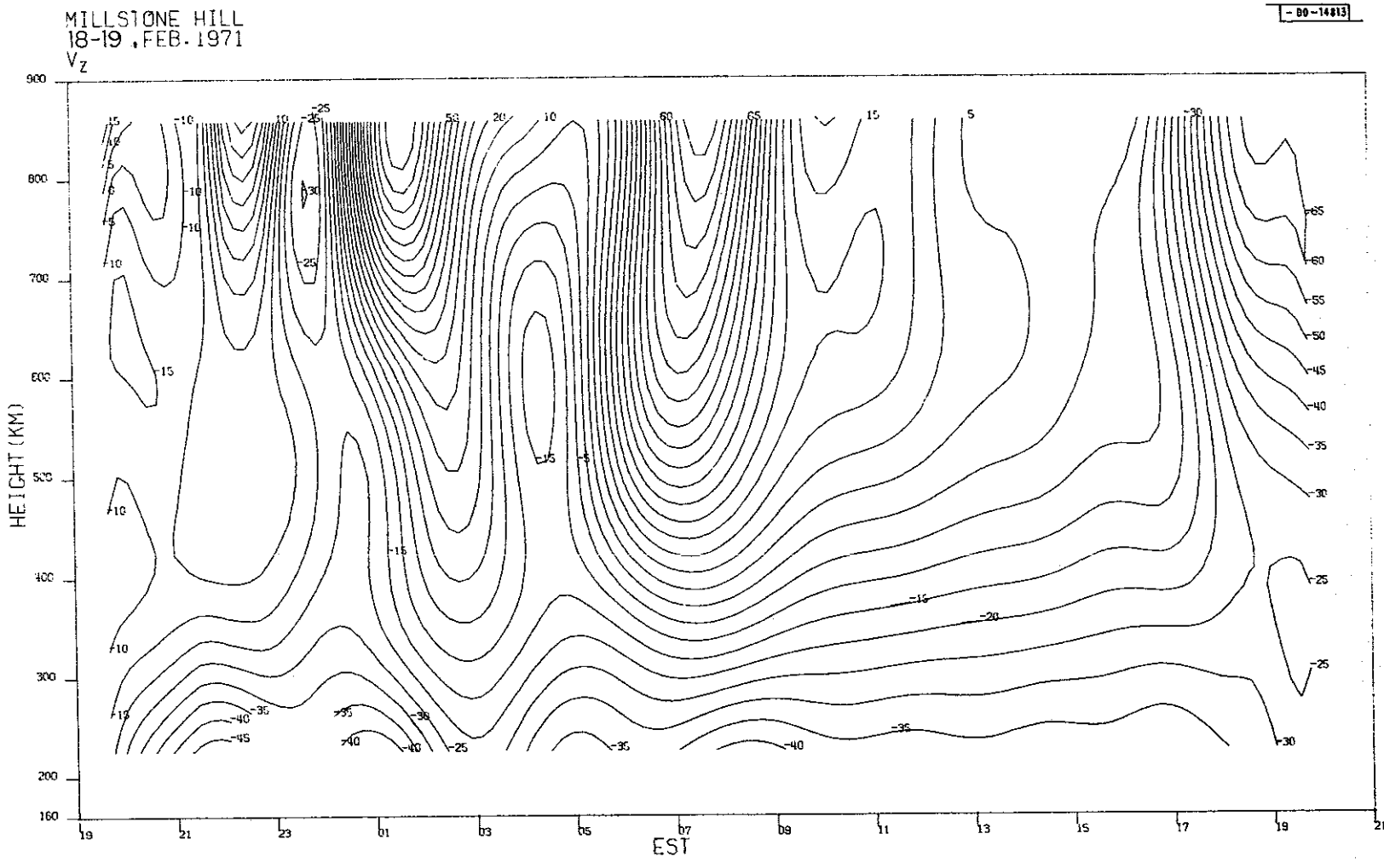

(d) V_z.

Fig. 9(a-d). Continued.

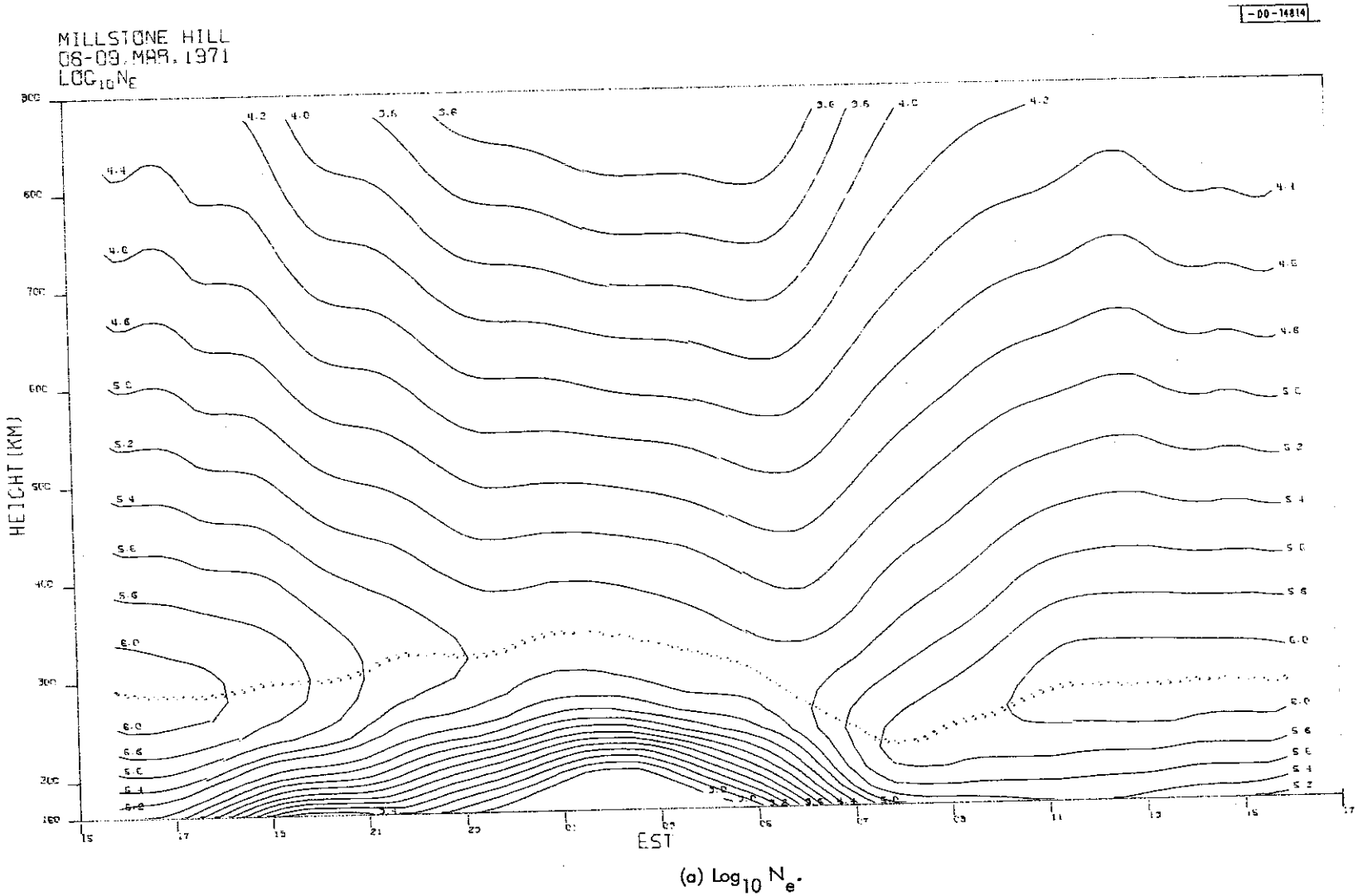

(a) $\text{Log}_{10} N_e$.

Fig. 10(a-d). Contours of density, temperature, and vertical velocity for 8-9 March 1971.

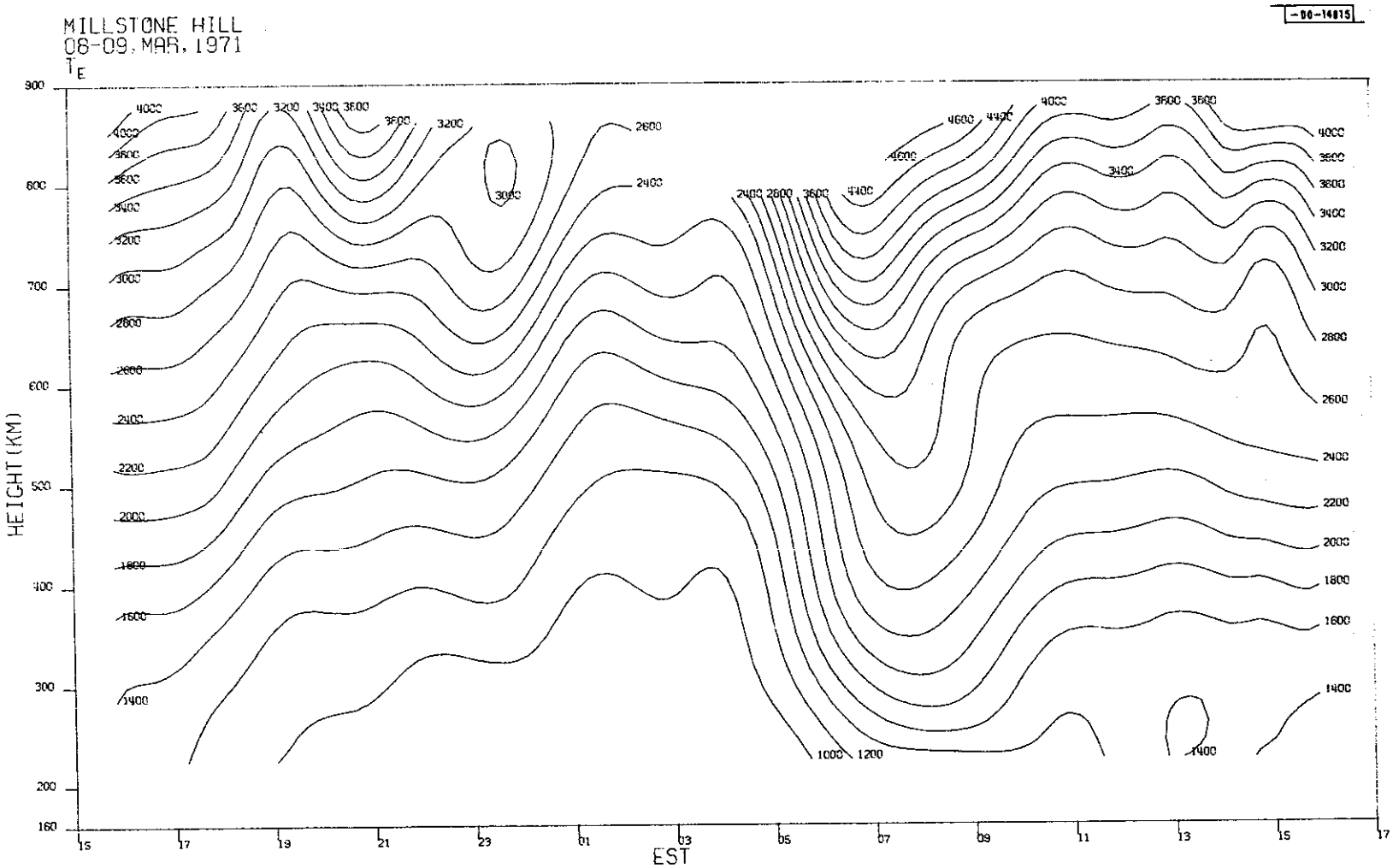

(b) T_e.

Fig. 10(a-d). Continued.

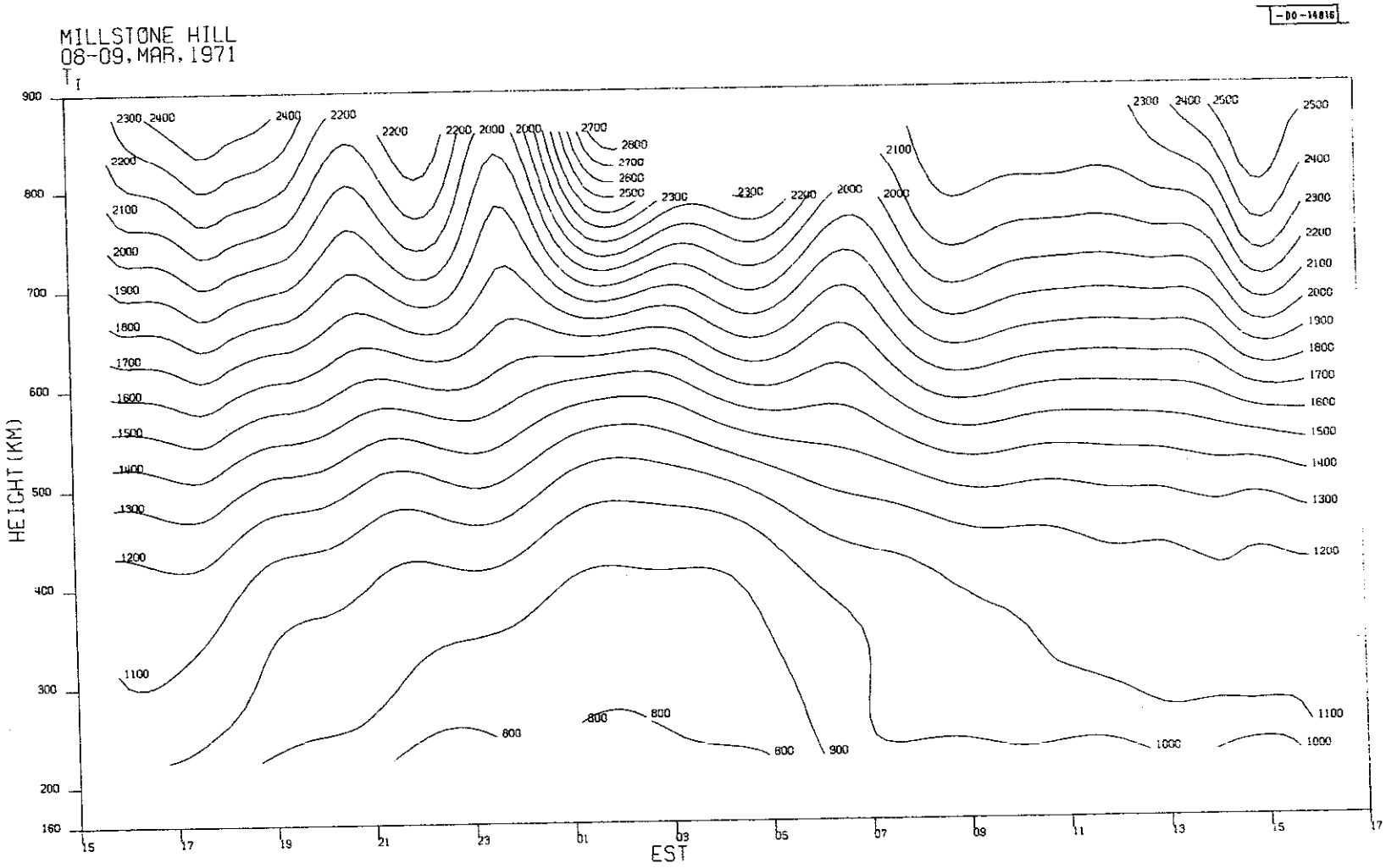

(c) T_i.

Fig. 10(a-d). Continued.

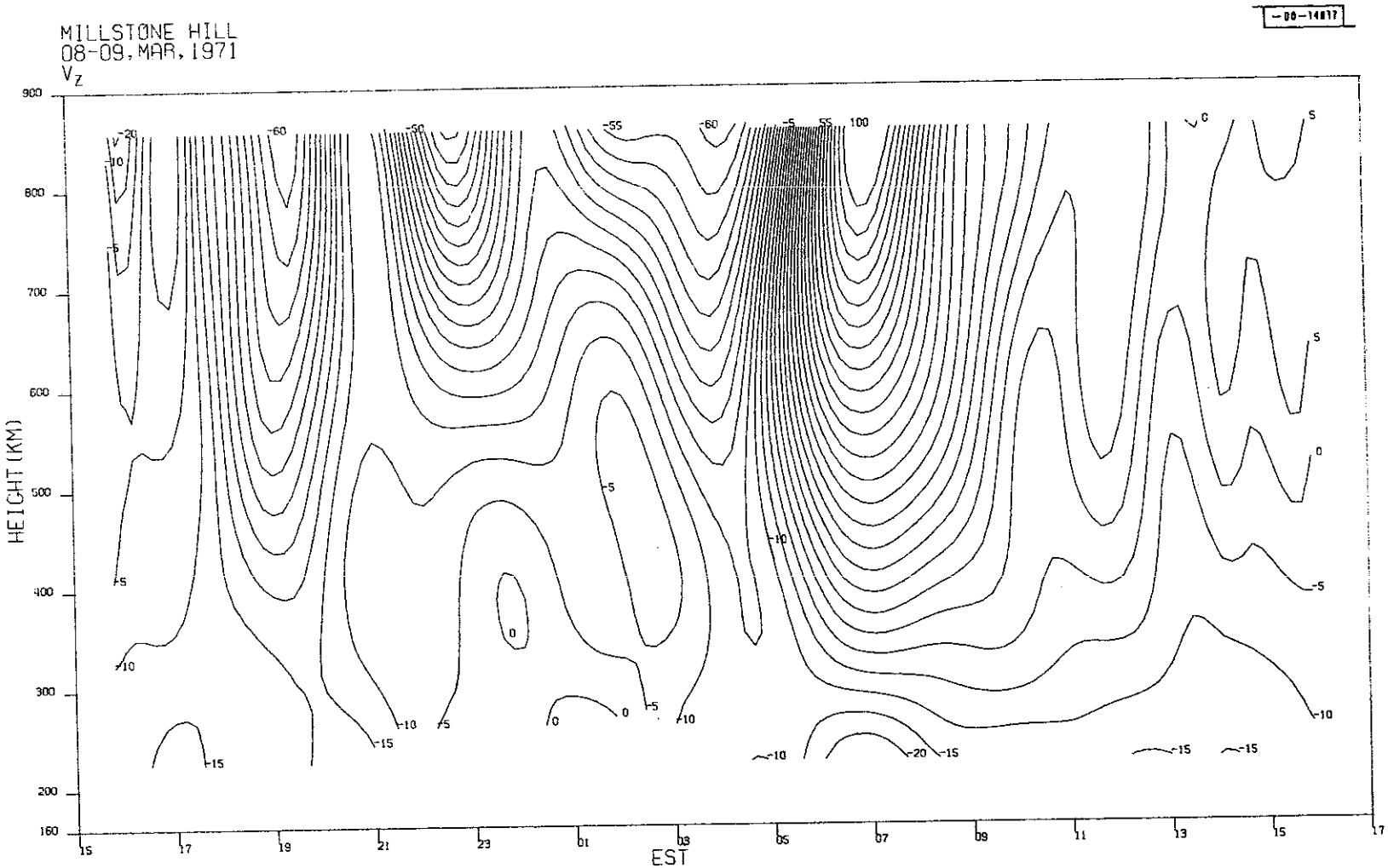

(d) V_z.

Fig. 10(a-d). Continued.

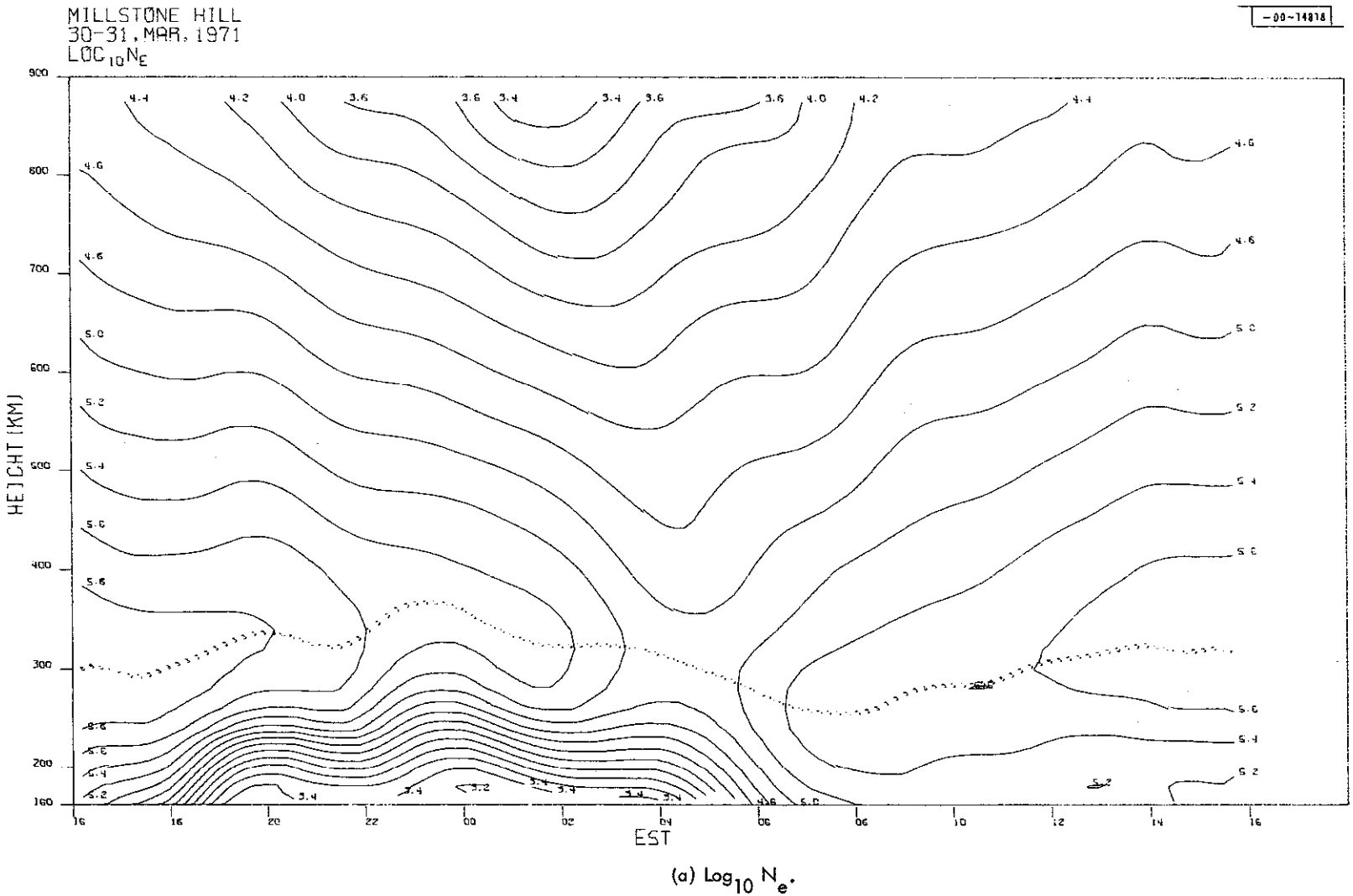

(a) $\text{Log}_{10} N_e$.

Fig. 11(a-d). Contours of density, temperature, and vertical velocity for 30-31 March 1971.

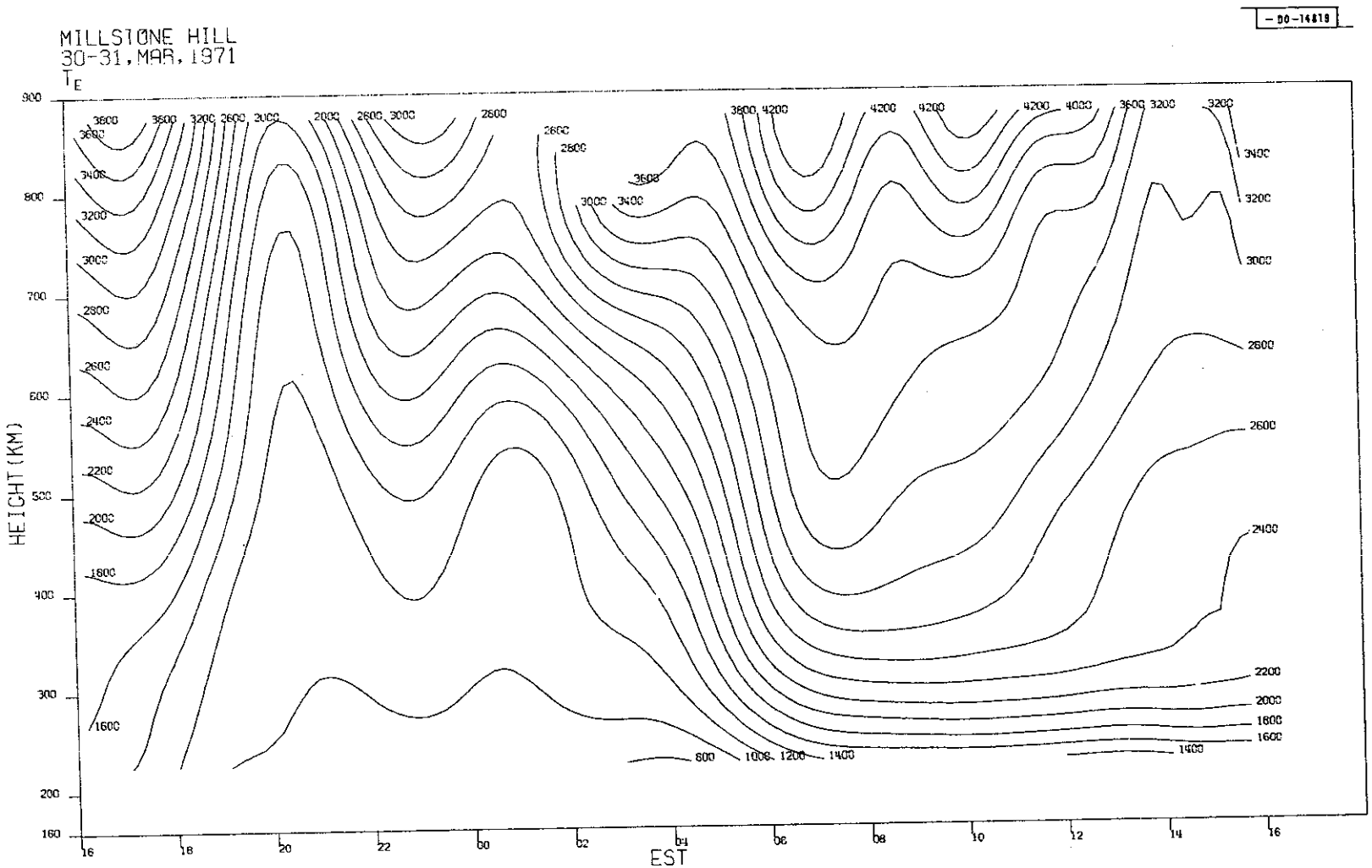

(b) T_e.

Fig. 11(a-d). Continued.

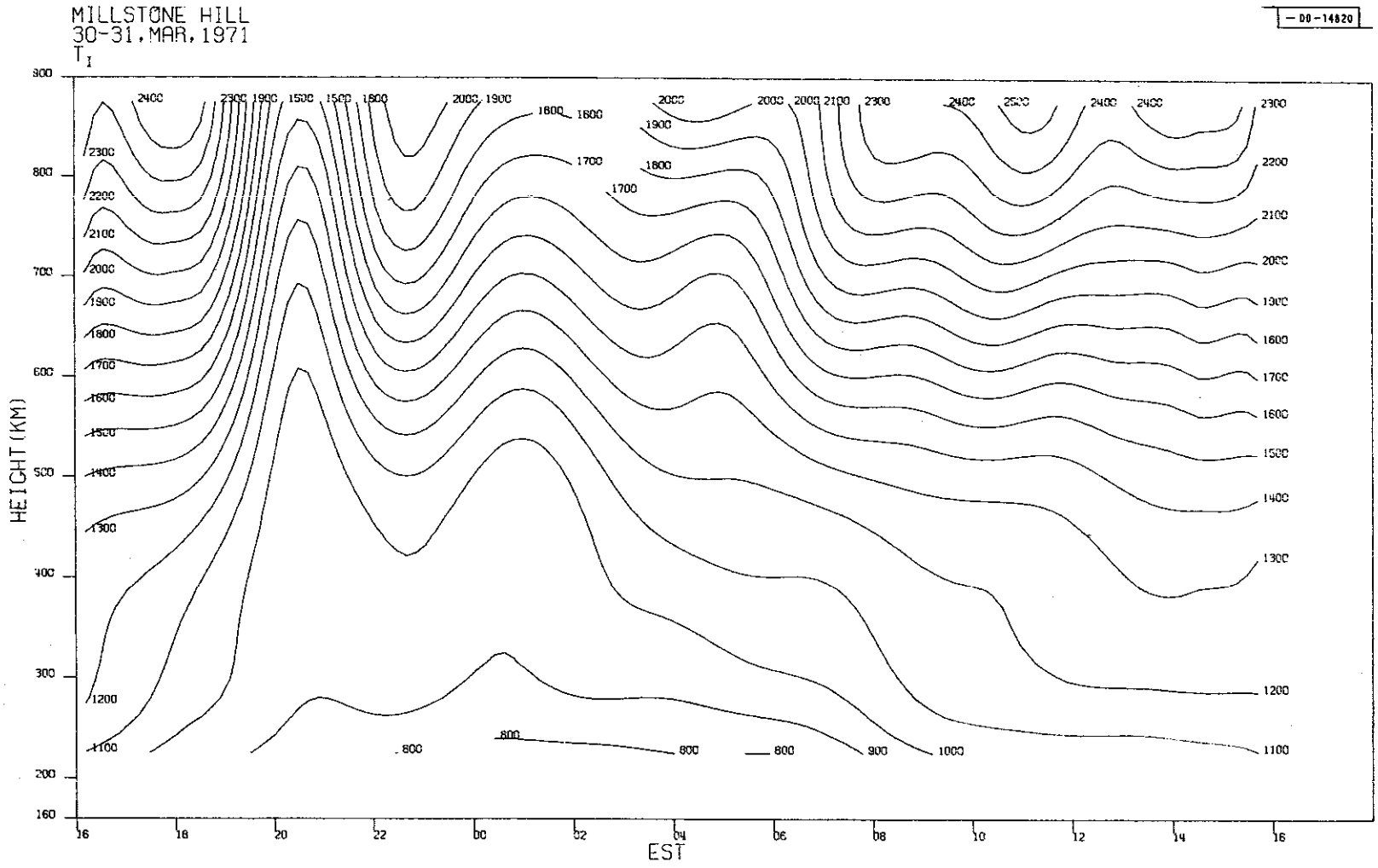

(c) T_i.

Fig. 11(a-d). Continued.

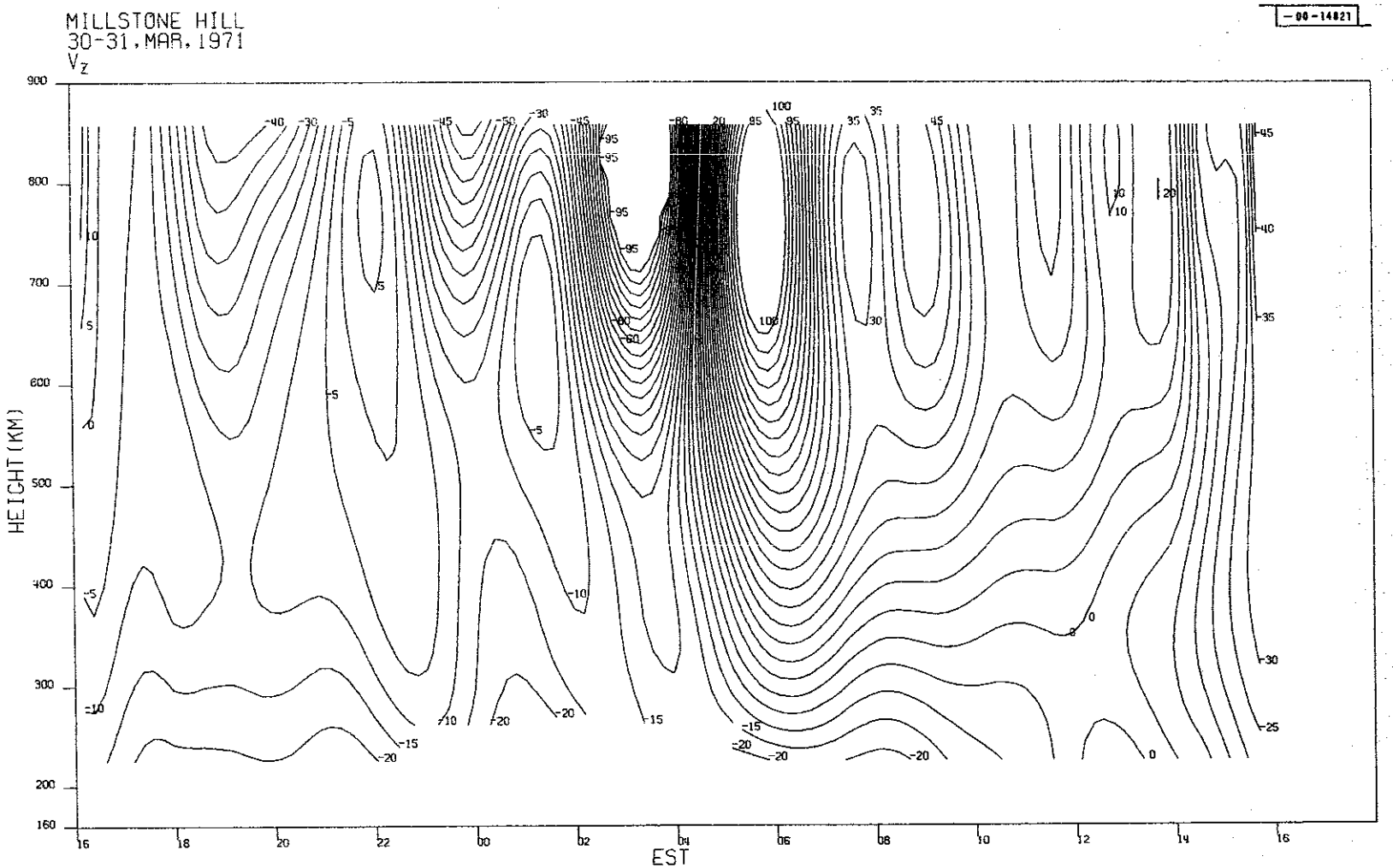

(d) V_z.

Fig. 11(a-d). Continued.

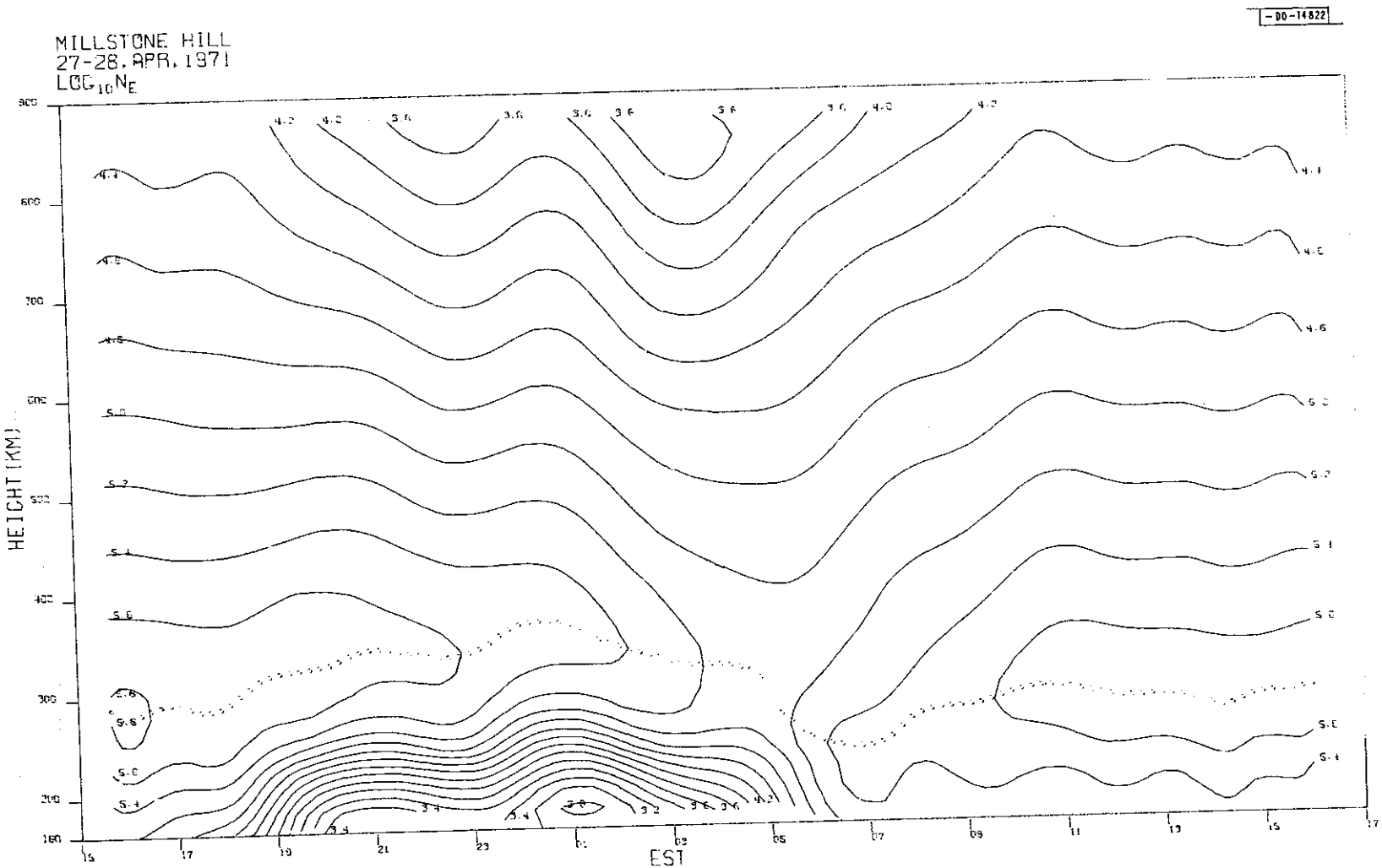

(a) $Log_{10} N_e$.

Fig. 12(a-d). Contours of density, temperature, and vertical velocity for 27-28 April 1971.

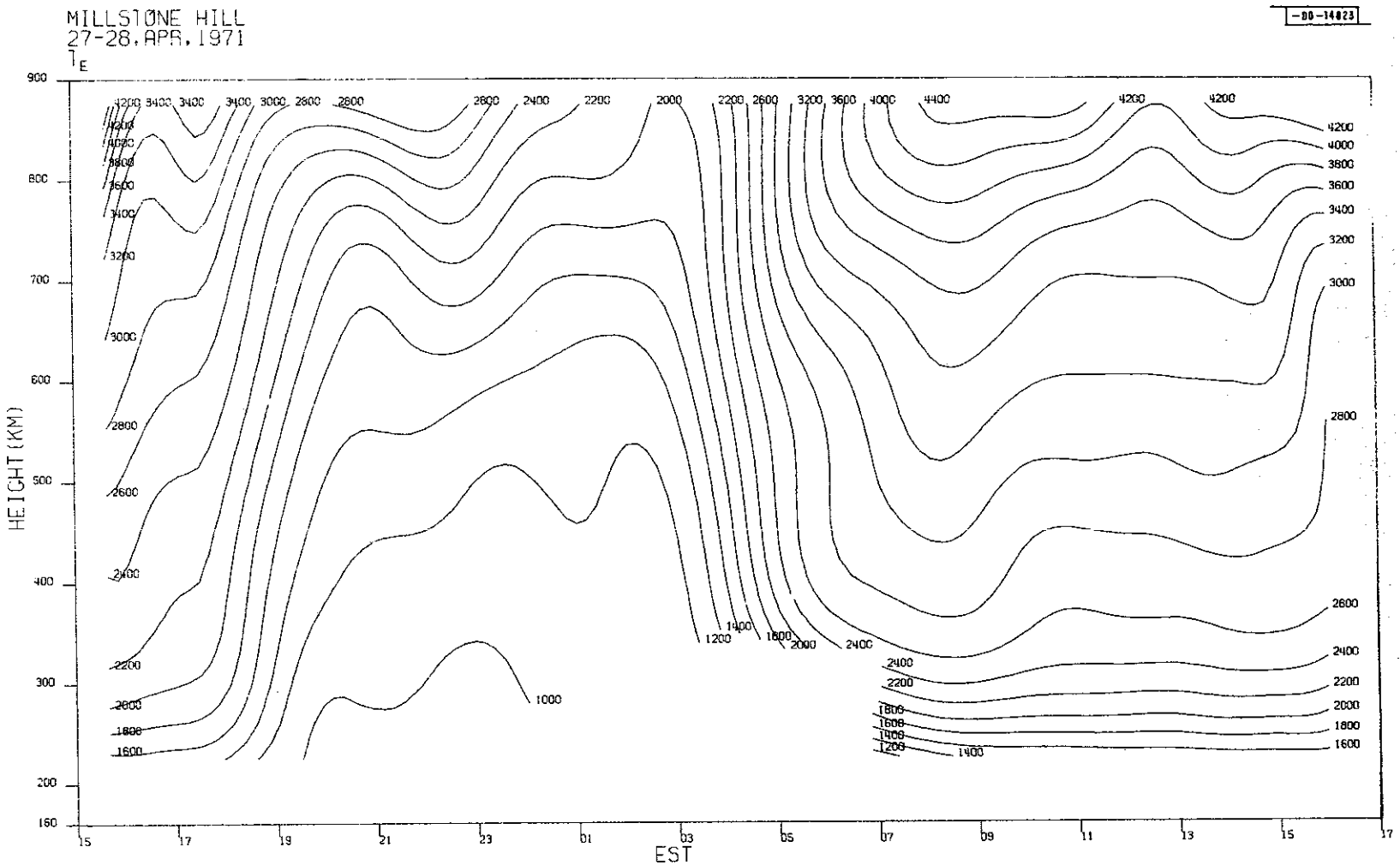

(b) T_e.

Fig. 12(a-d). Continued.

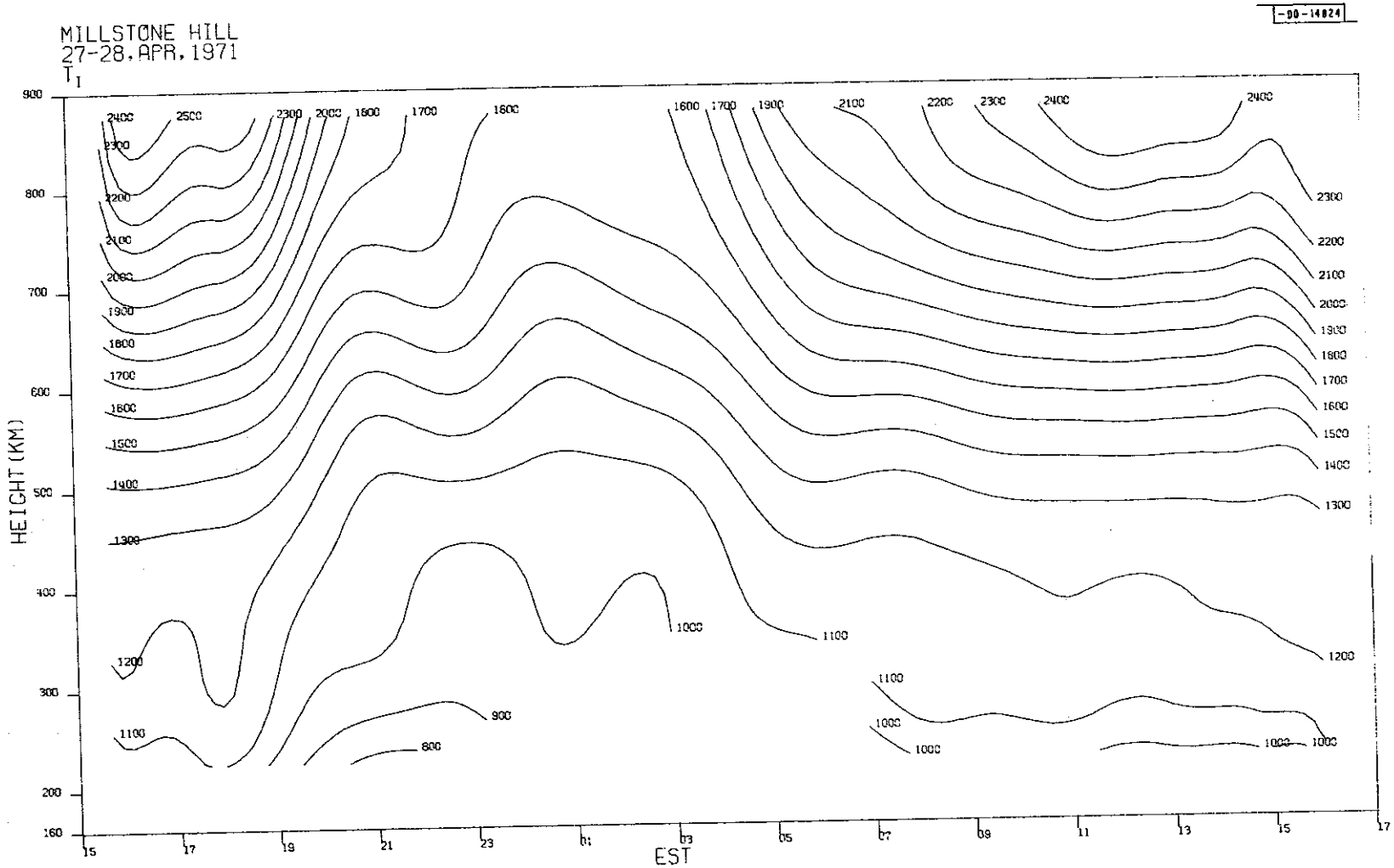

(c) T_i.

Fig. 12(a-d). Continued.

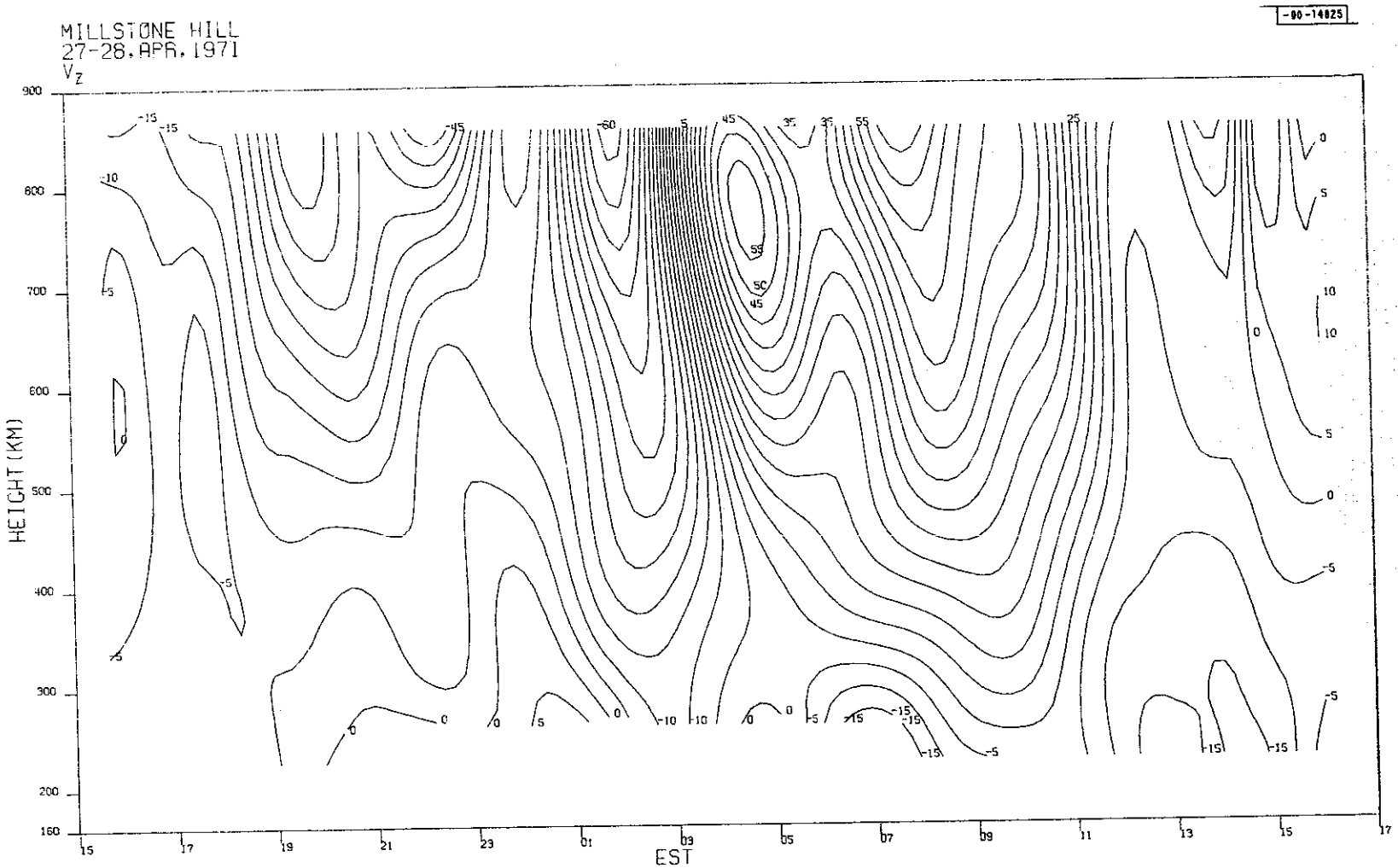

(d) V_z.

Fig. 12(a-d). Continued.

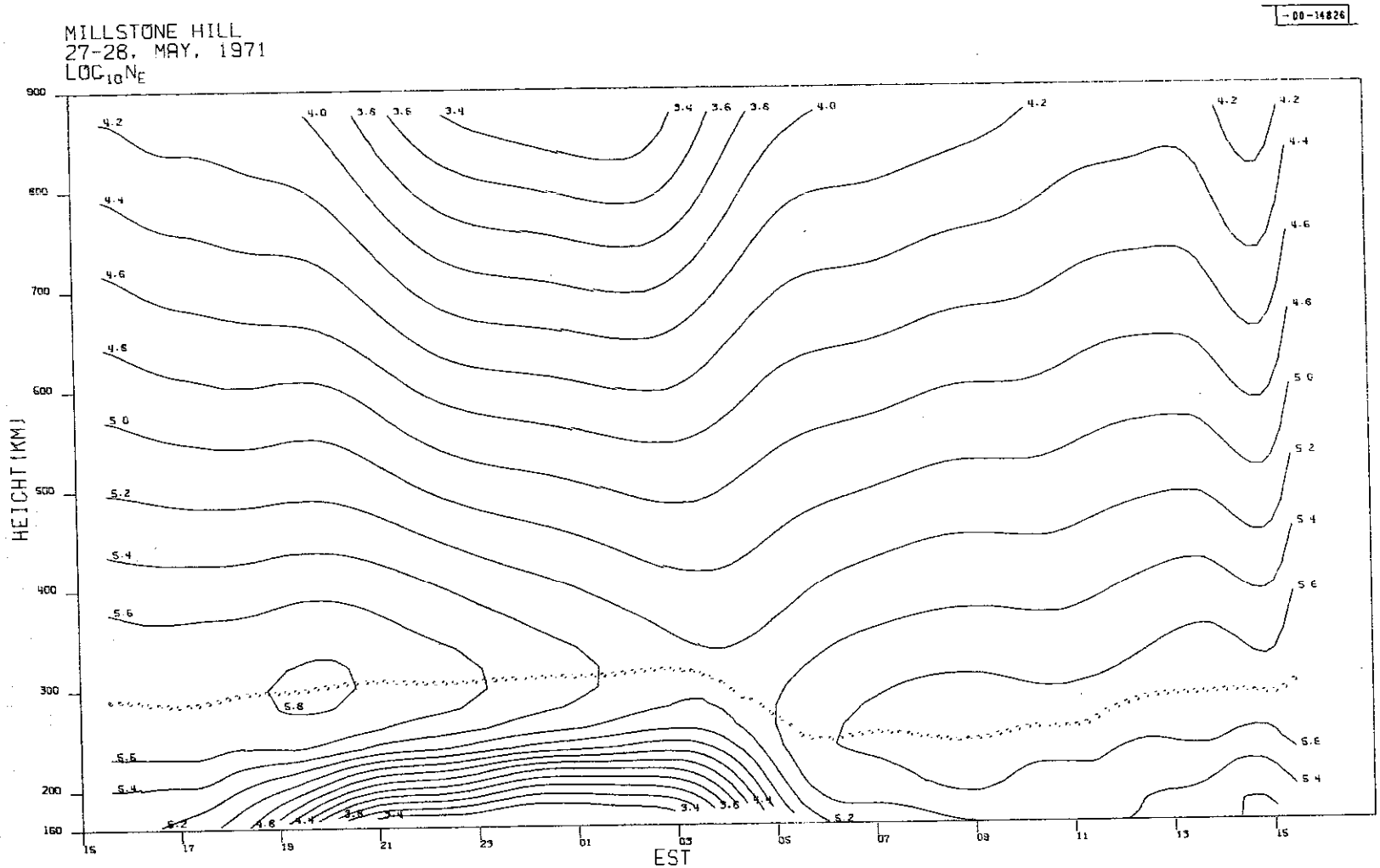

(a) $\text{Log}_{10} N_e$.

Fig. 13(a-d). Contours of density, temperature, and vertical velocity for 27-28 May 1971.

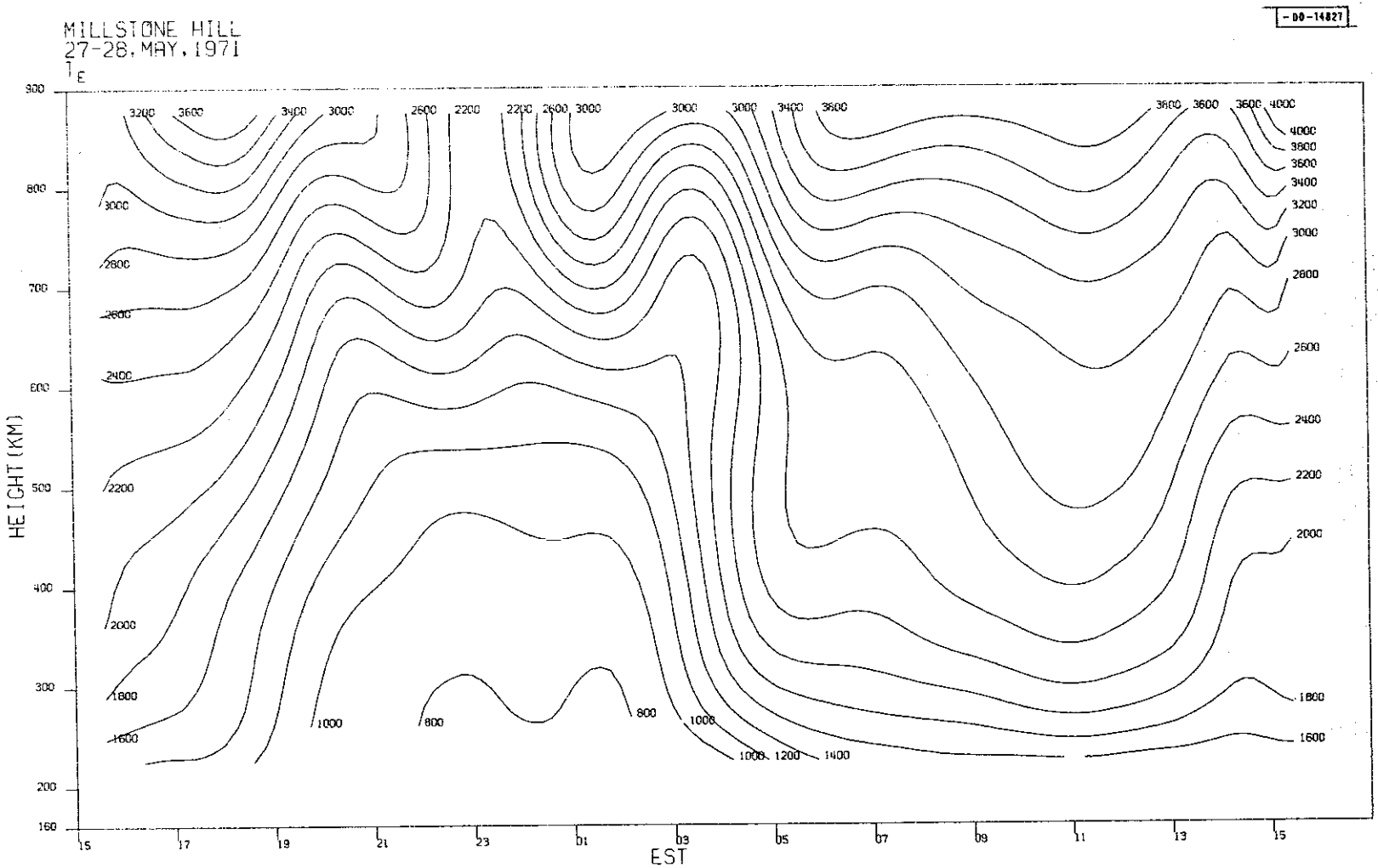

(b) T_e.

Fig. 13(a-d). Continued.

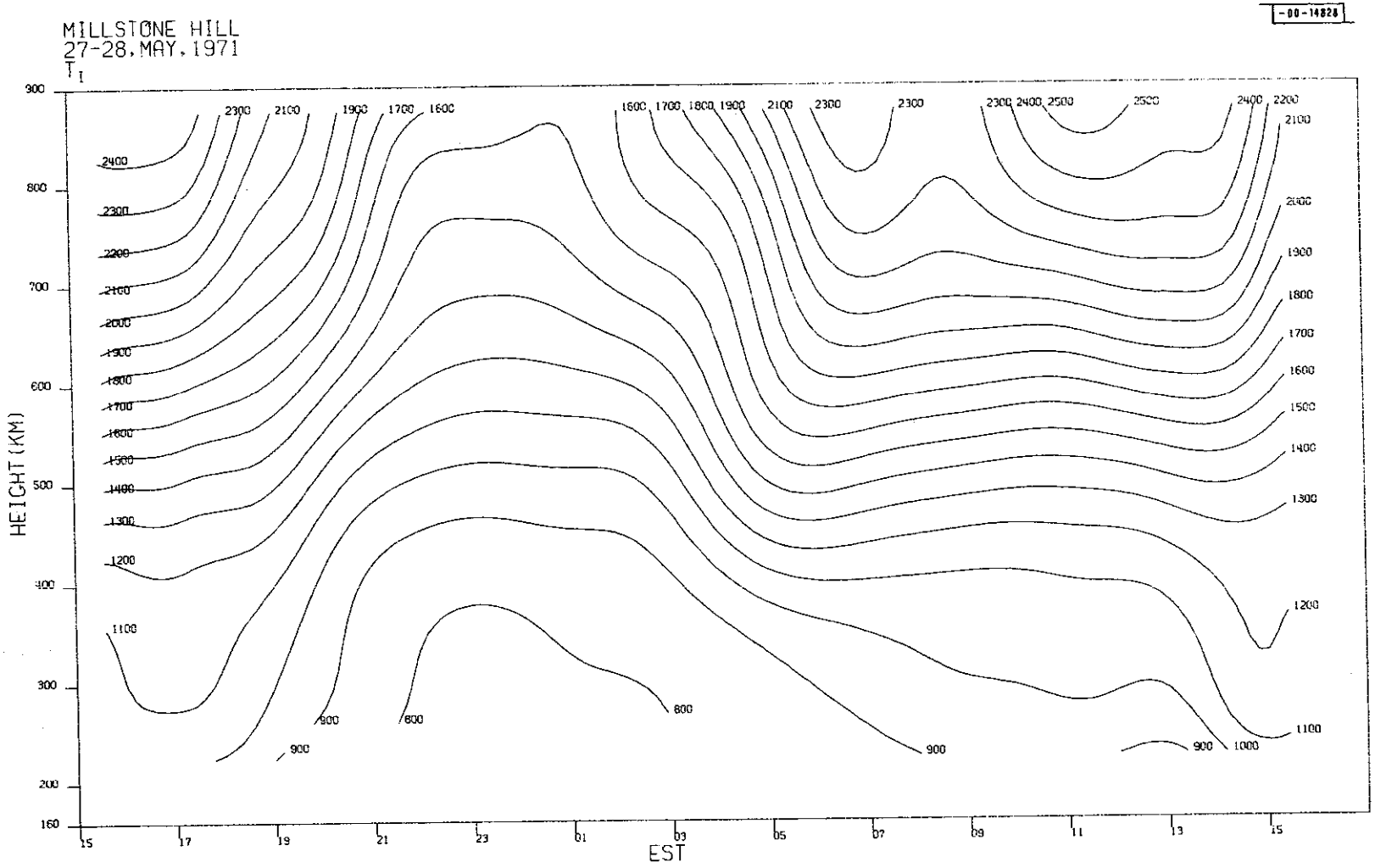

(c) T_i.

Fig. 13(a-d). Continued.

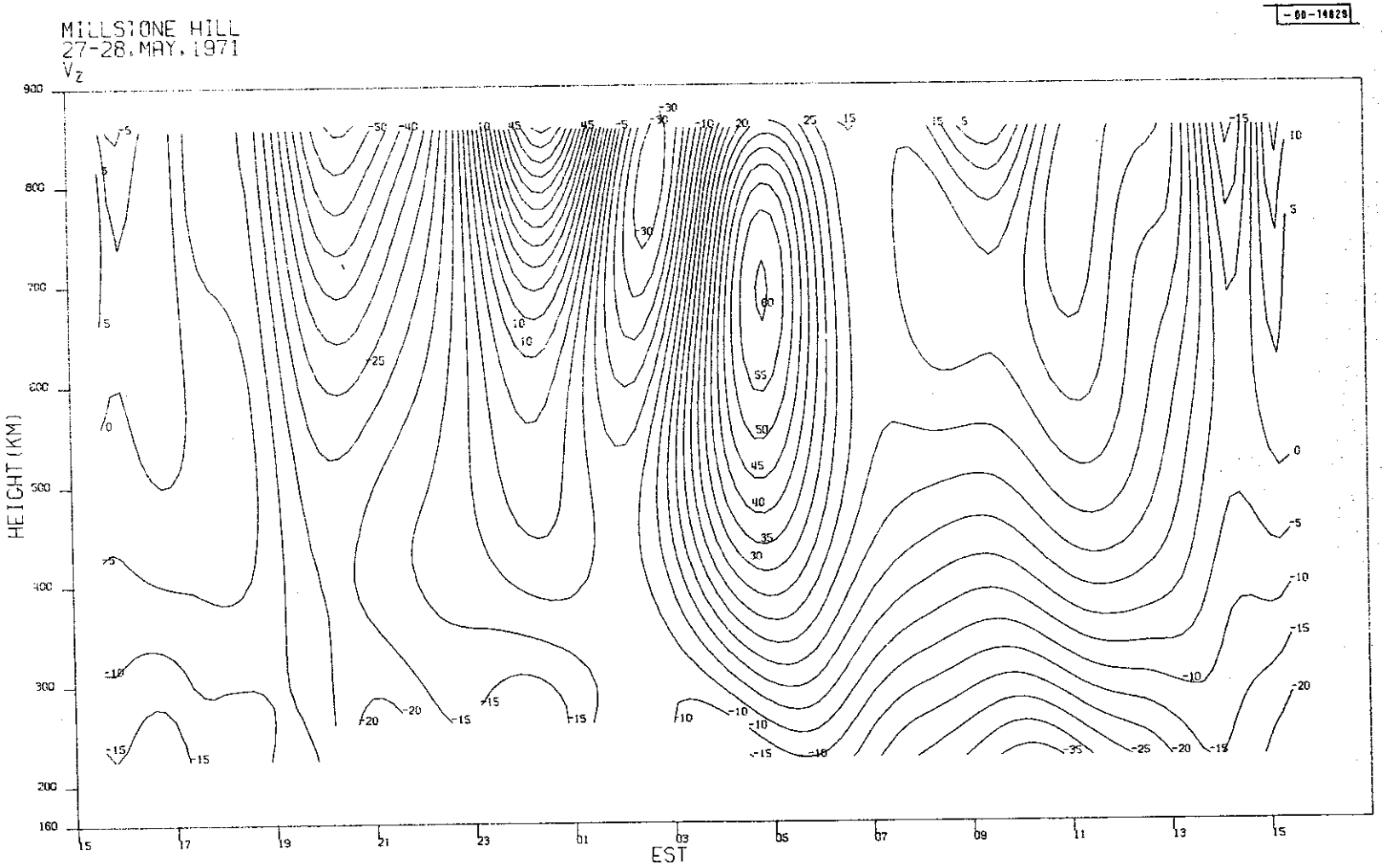

(d) V_z.

Fig. 13(a-d). Continued.

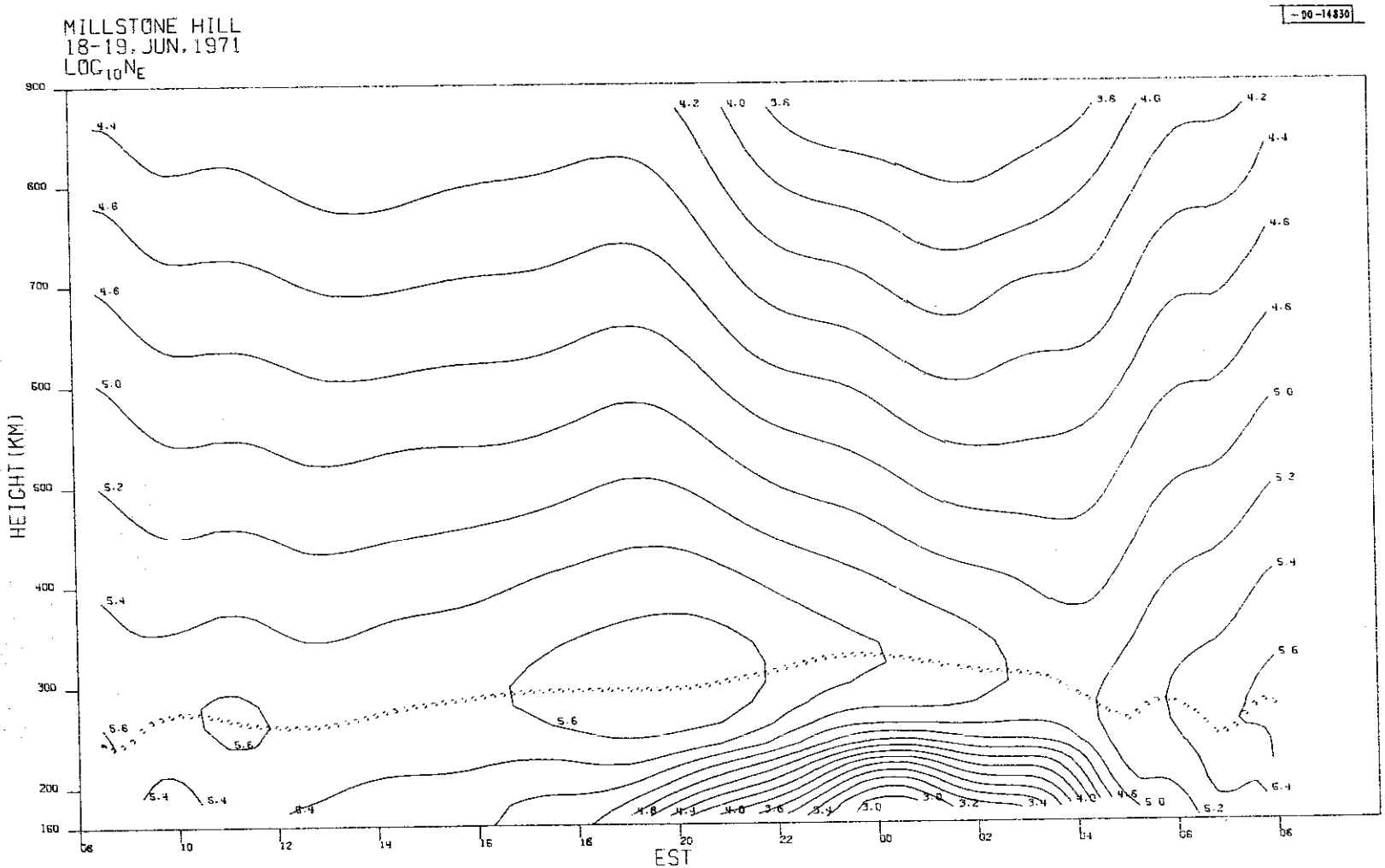

(a) $\text{Log}_{10} N_e$.

Fig. 14(a-d). Contours of density, temperature, and vertical velocity for 18-19 June 1971.

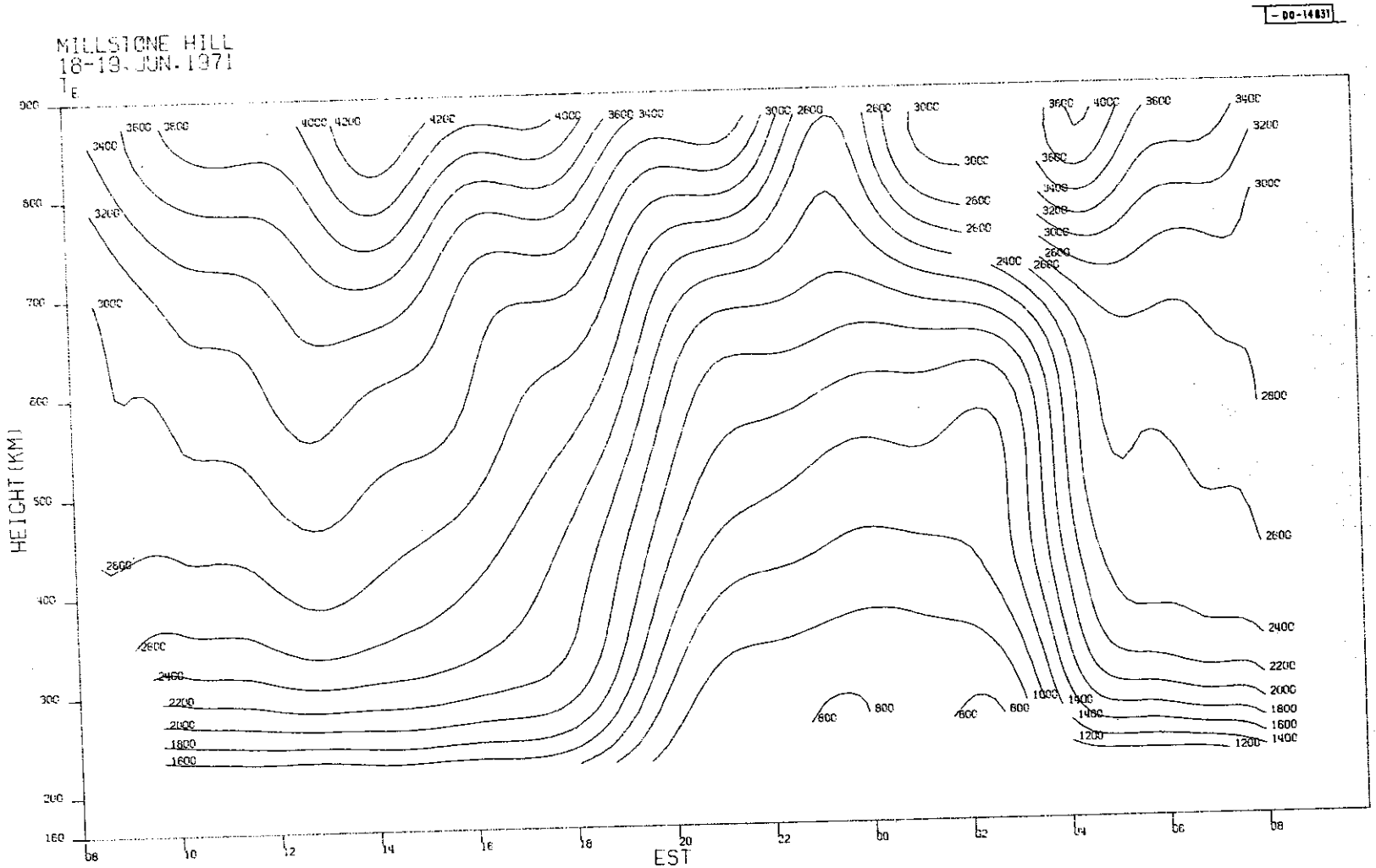

(b) T_e.

Fig. 14(a-d). Continued.

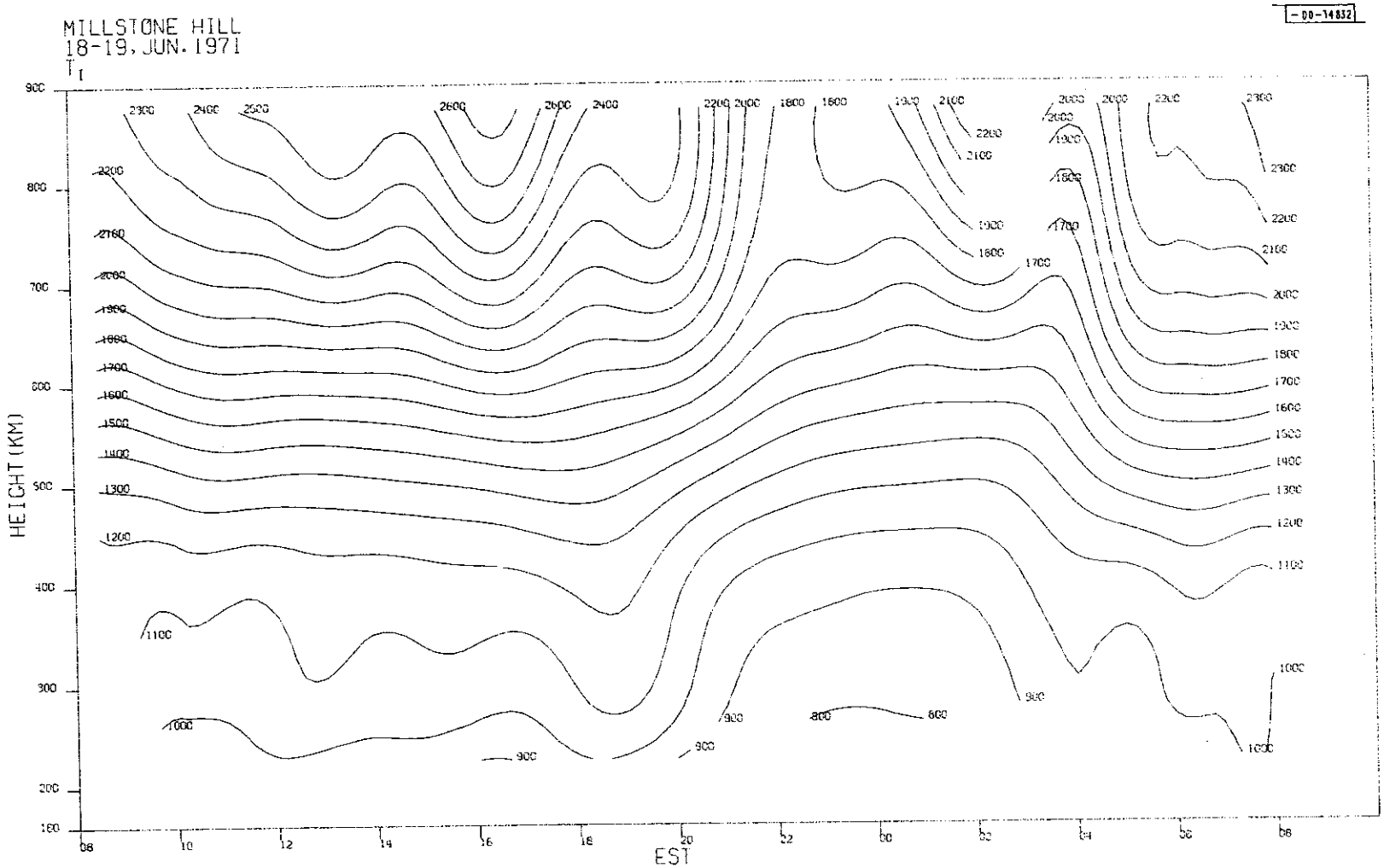

(c) T_i.

Fig. 14(a-d). Continued.

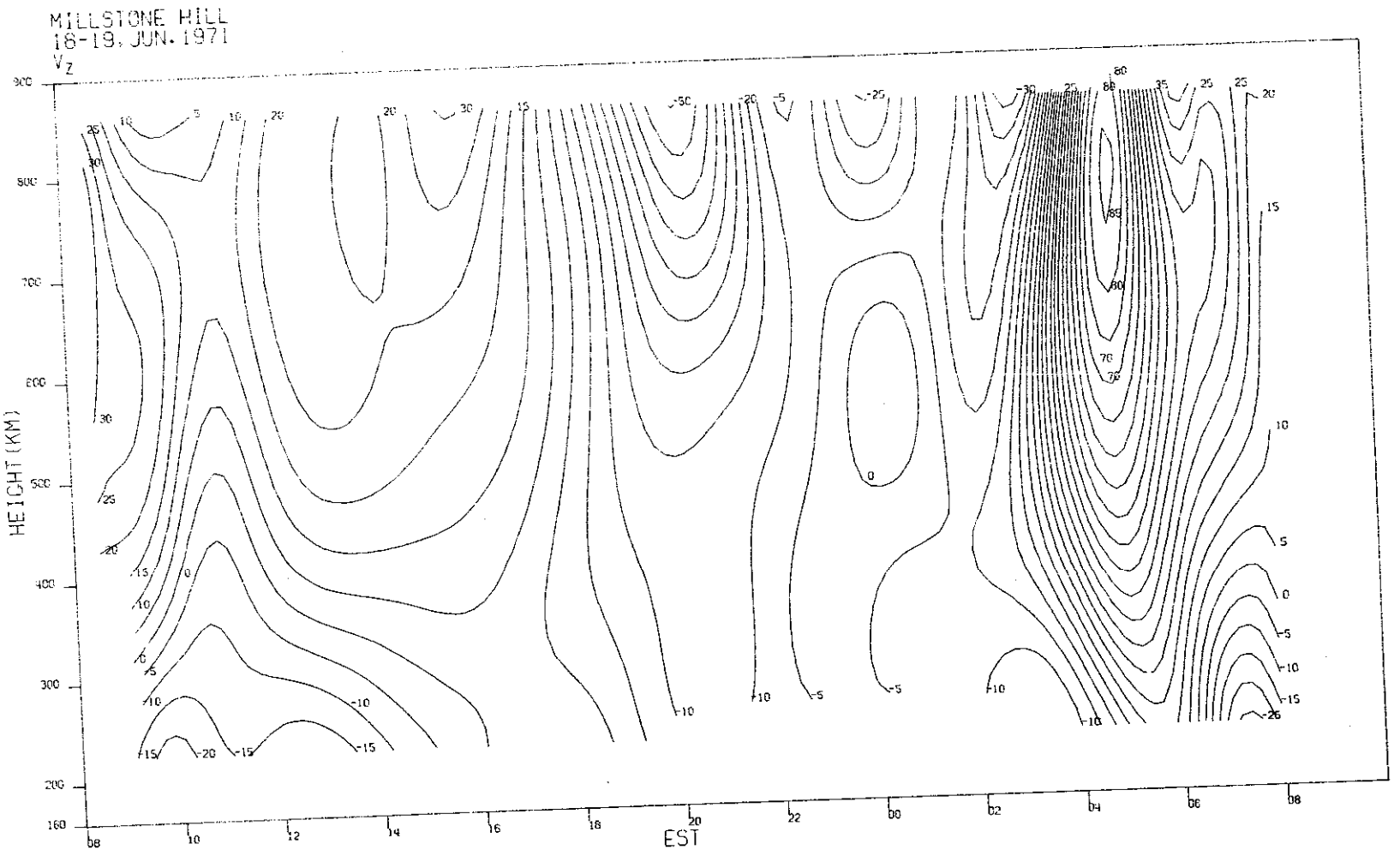

(d) V_z.

Fig. 14(a-d). Continued.

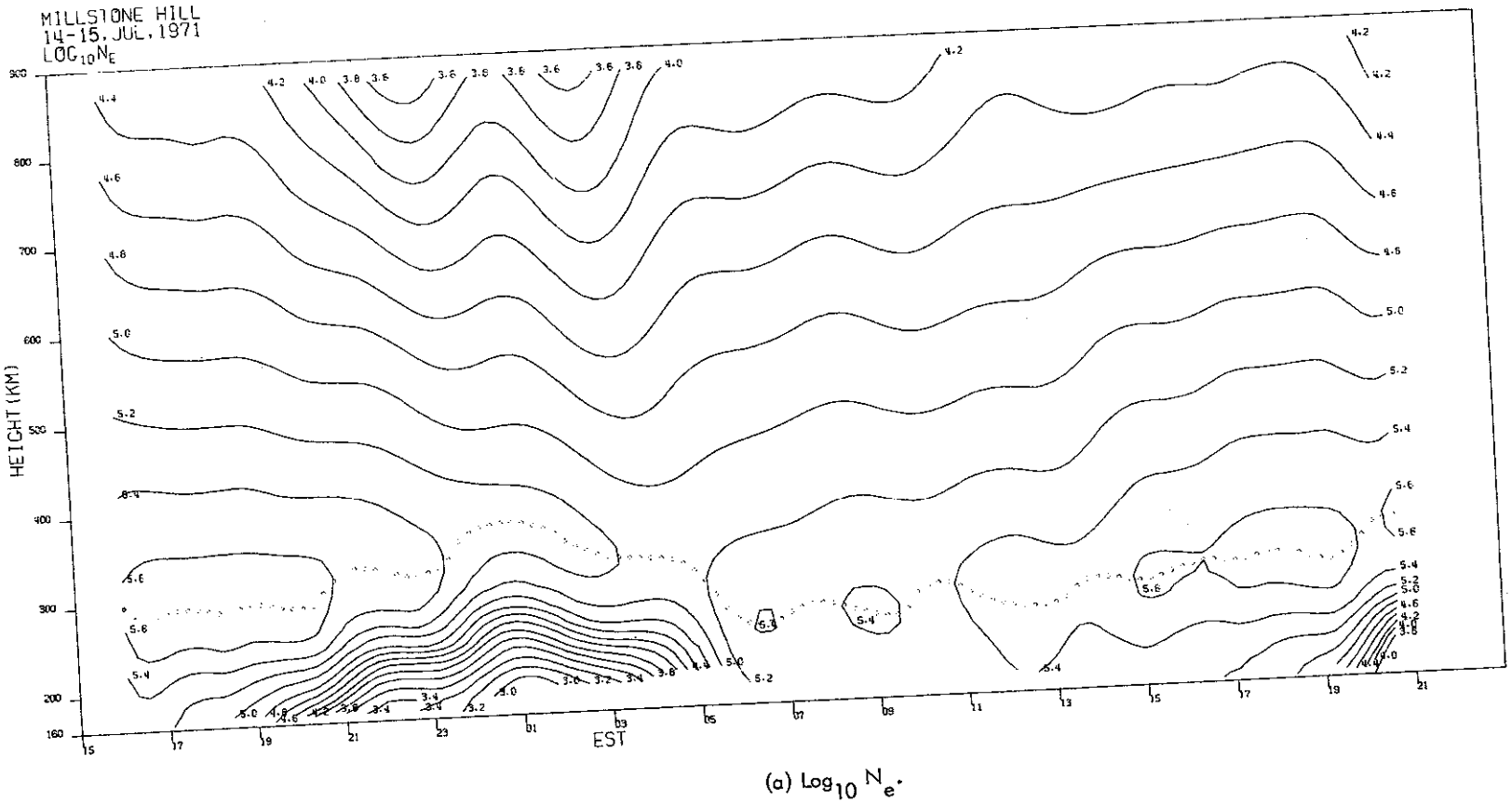

(a) $\text{Log}_{10} N_e$.

Fig. 15(a-d). Contours of density, temperature, and vertical velocity for 14-15 July 1971.

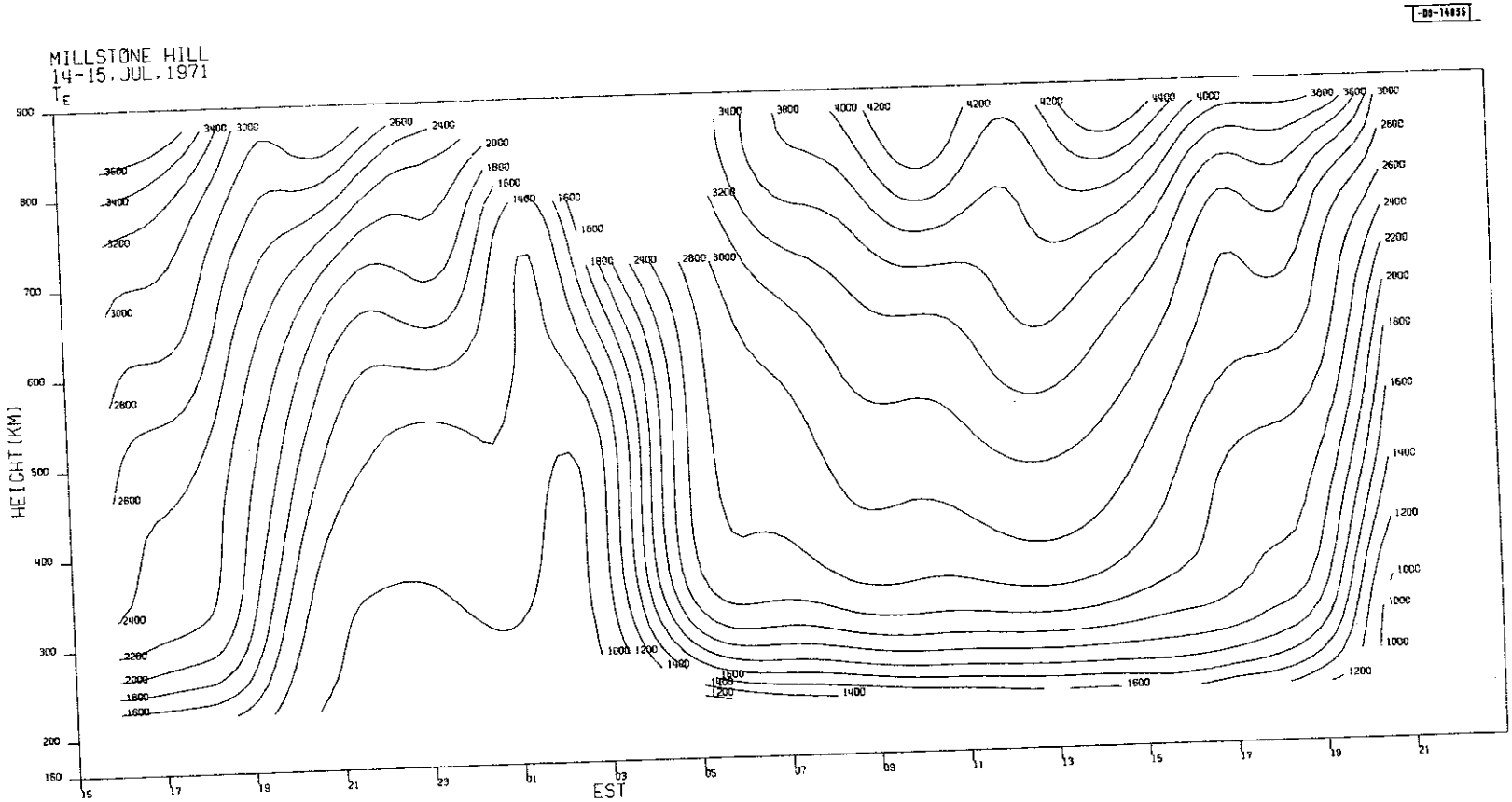

(b) T_e.

Fig. 15(a-d). Continued.

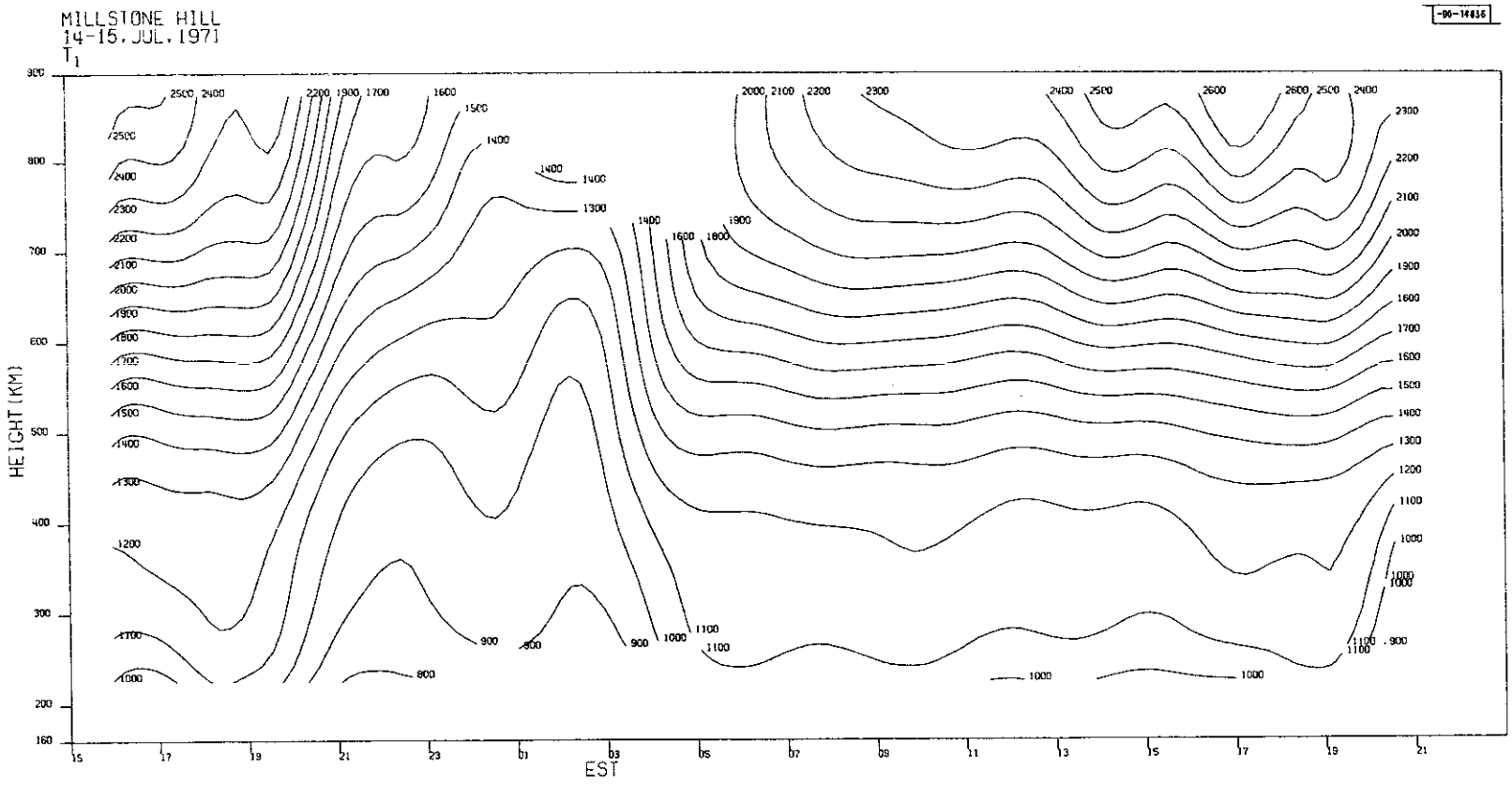

(c) T_i.

Fig. 15(a-d). Continued.

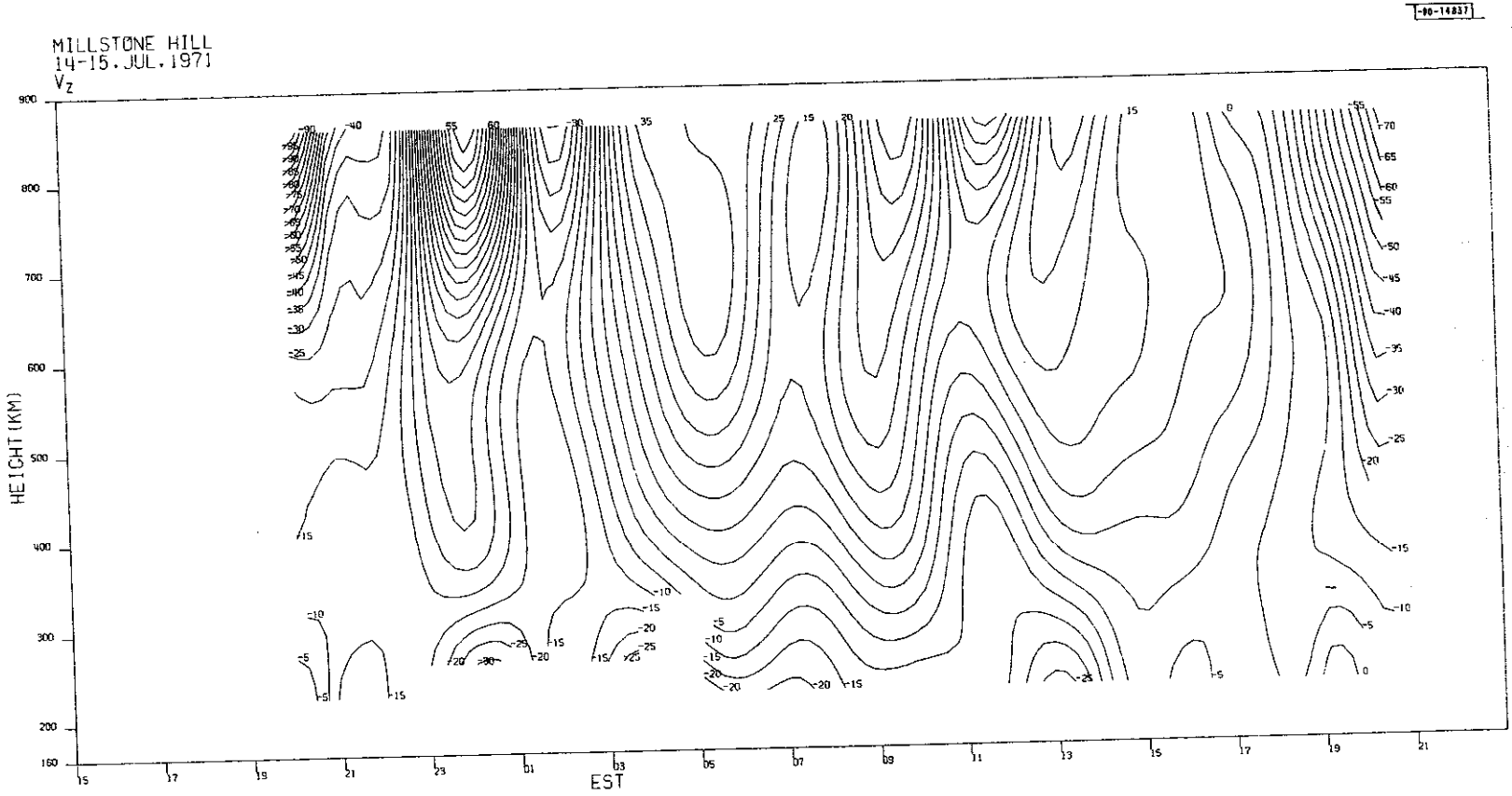

(d) V_z.

Fig. 15(a-d). Continued.

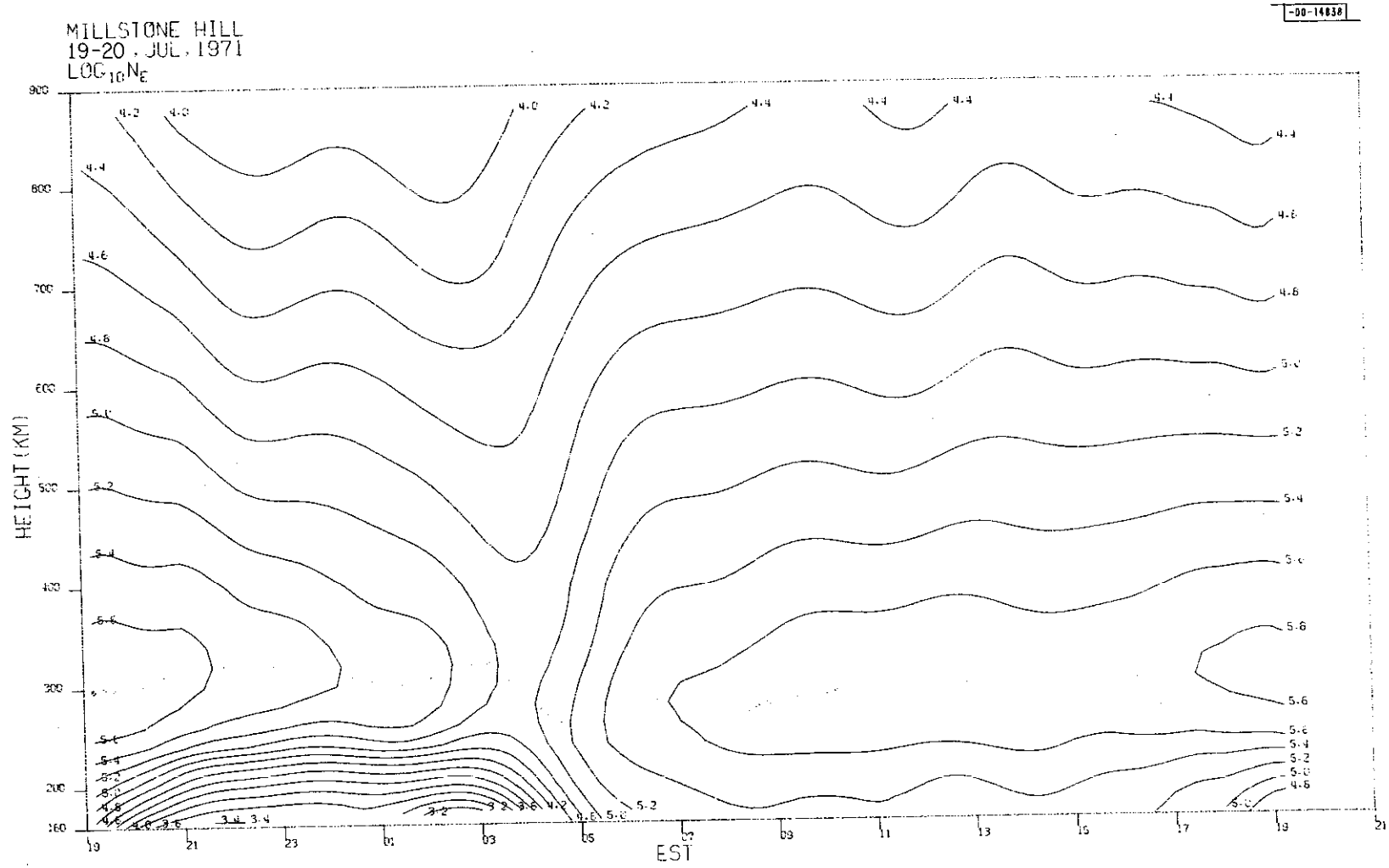

(a) $\text{Log}_{10} N_e$.

Fig. 16(a-d). Contours of density, temperature, and vertical velocity for 19-20 July 1971.

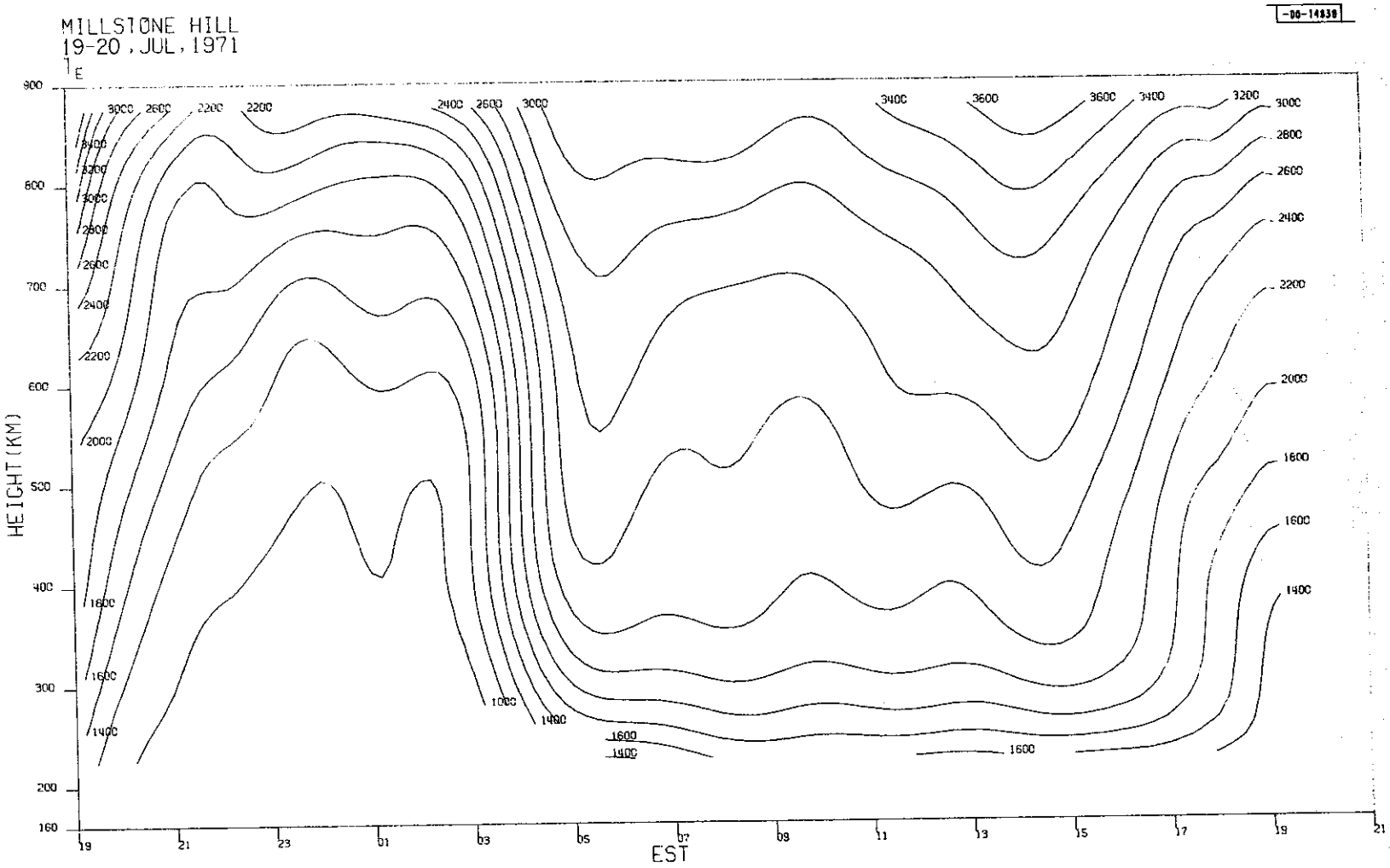

(b) T_e.

Fig. 16(a-d). Continued.

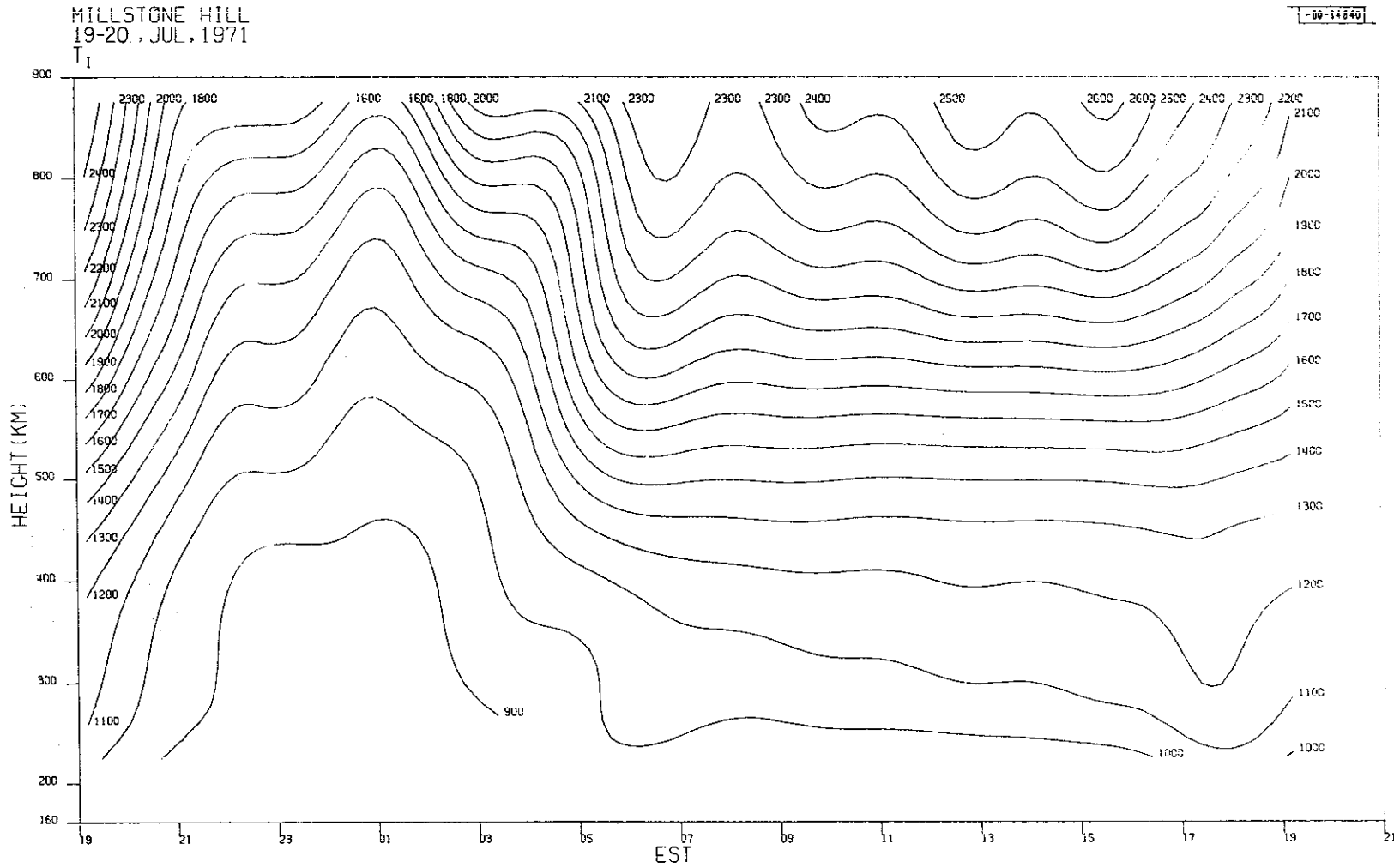

(c) T_i.

Fig. 16(a-d). Continued.

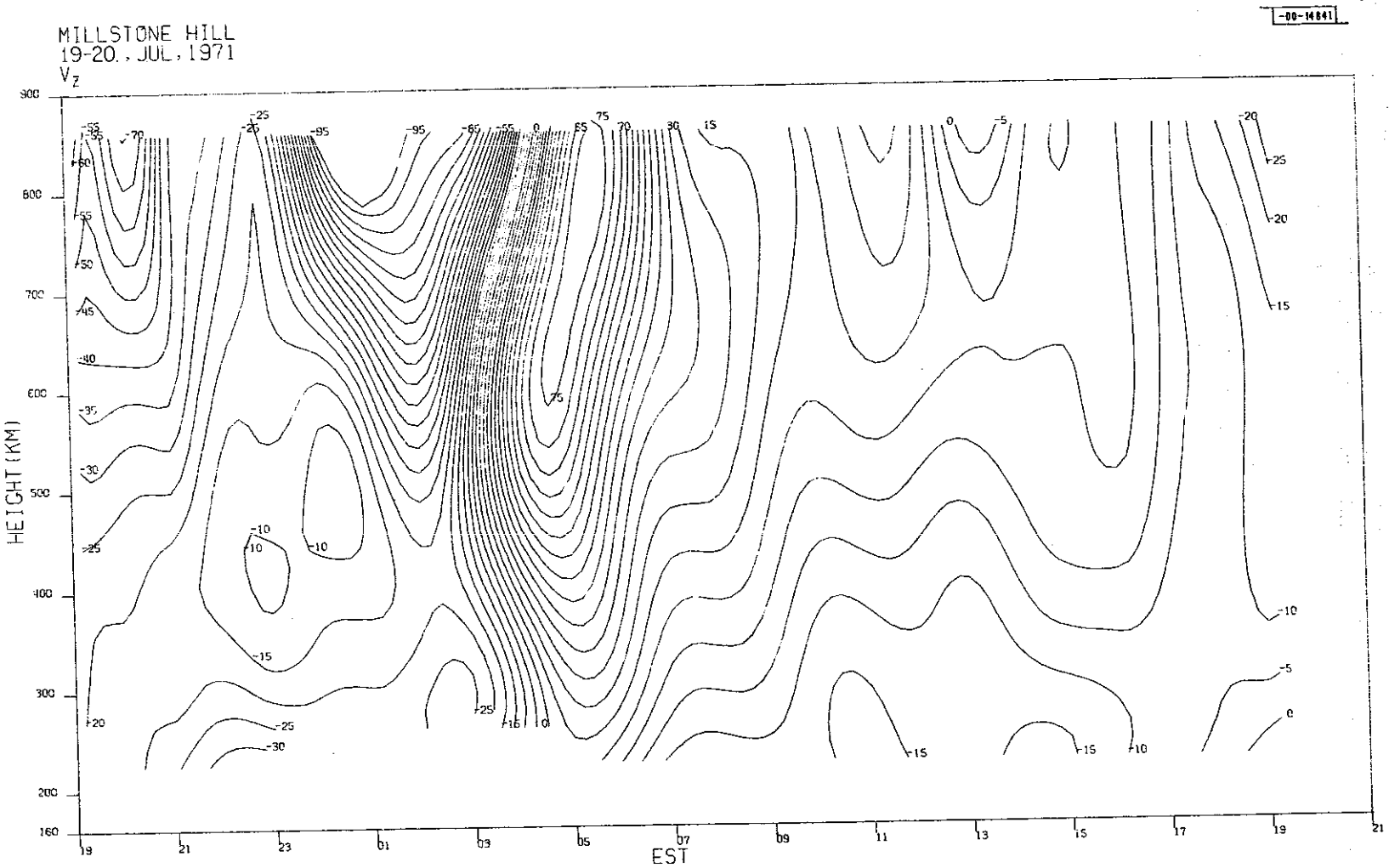

(d) V_z.

Fig. 16(a-d). Continued.

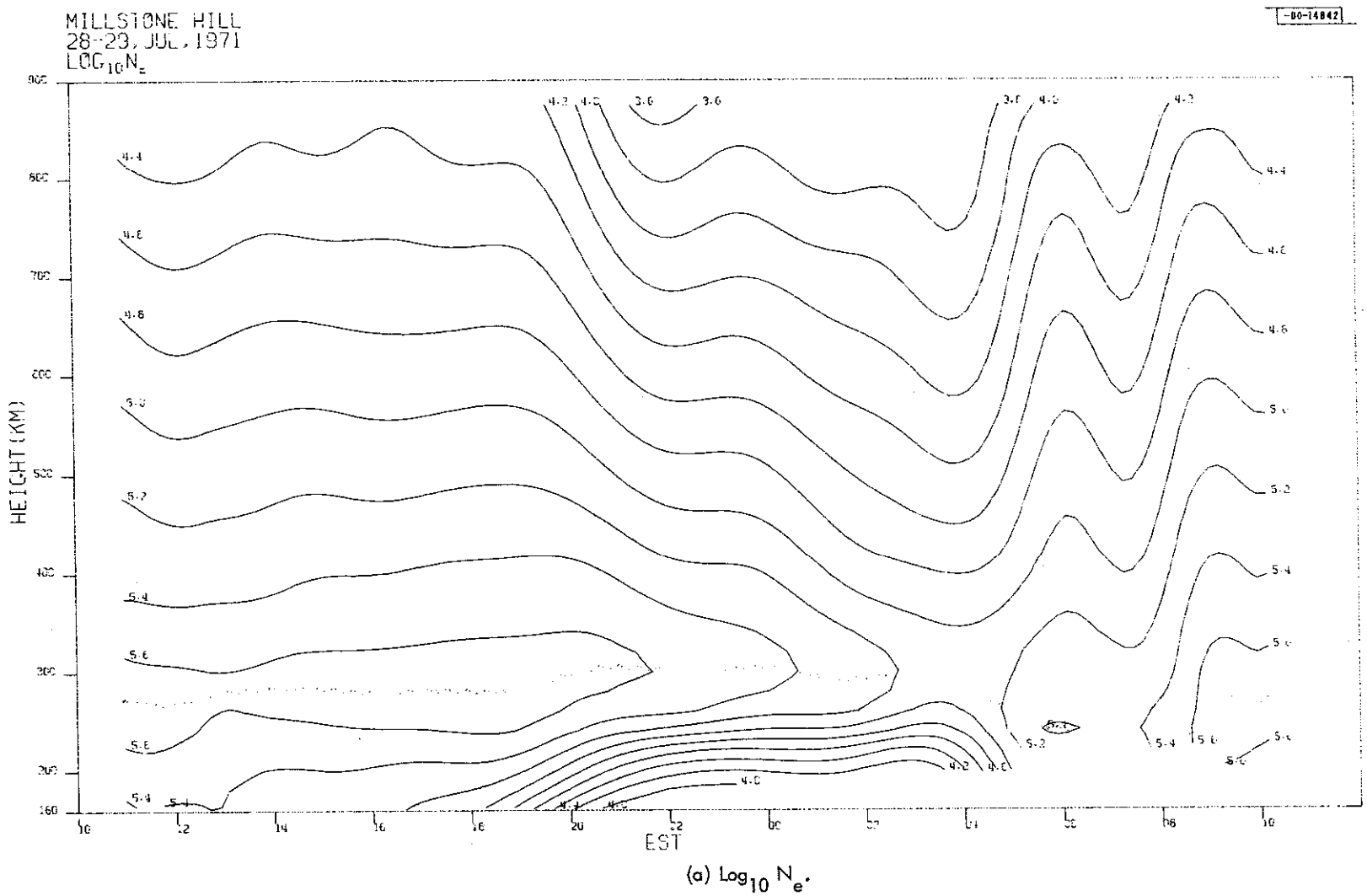

(a) $\text{Log}_{10} N_e$.

Fig. 17(a-d). Contours of density, temperature, and vertical velocity for 28-29 July 1971.

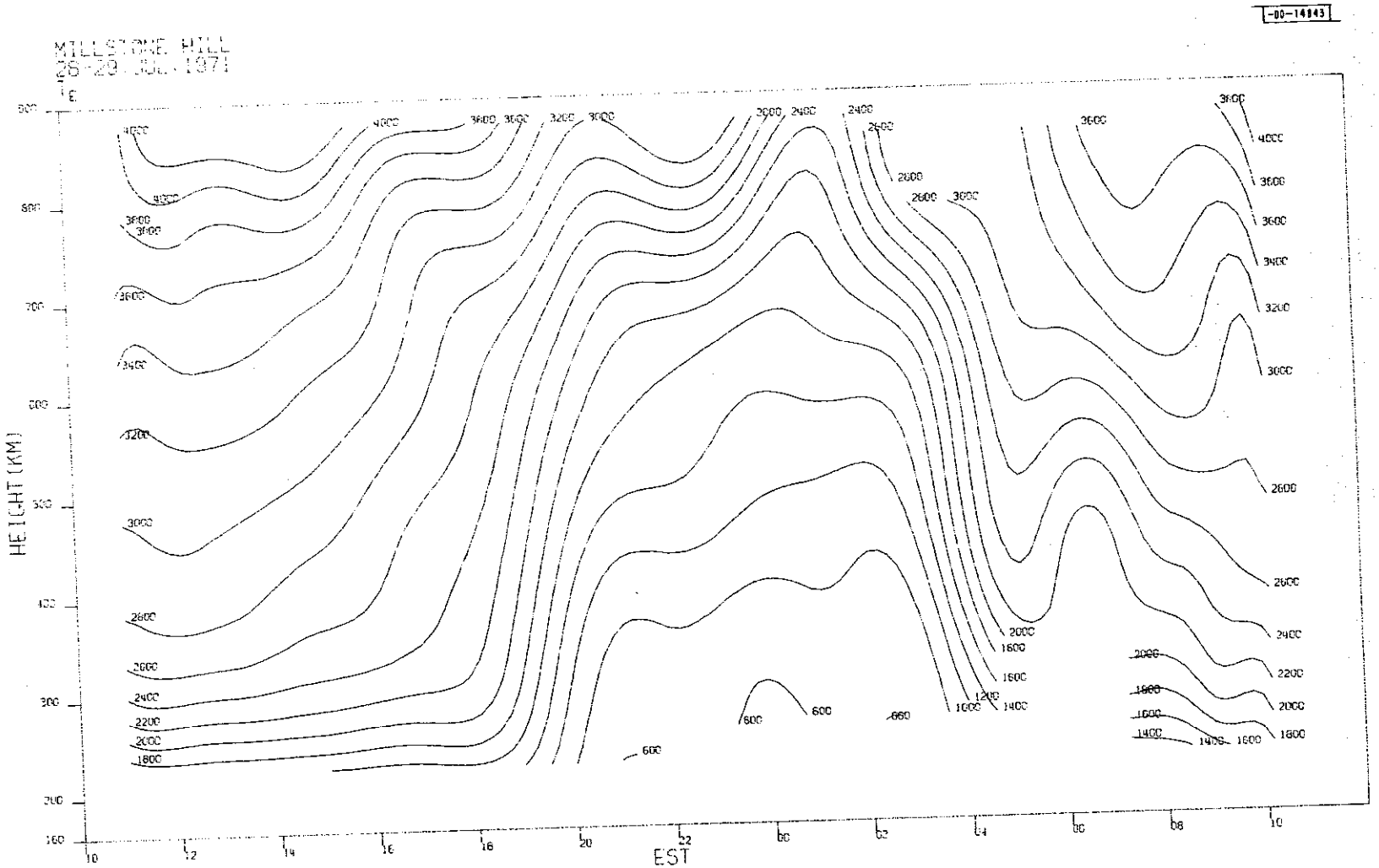

(b) T_e.

Fig. 17(a-d). Continued.

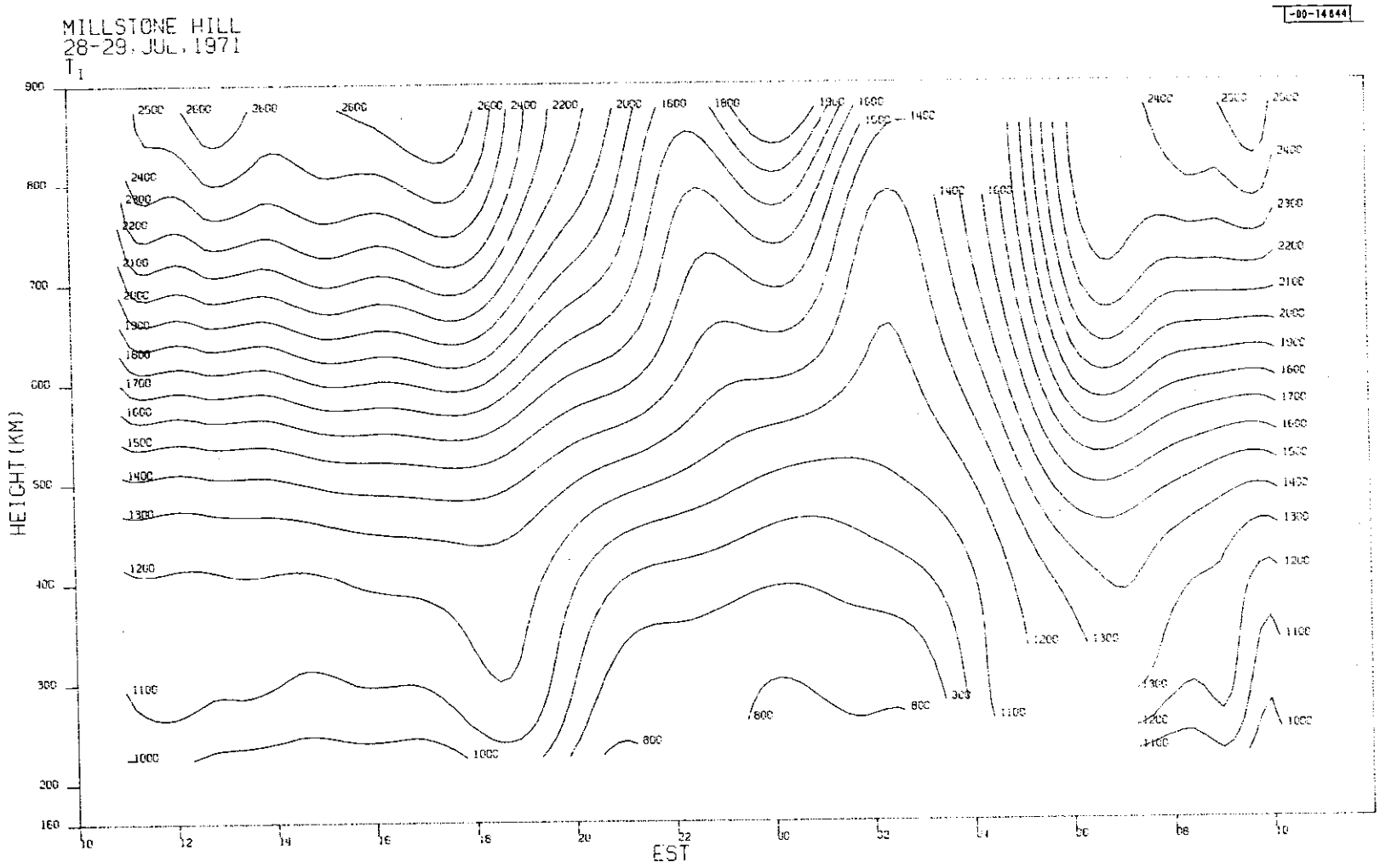

(c) T_i.

Fig. 17(a-d). Continued.

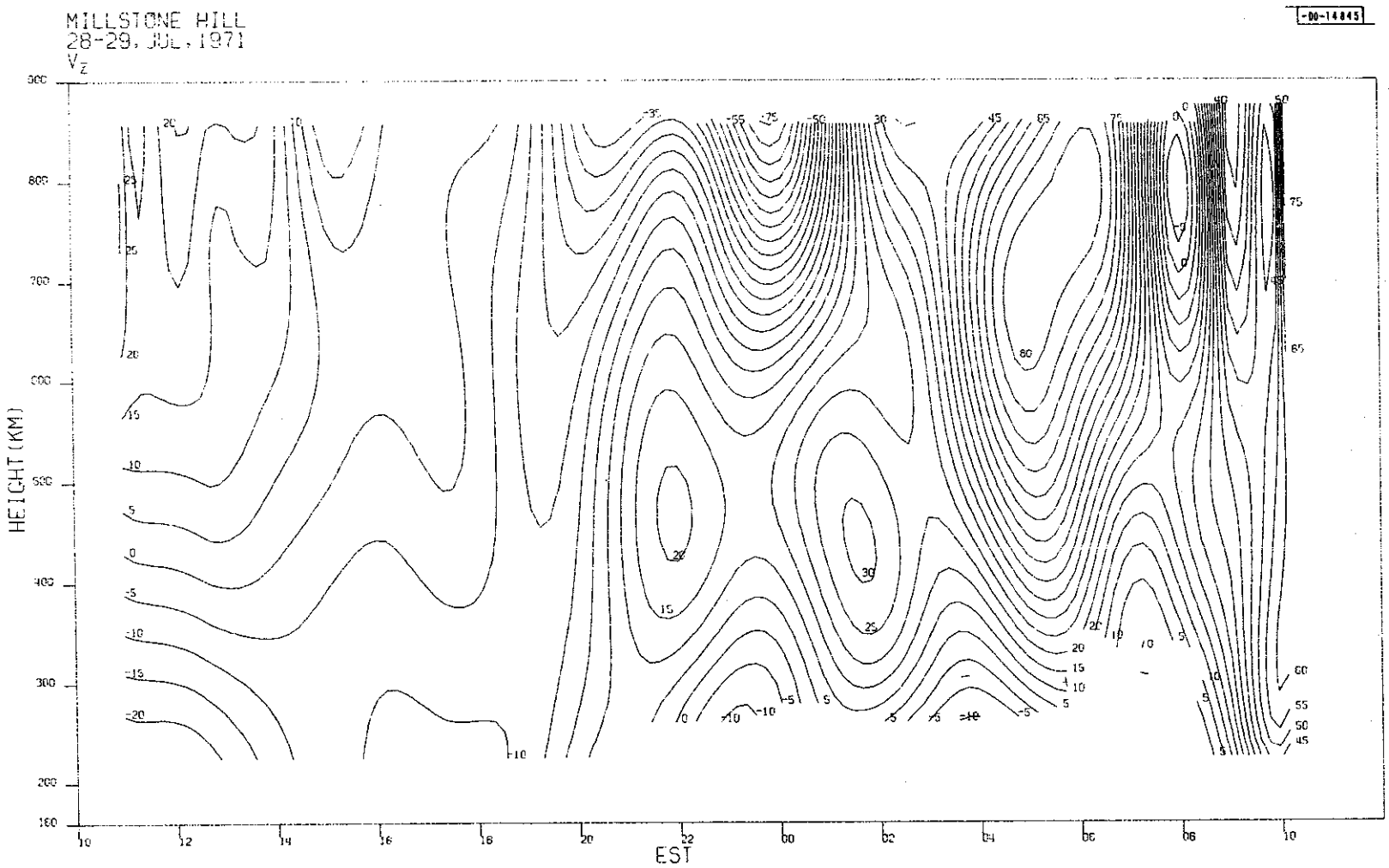

(d) V_z.

Fig. 17(a-d). Continued.

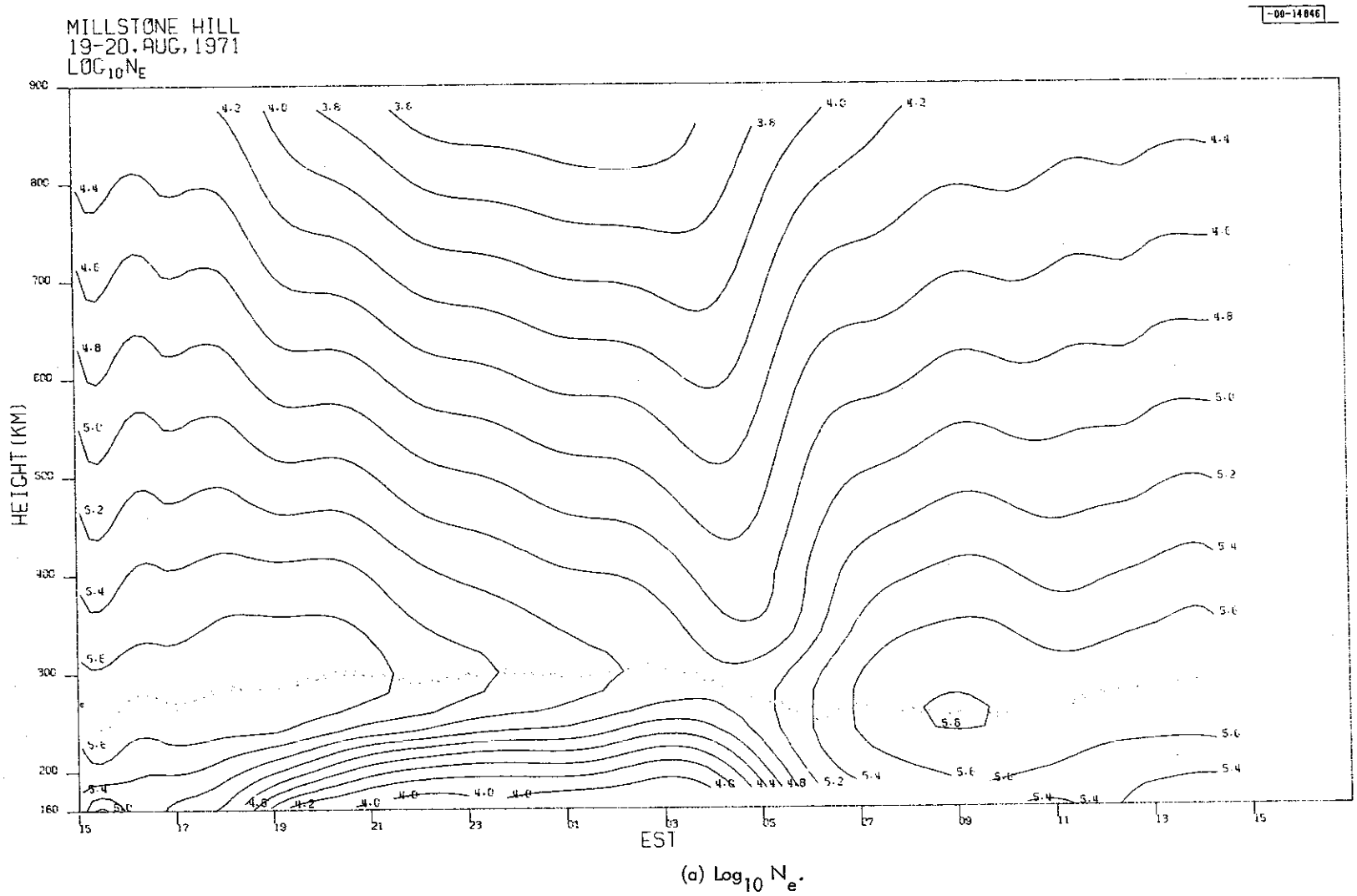

(a) $\text{Log}_{10} N_e$.

Fig. 18(a-d). Contours of density, temperature, and vertical velocity for 19-20 August 1971.

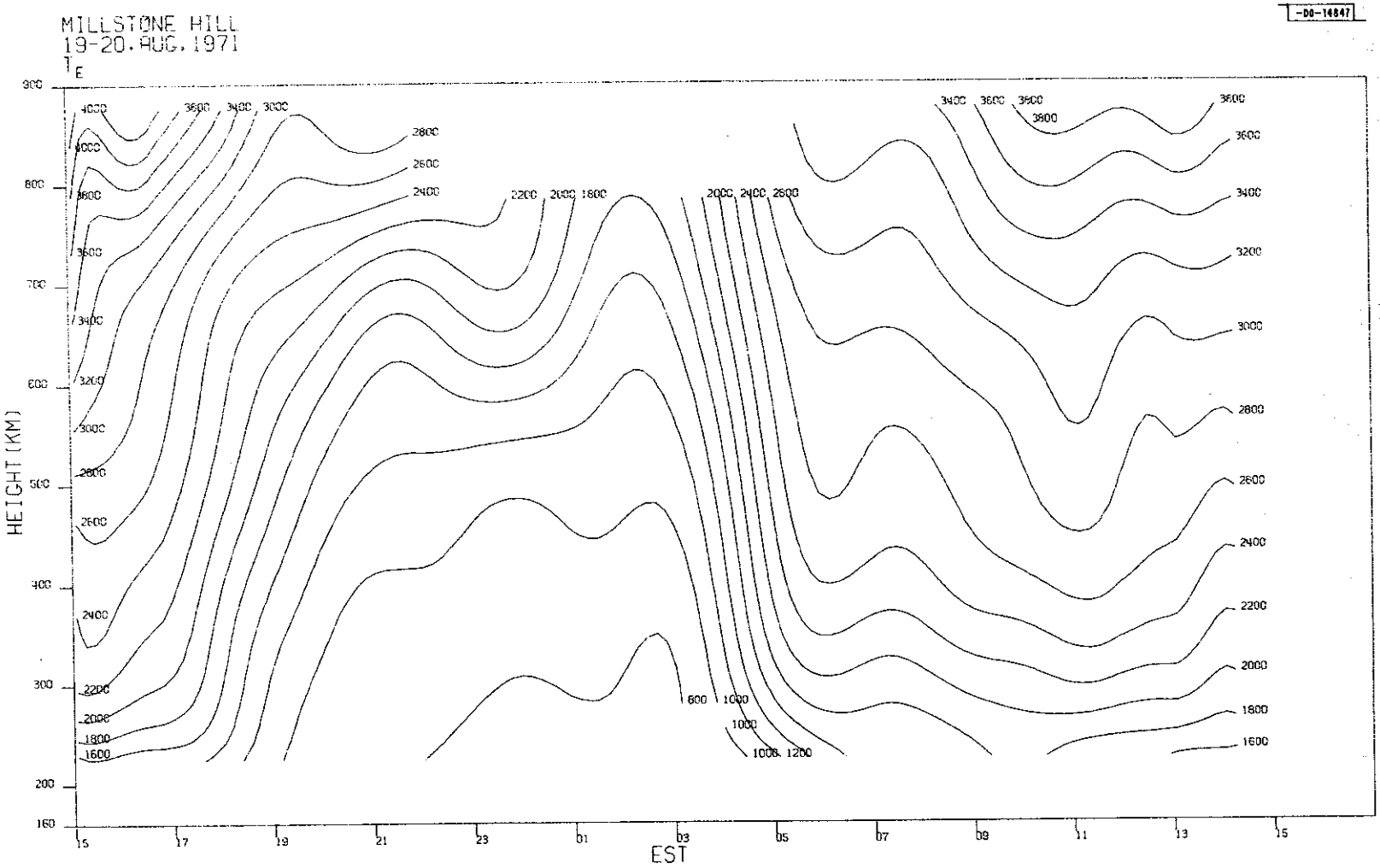

(b) T_e.

Fig. 18(a-d). Continued.

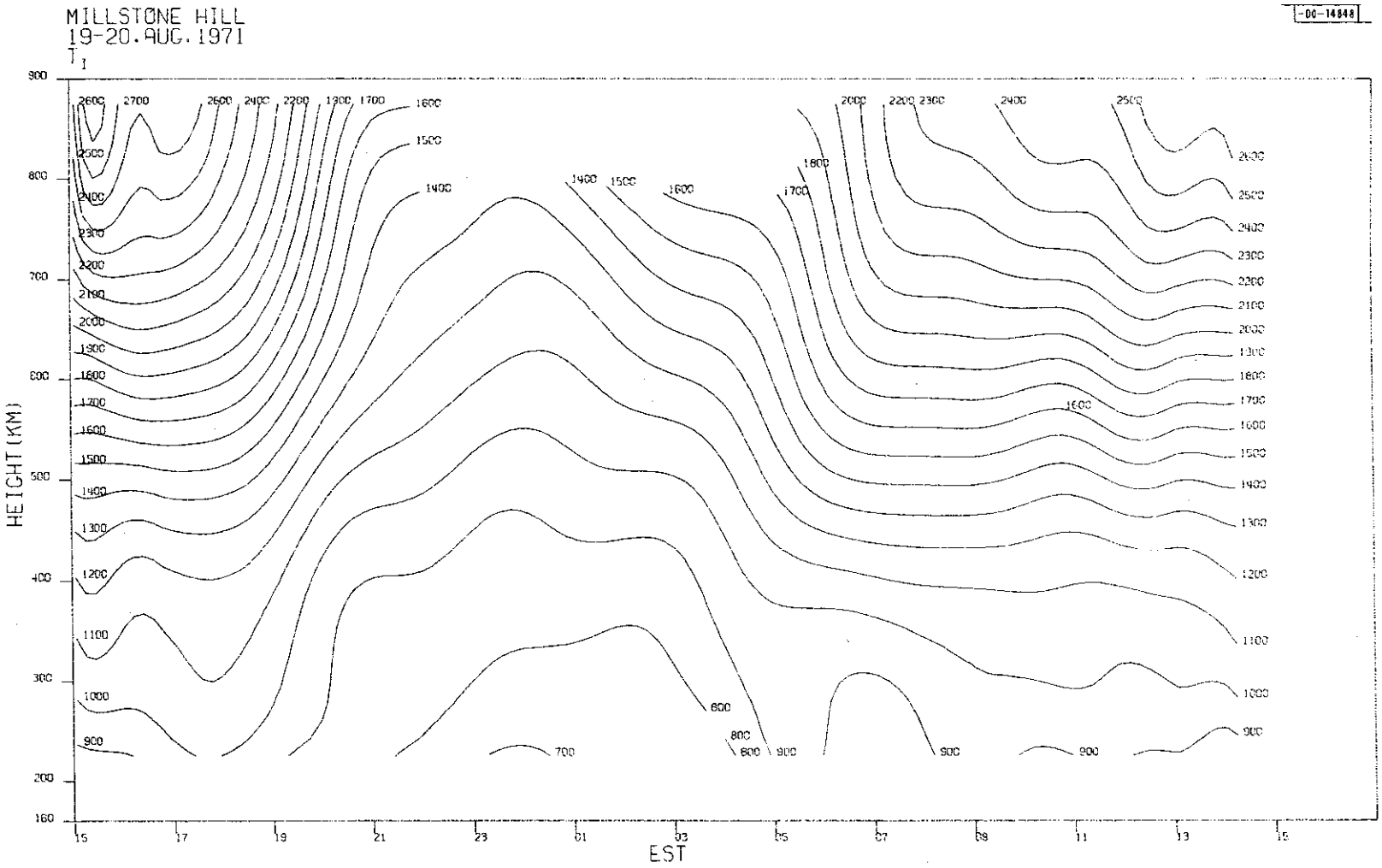

(c) T_i.

Fig. 18(a-d). Continued.

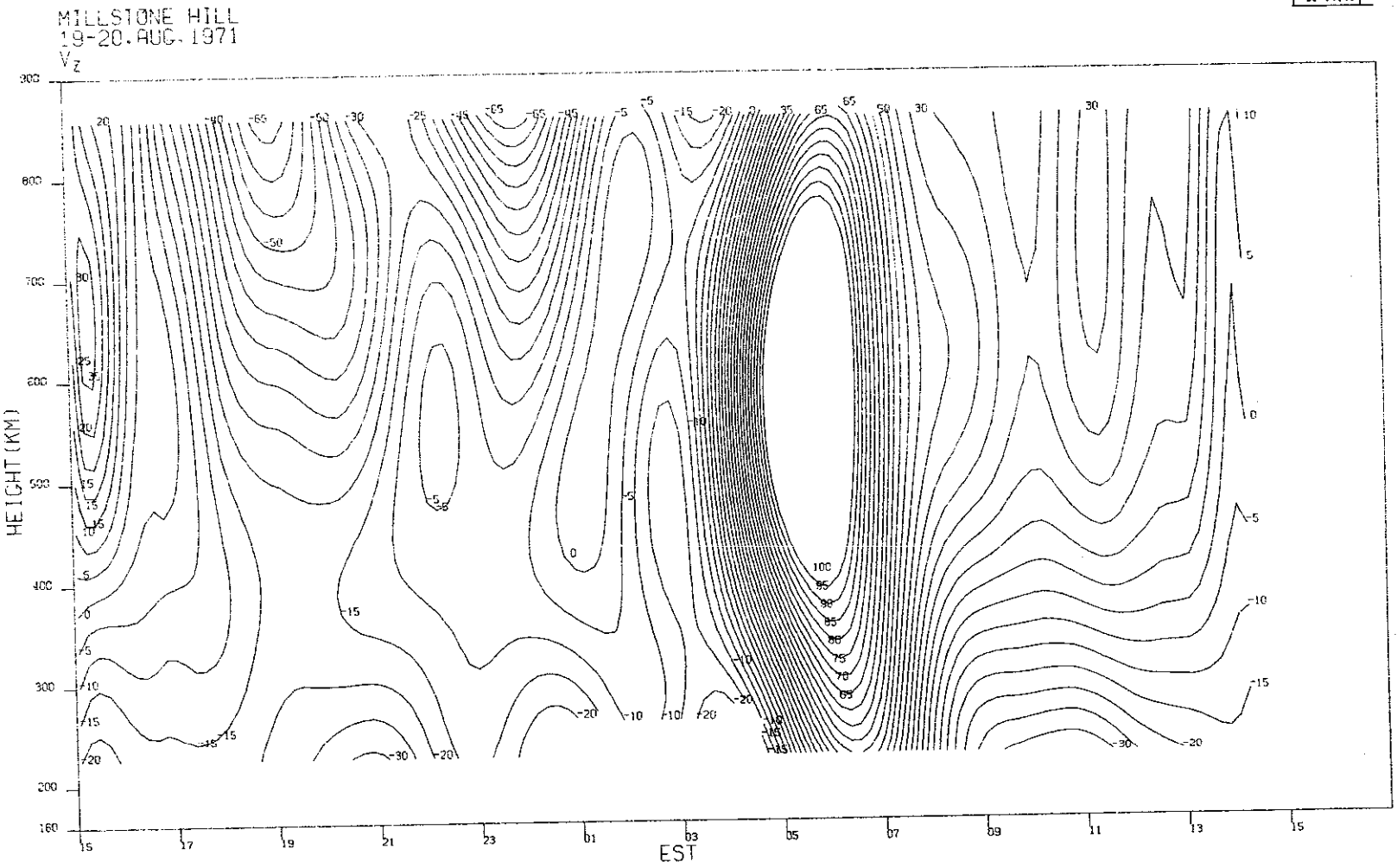

(d) V_z.

Fig. 18(a-d). Continued.

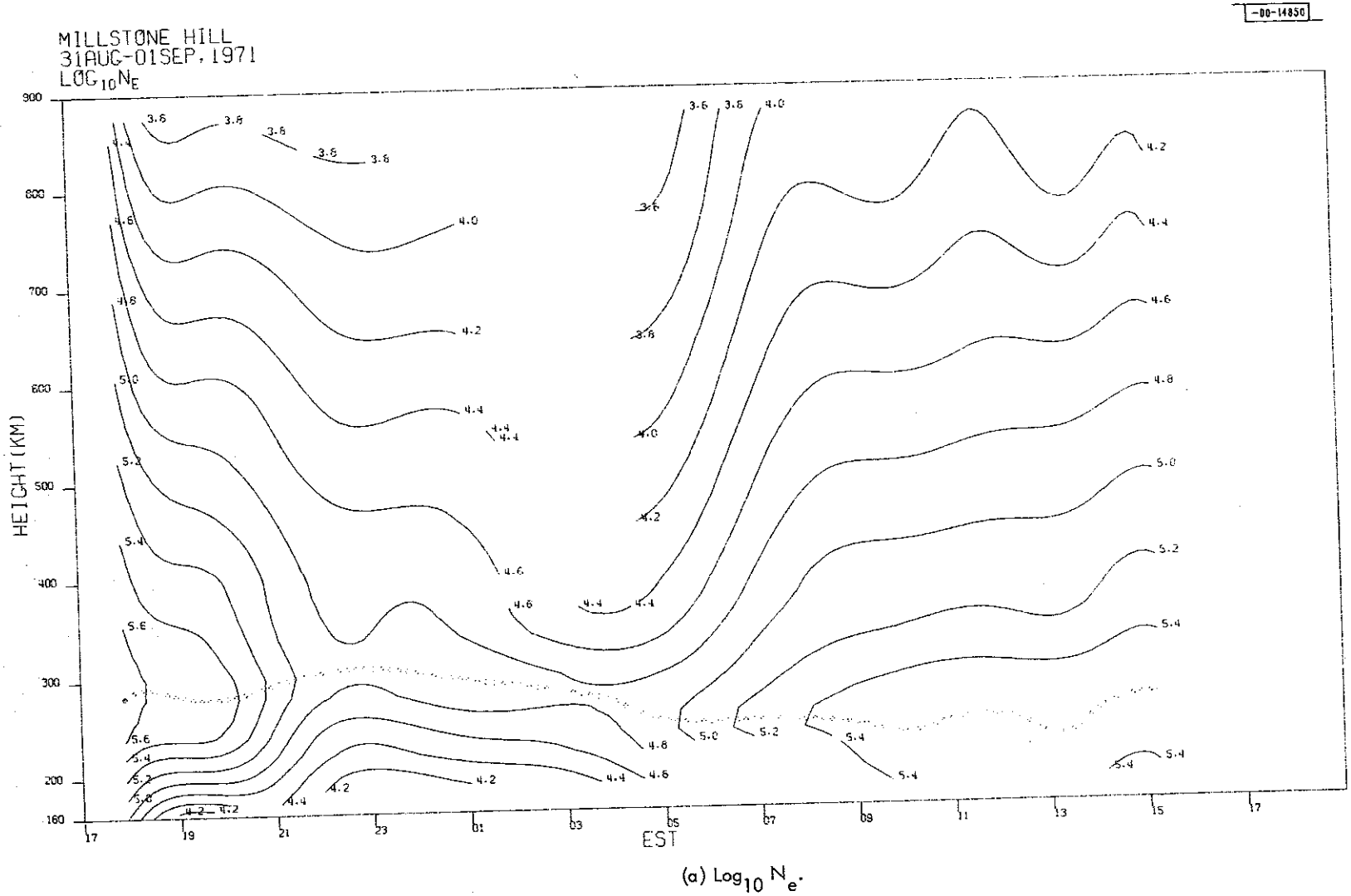

(a) $\text{Log}_{10} N_e$.

Fig. 19(a-d). Contours of density, temperature, and vertical velocity for 31 August – 1 September 1971.

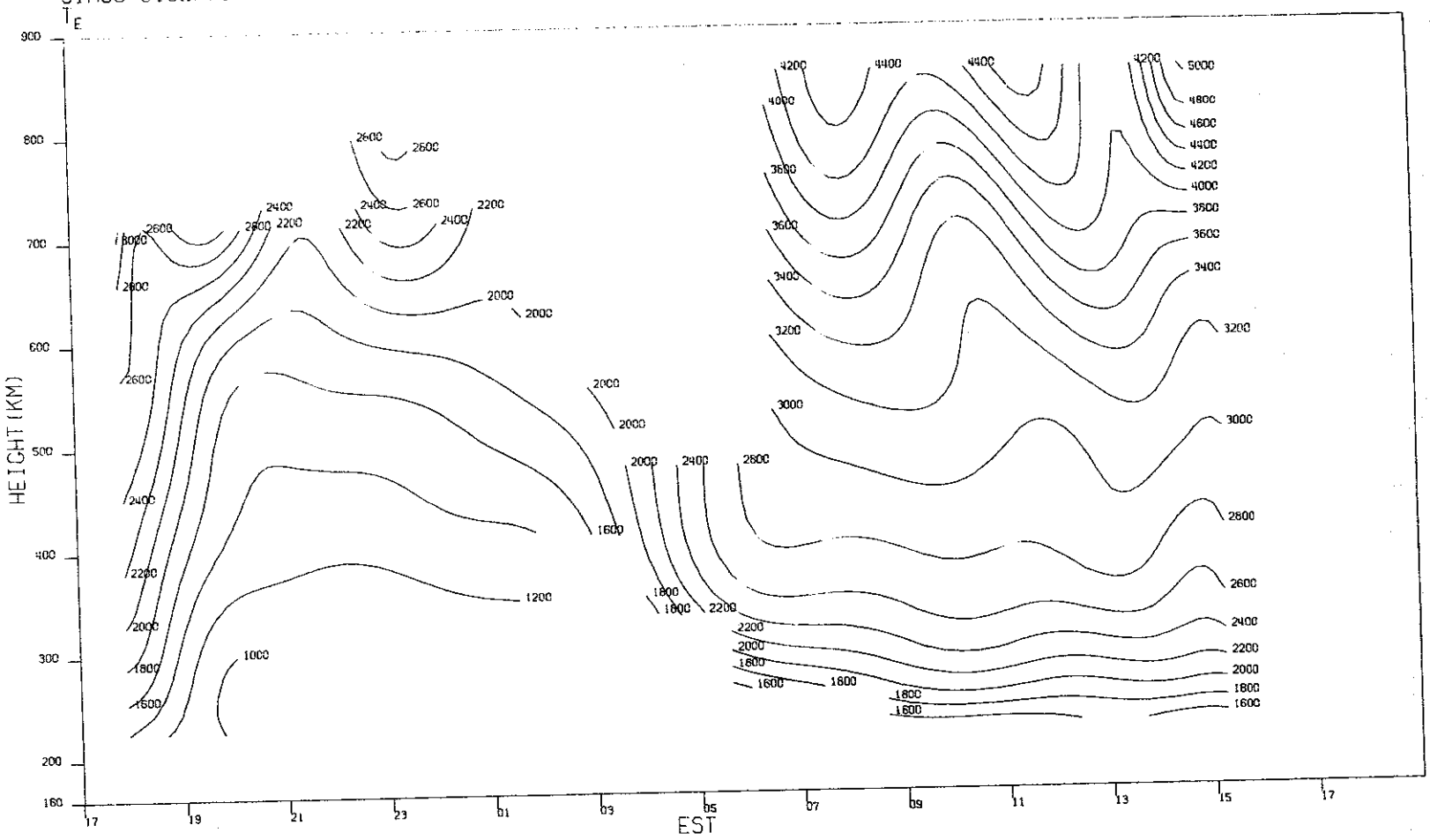

(b) T_e.

Fig. 19(a-d). Continued.

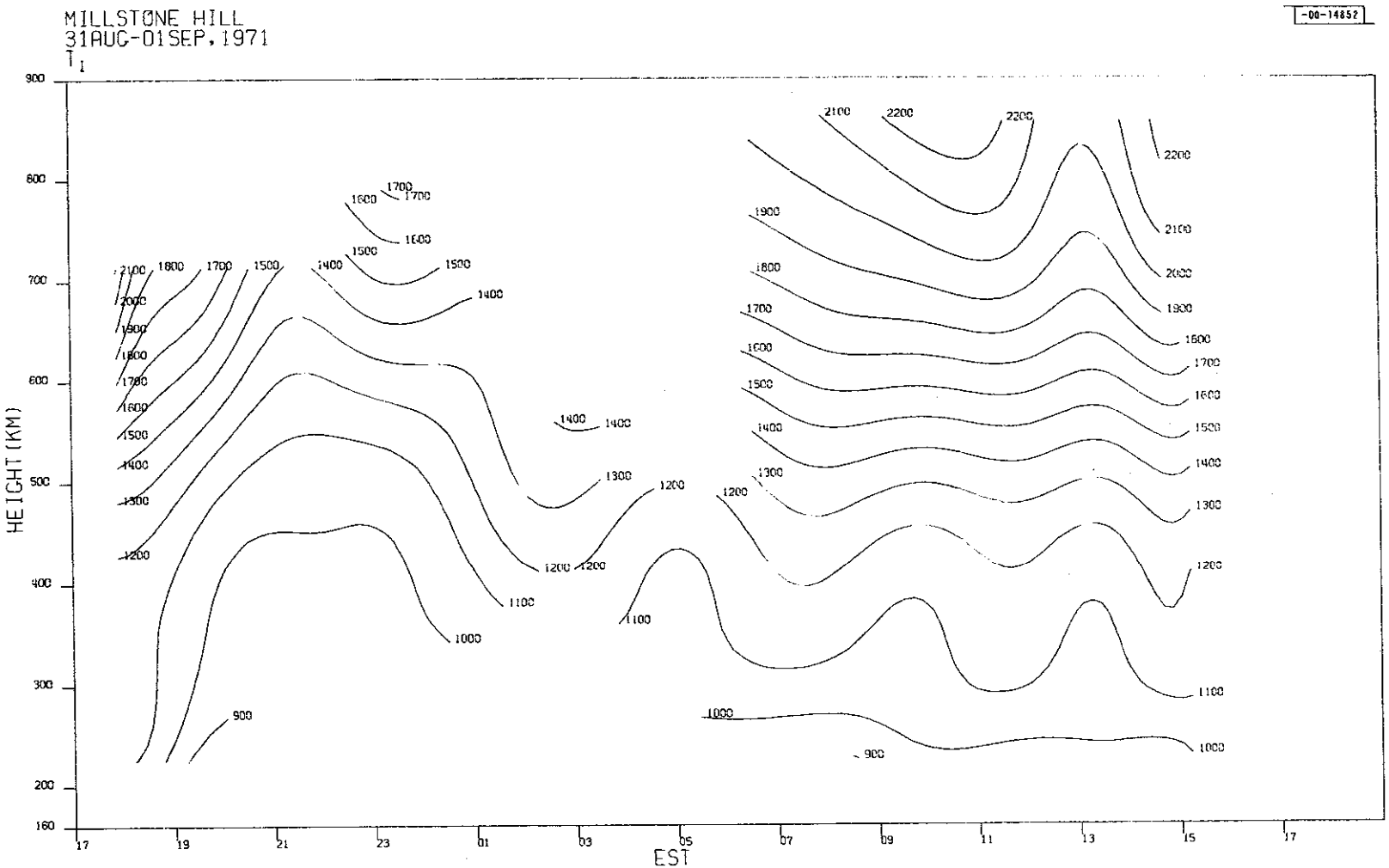

(c) T_i.

Fig. 19(a-d). Continued.

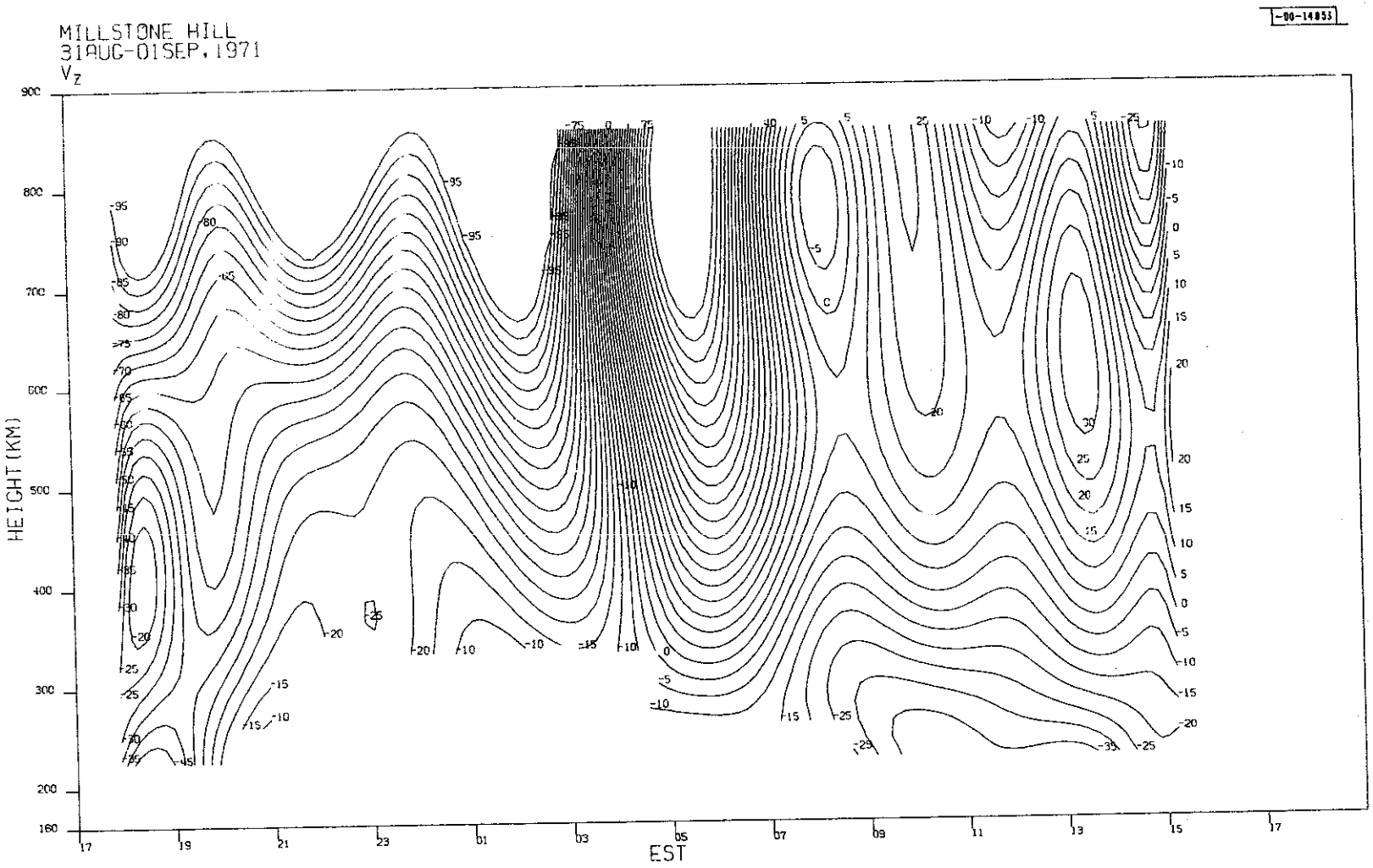

(d) V_z.

Fig. 19(a-d). Continued.

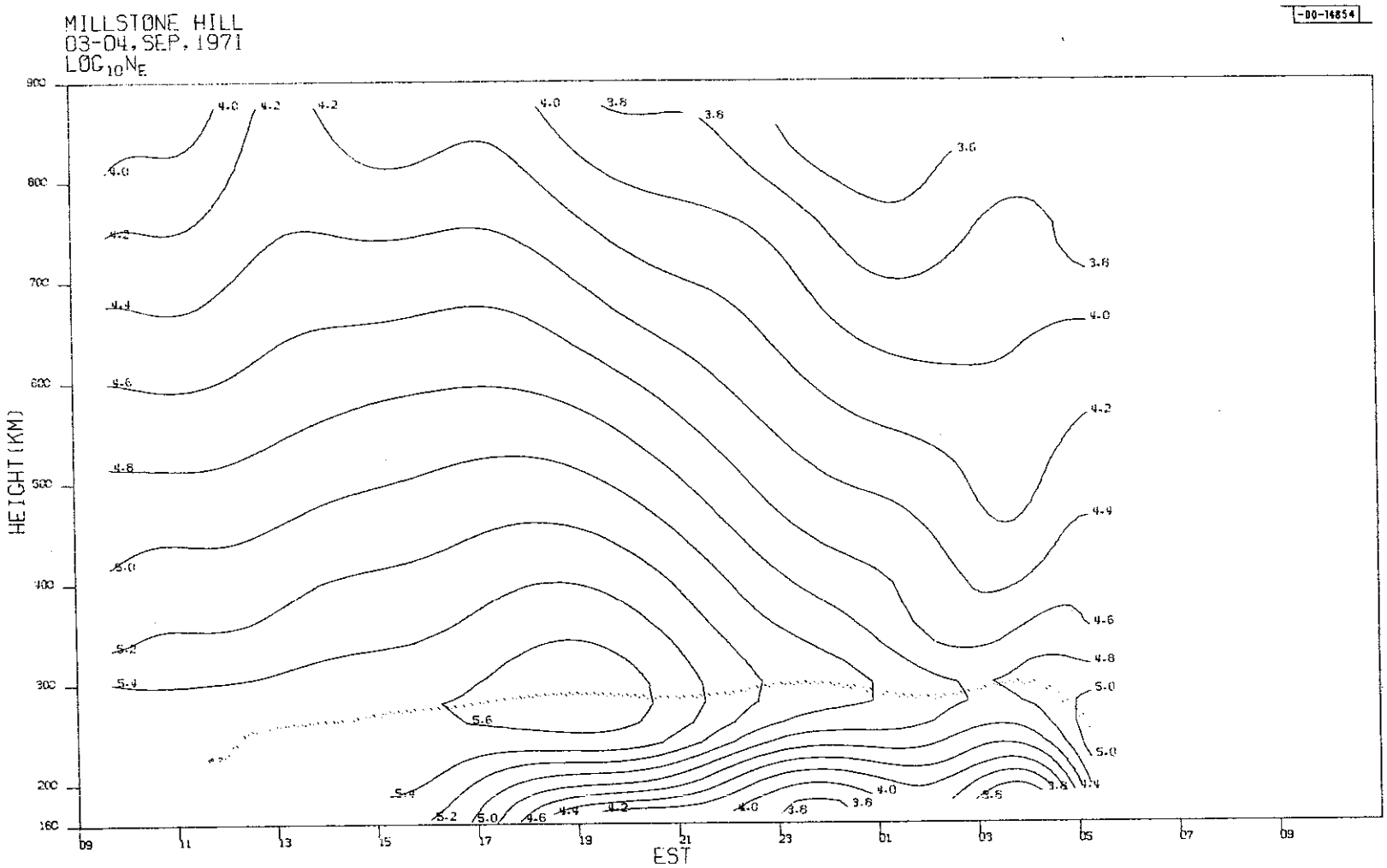

(a) $\text{Log}_{10} N_e$.

Fig. 20(a-c). Contours of density and temperature for 3-4 September 1971.

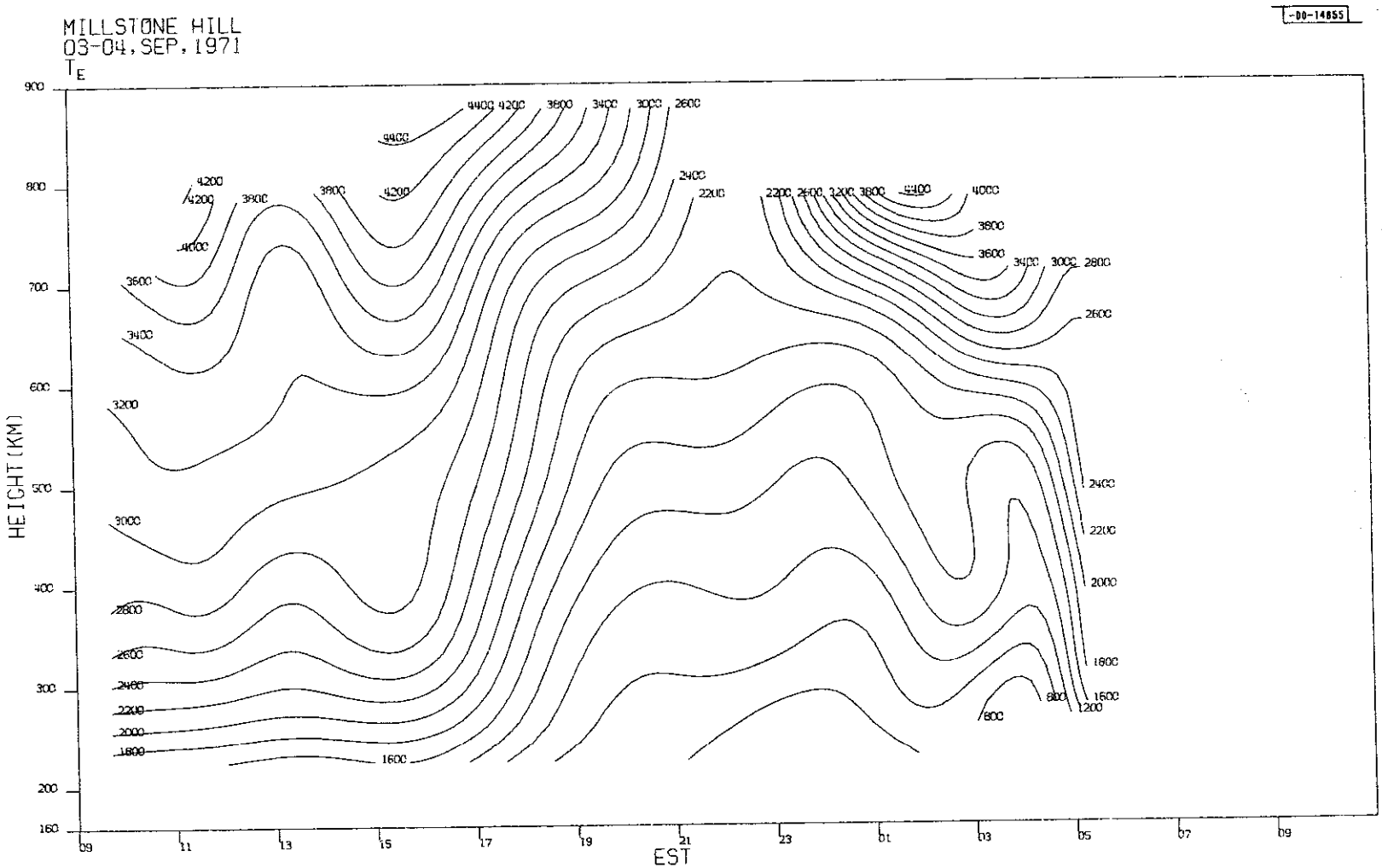

(b) T_e.

Fig. 20(a-c). Continued.

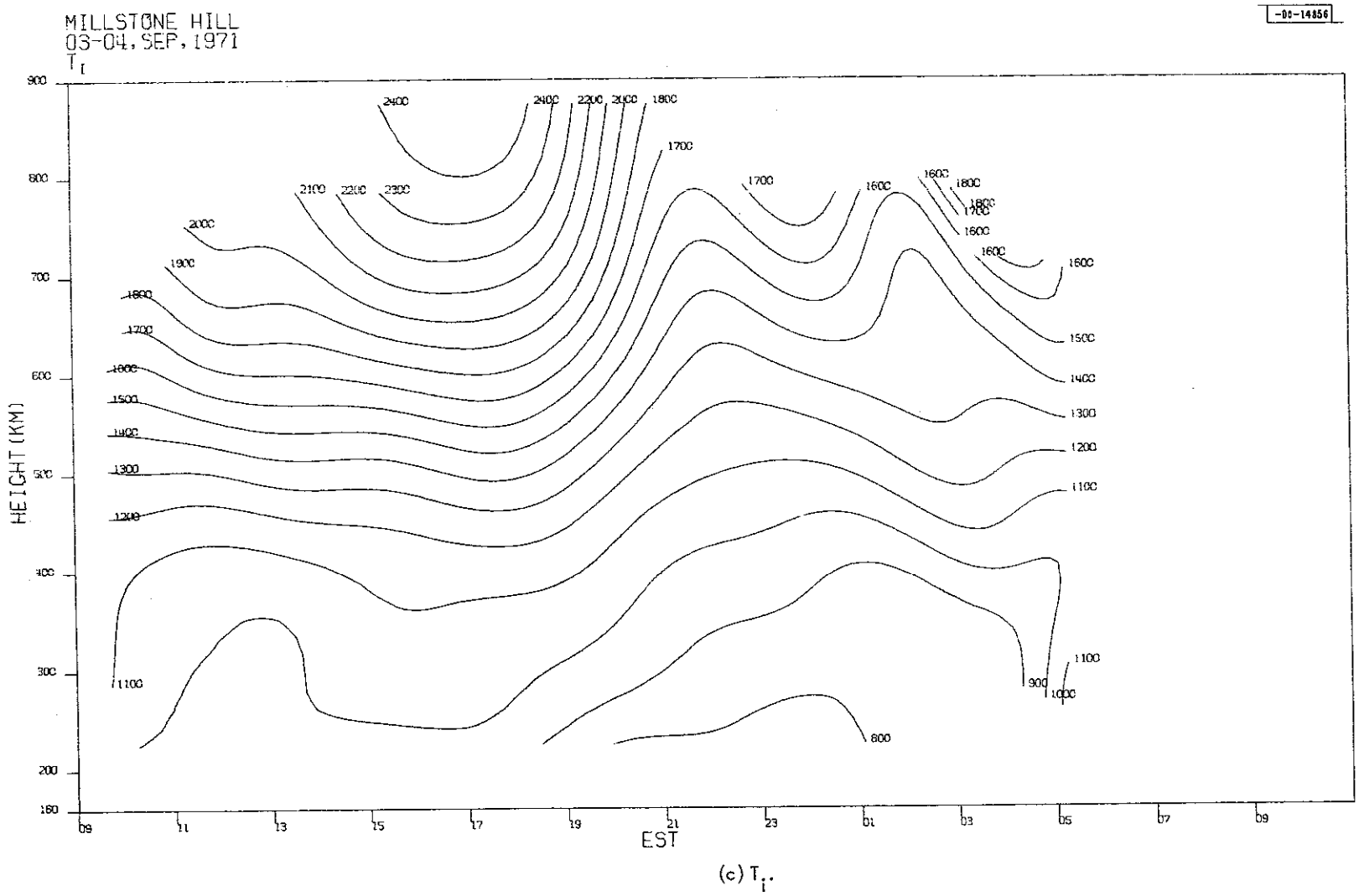

(c) T_i.

Fig. 20(a-c). Continued.

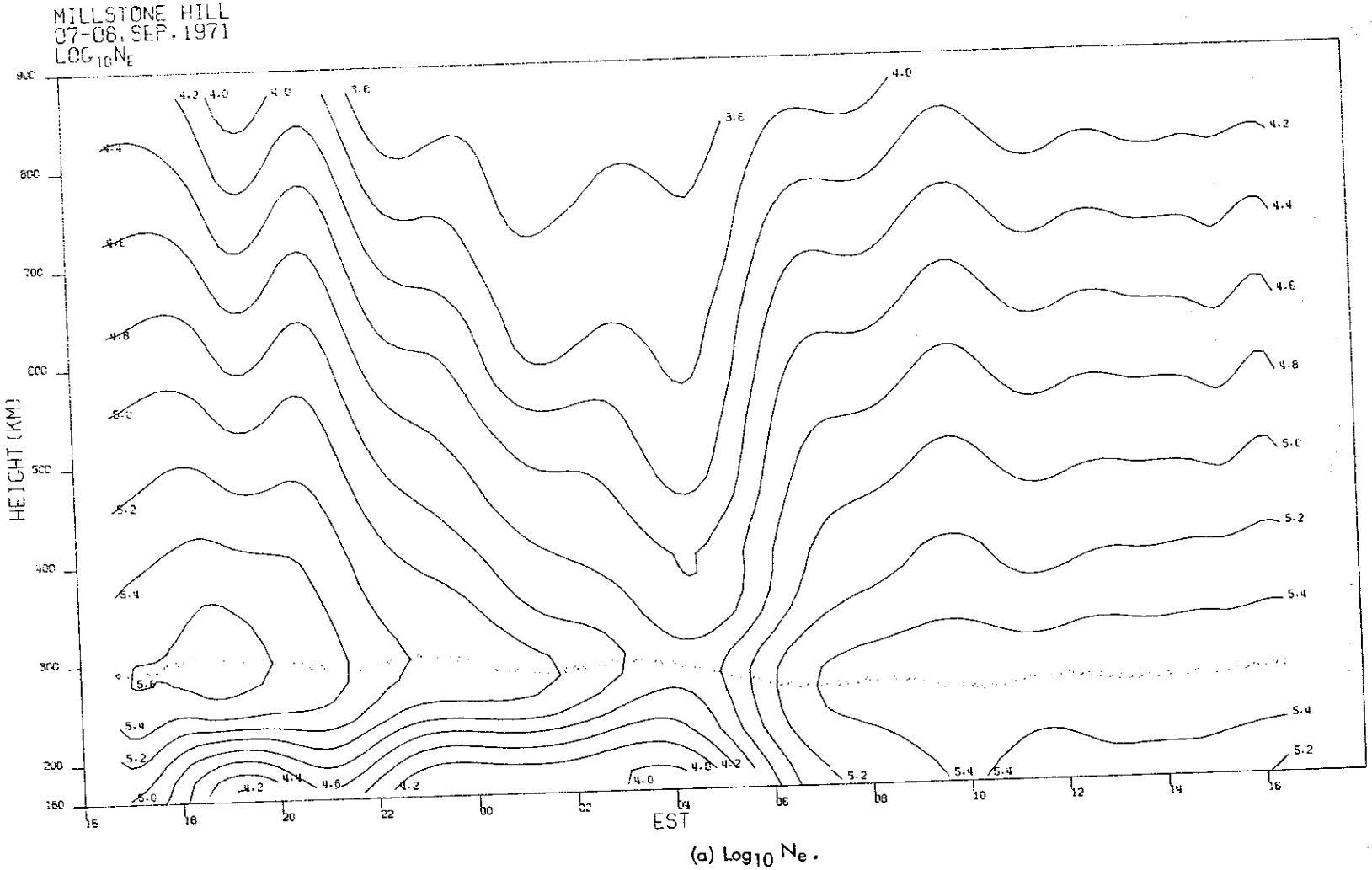

(a) $Log_{10} N_e$.

Fig. 21(a-d). Contours of density and temperature for 7-8 September 1971.

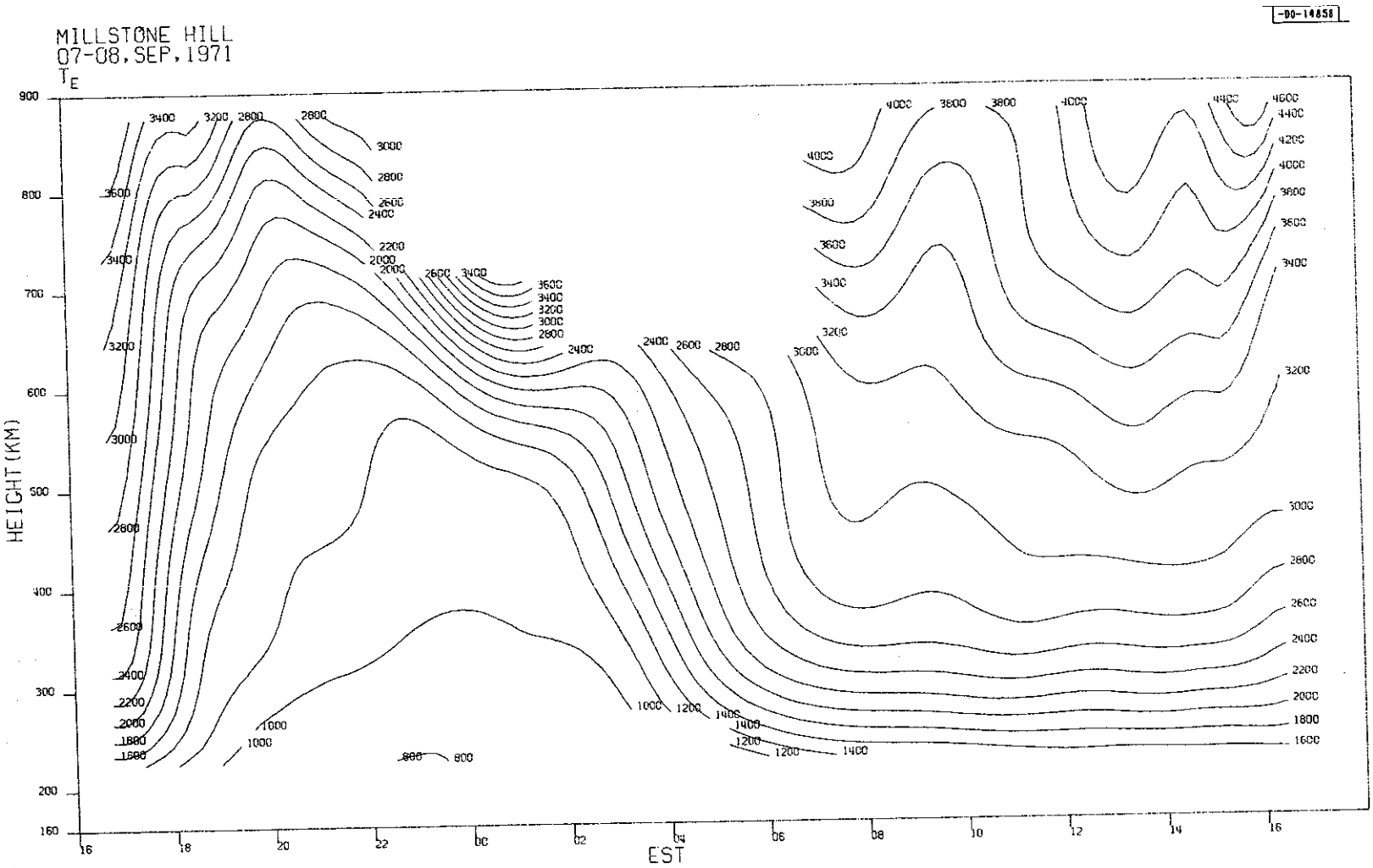

(b) T_e.

Fig. 21(a-d). Continued.

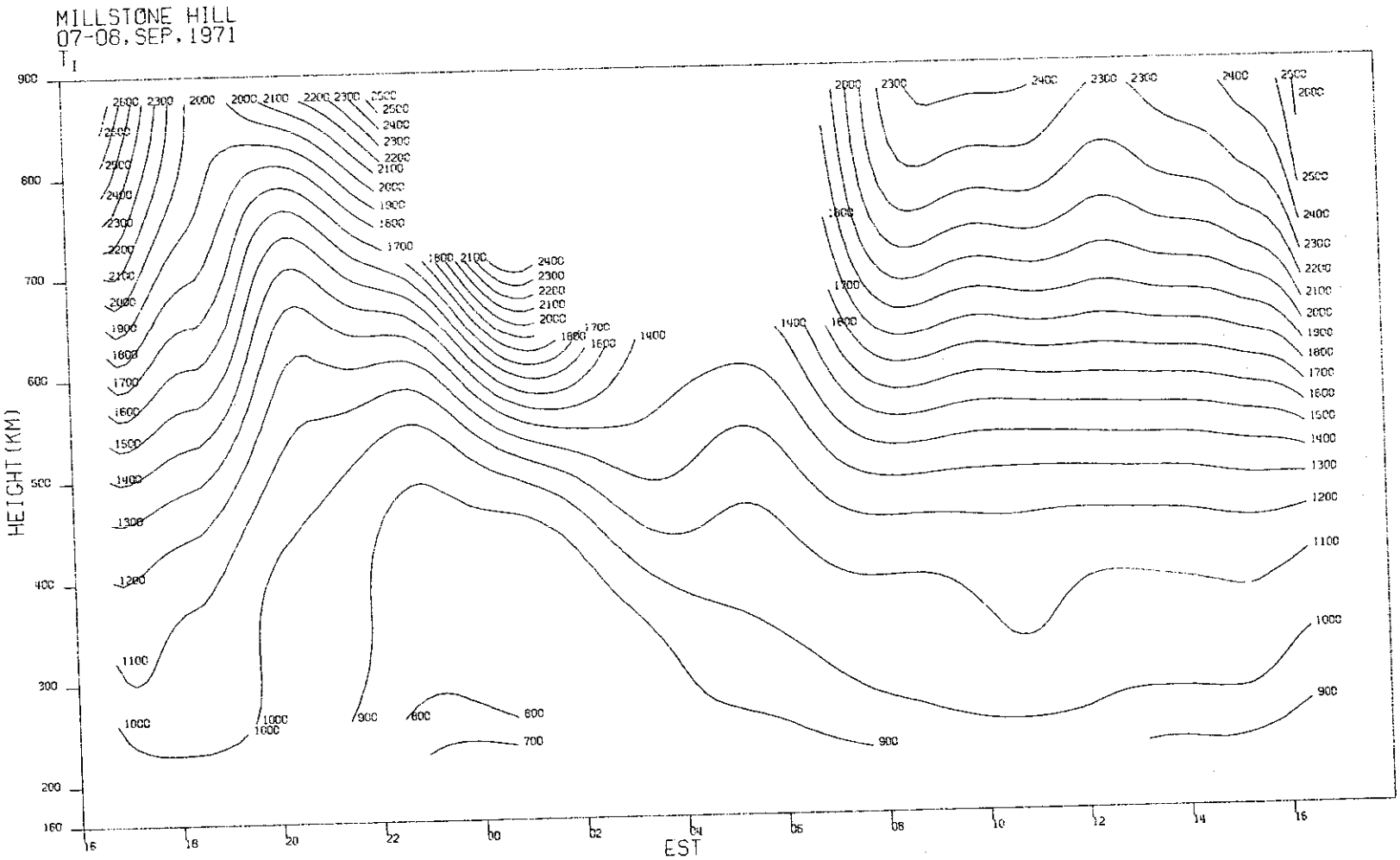

(c) T_i.

Fig. 21(a-d). Continued.

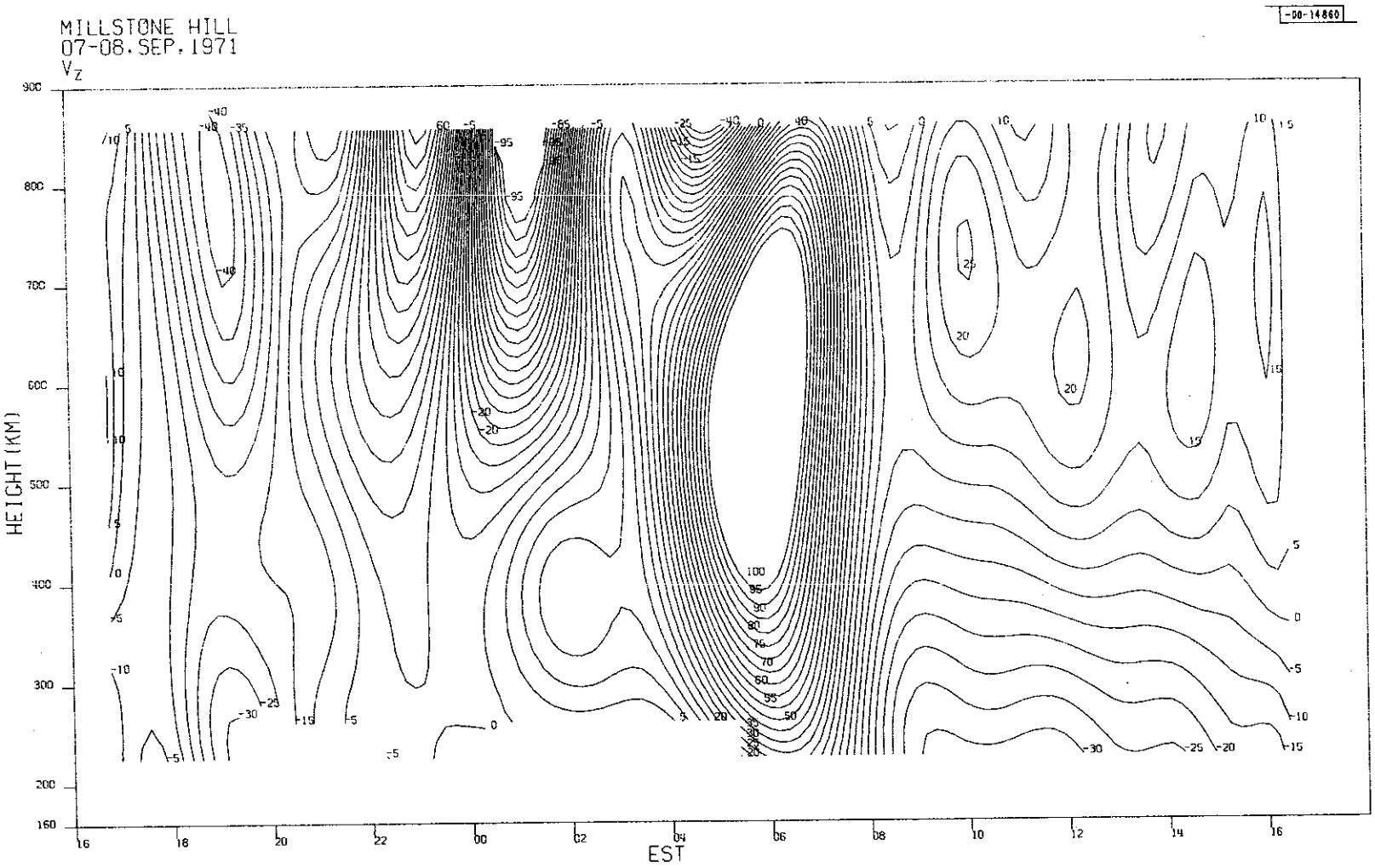

(d) V_z.

Fig. 21(a-d). Continued.

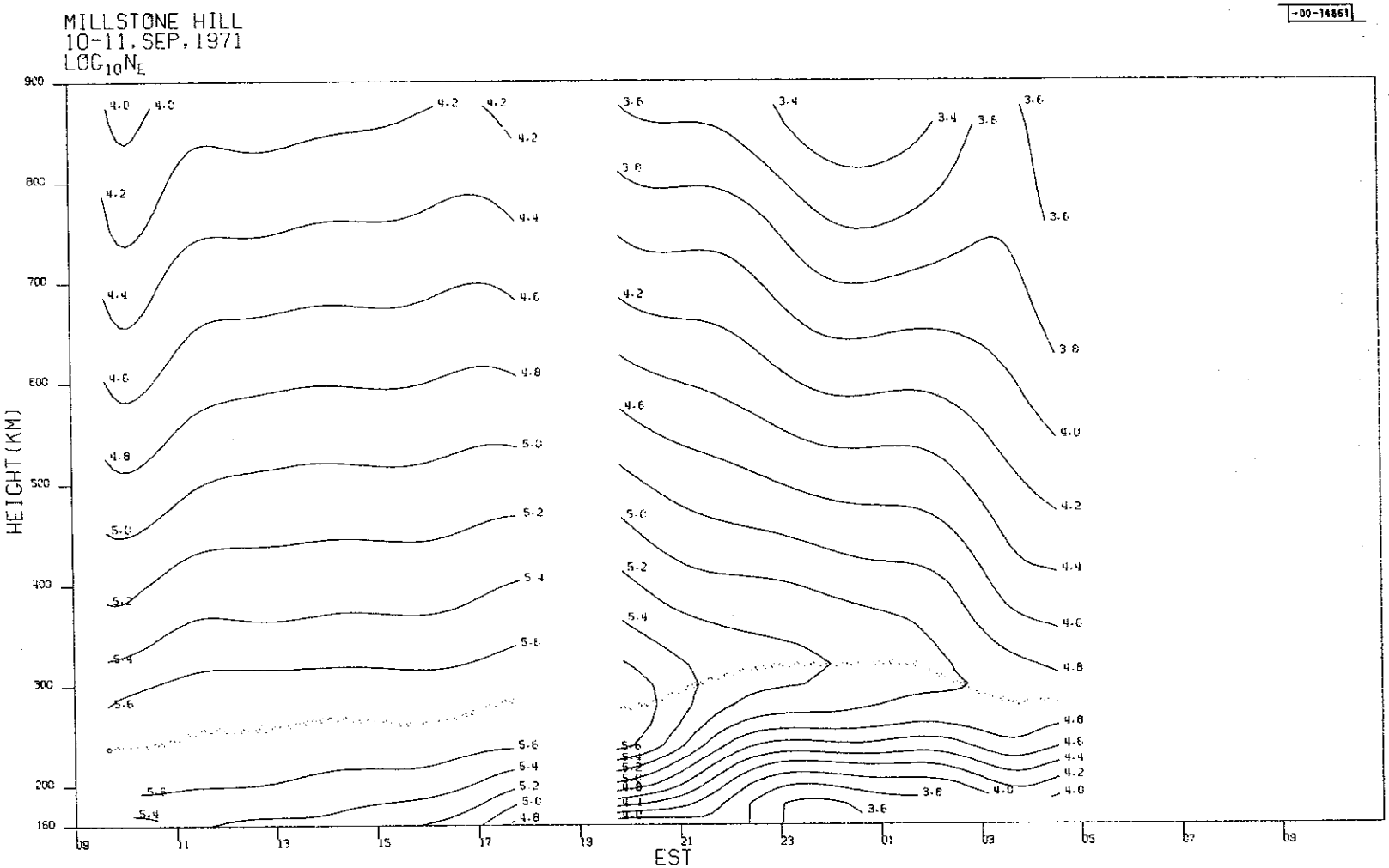

(a) $\text{Log}_{10} N_e$.

Fig. 22(a-c). Contours of density and temperature for 10-11 September 1971.

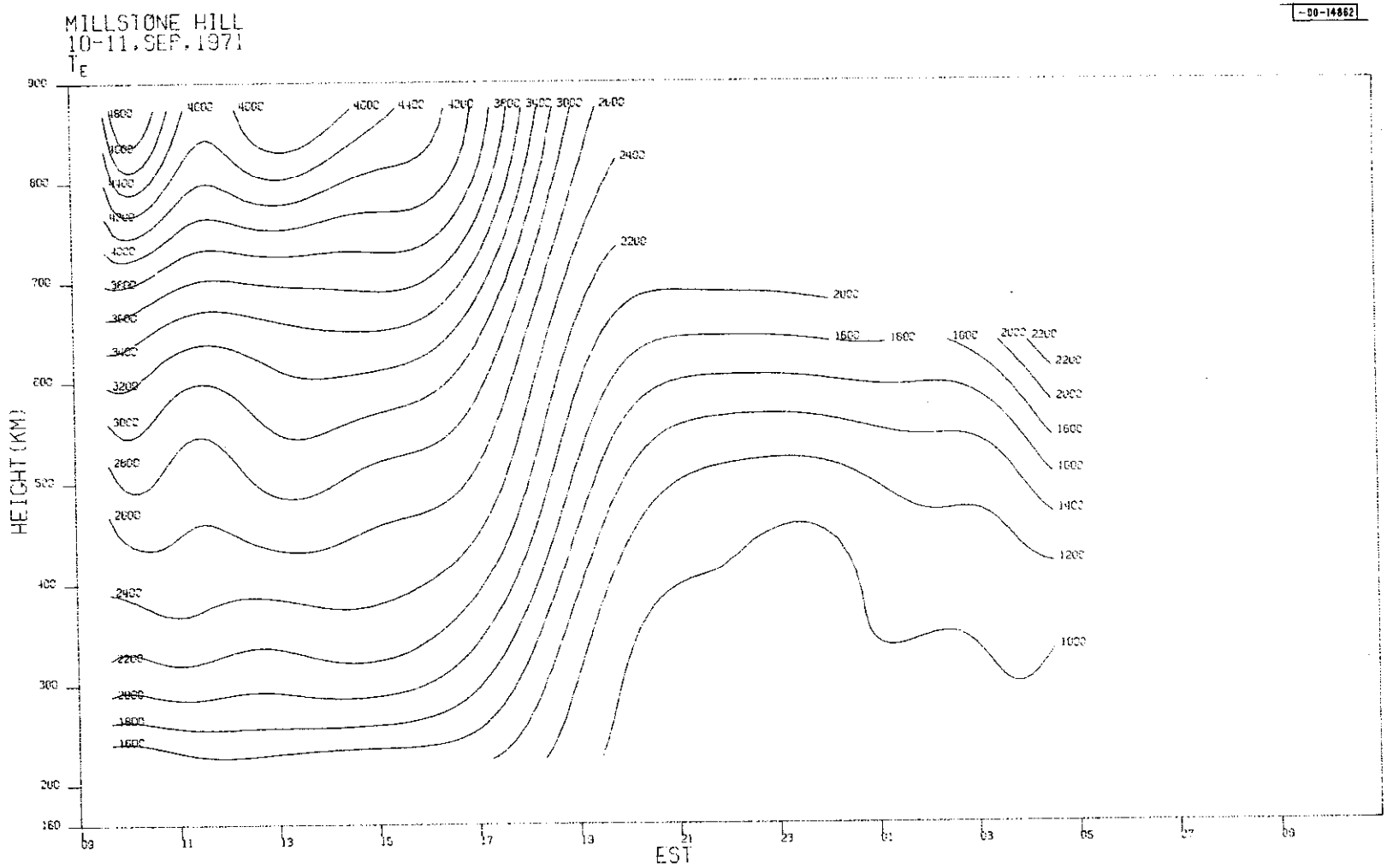

(b) T_e.

Fig. 22(a-c). Continued.

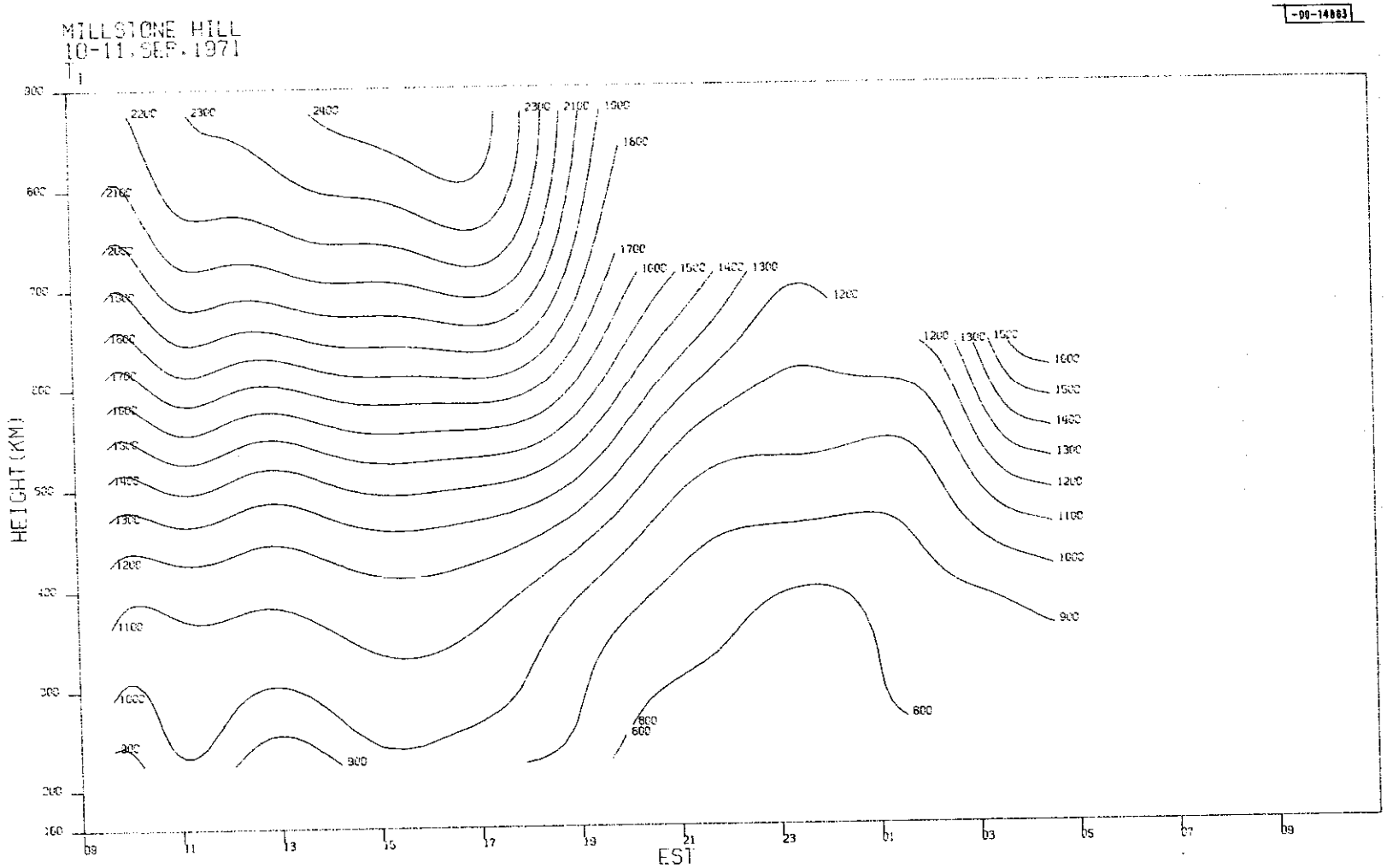

(c) T_i.

Fig. 22(a-c). Continued.

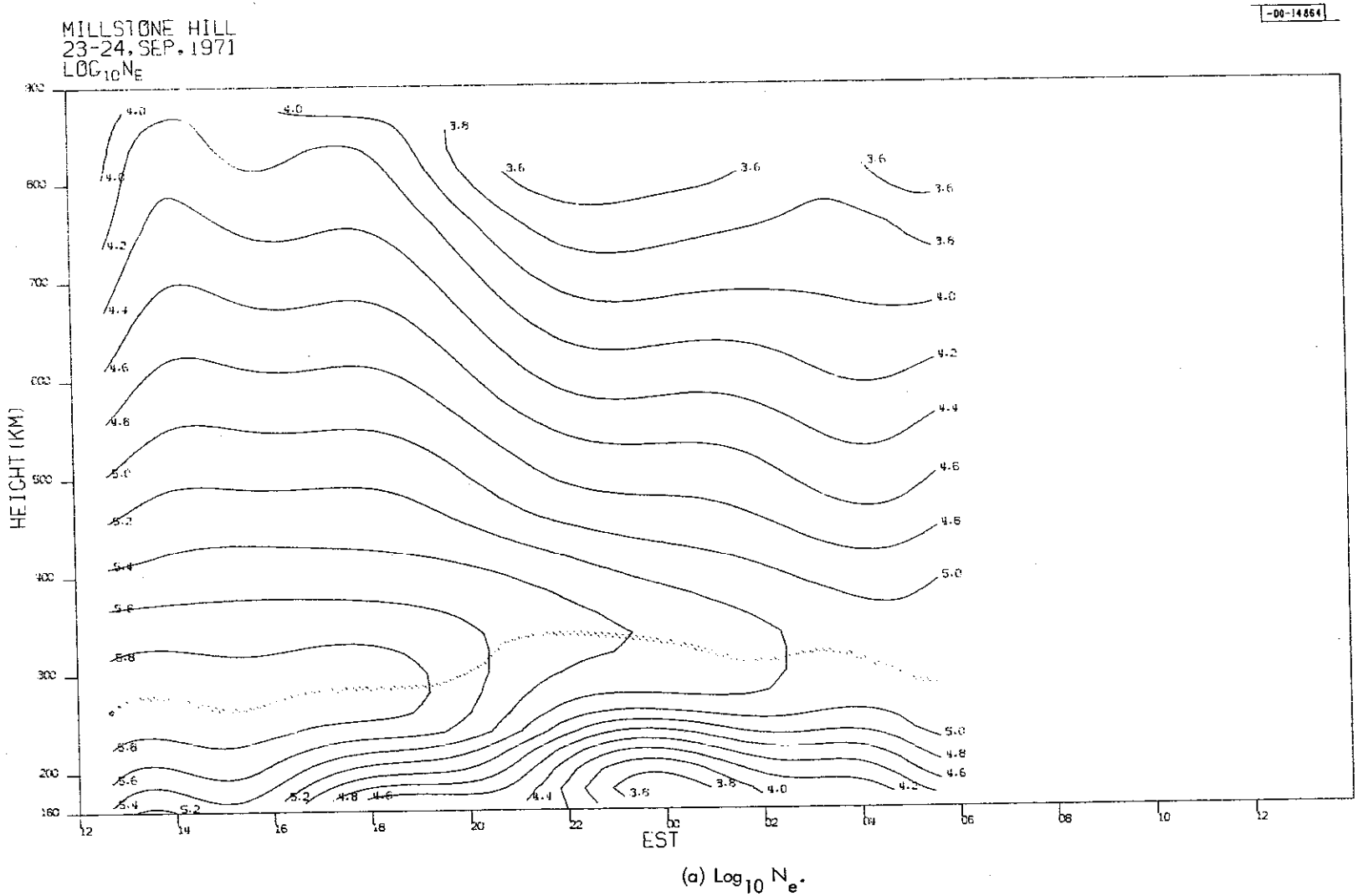

(a) $\text{Log}_{10} N_e$.

Fig. 23(a-c). Contours of density and temperature for 23-24 September 1971.

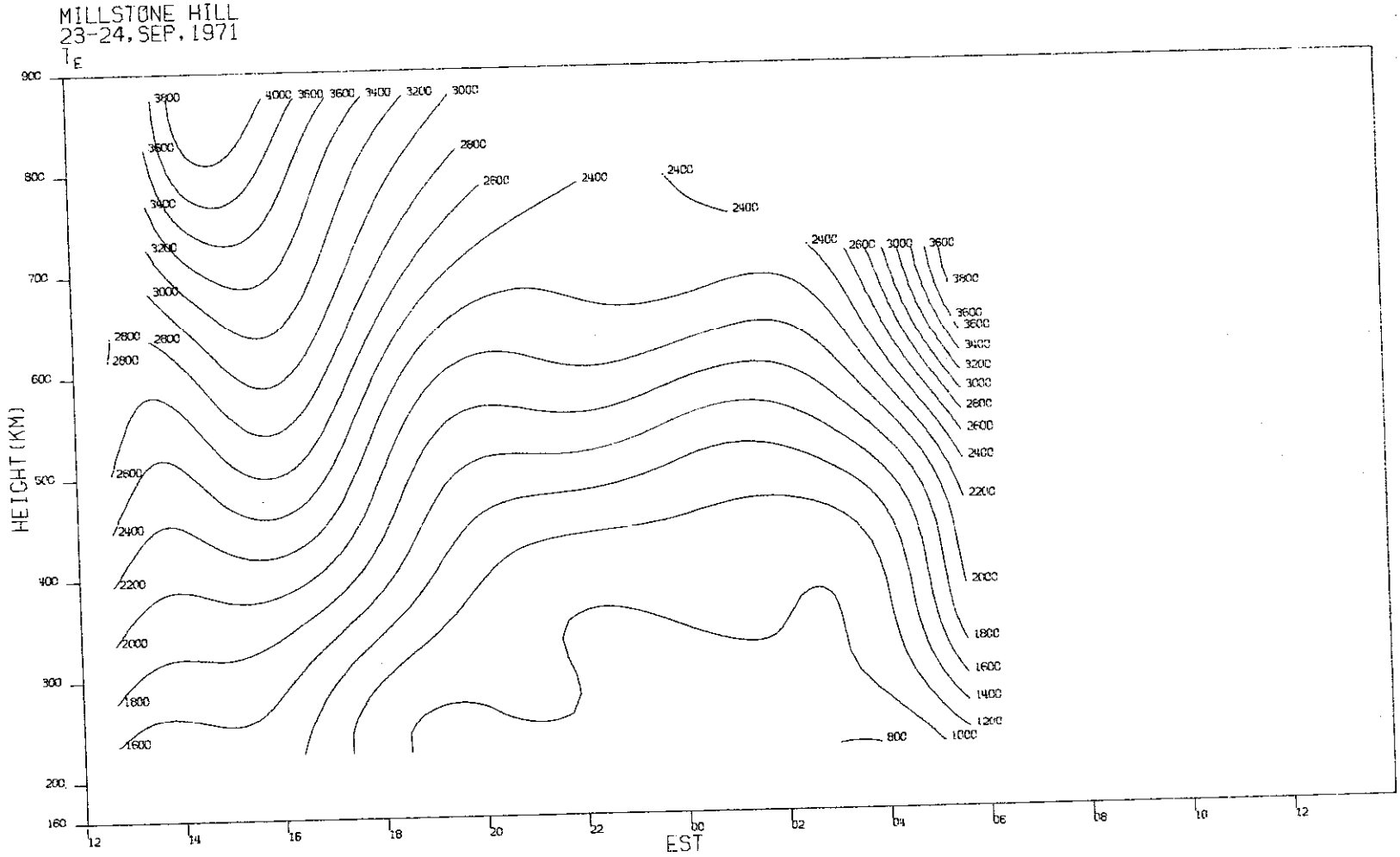

(b) T_e.

Fig. 23(a-c). Continued.

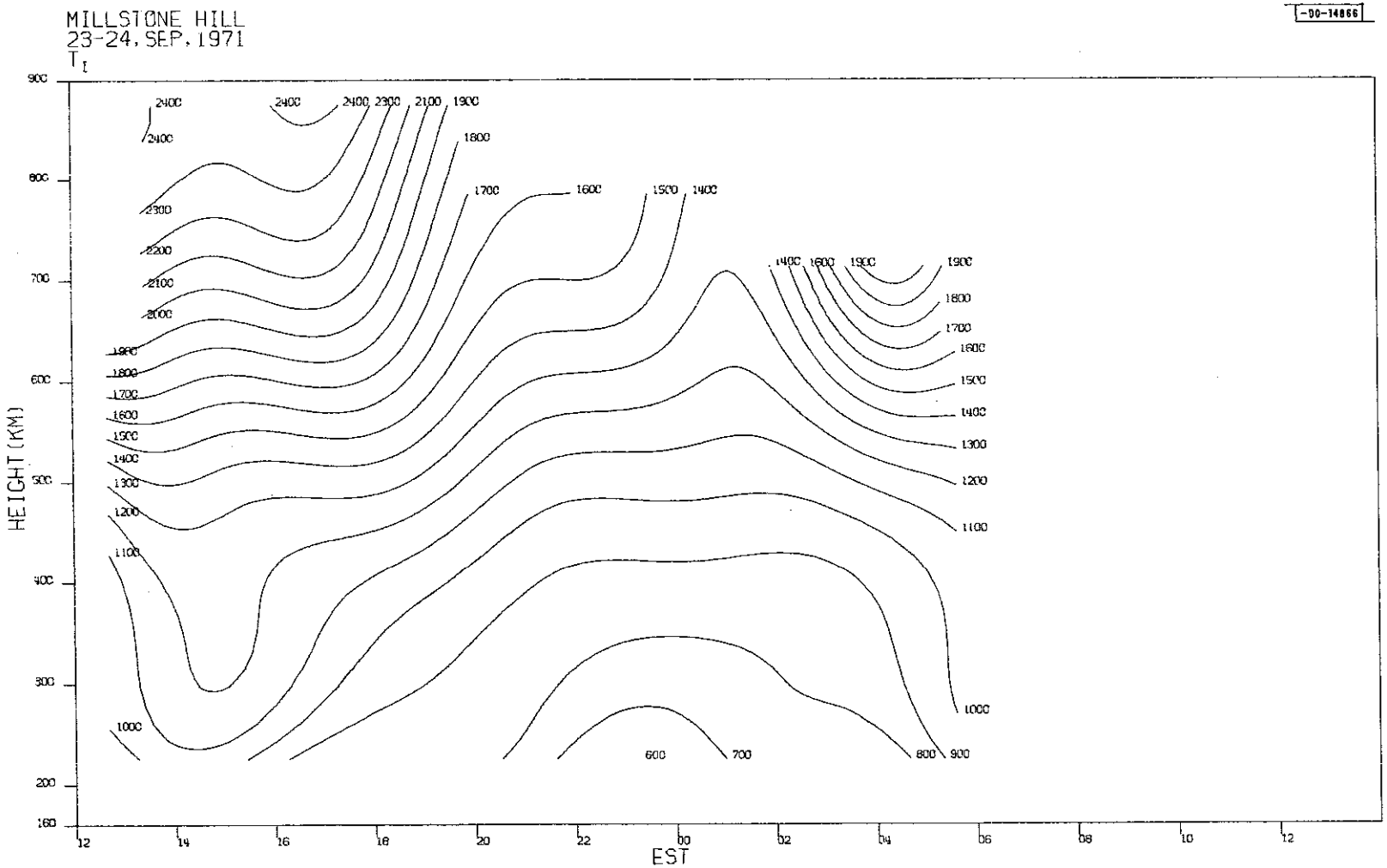

(c) T_i.

Fig. 23(a-c). Continued.

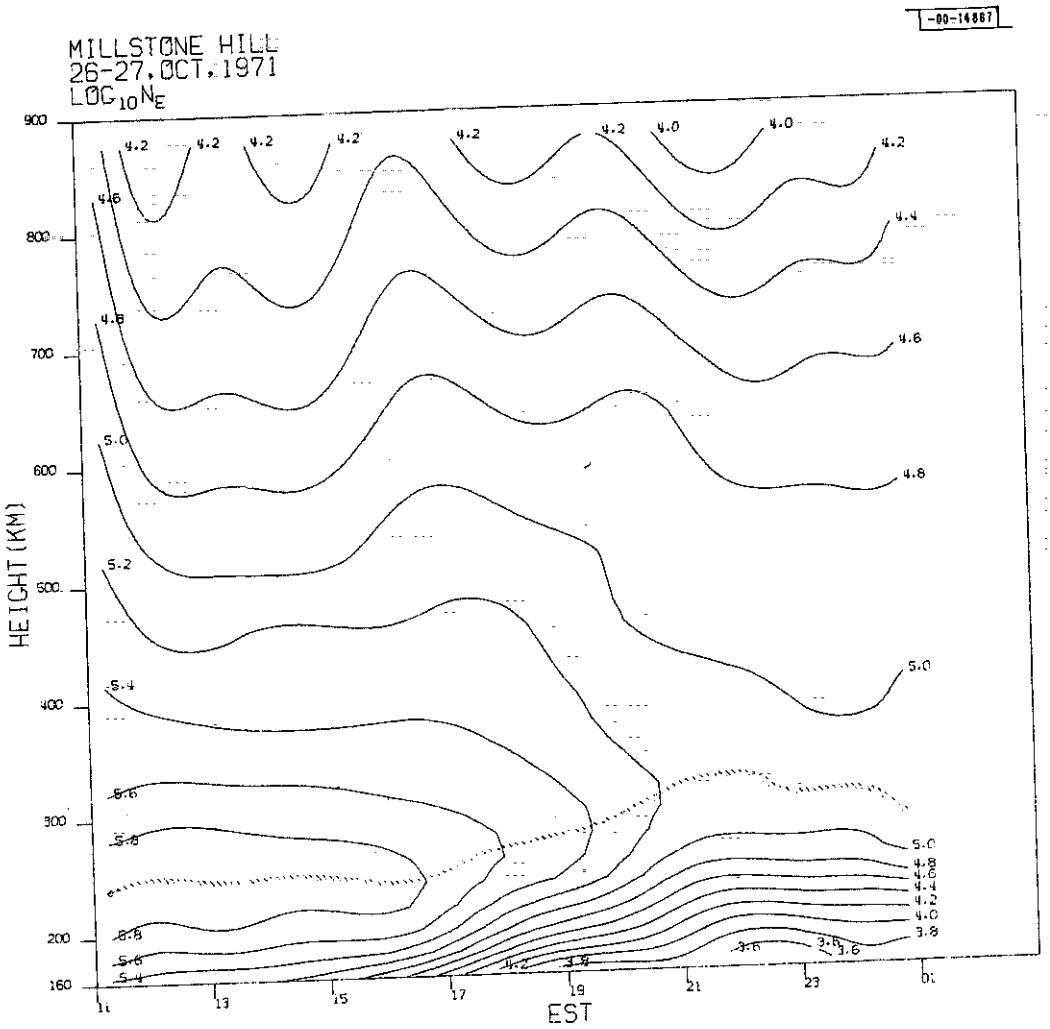

(a) $\text{Log}_{10} N_e$.

Fig. 24(a-d). Contours of density, temperature, and vertical velocity for 26-27 October 1971.

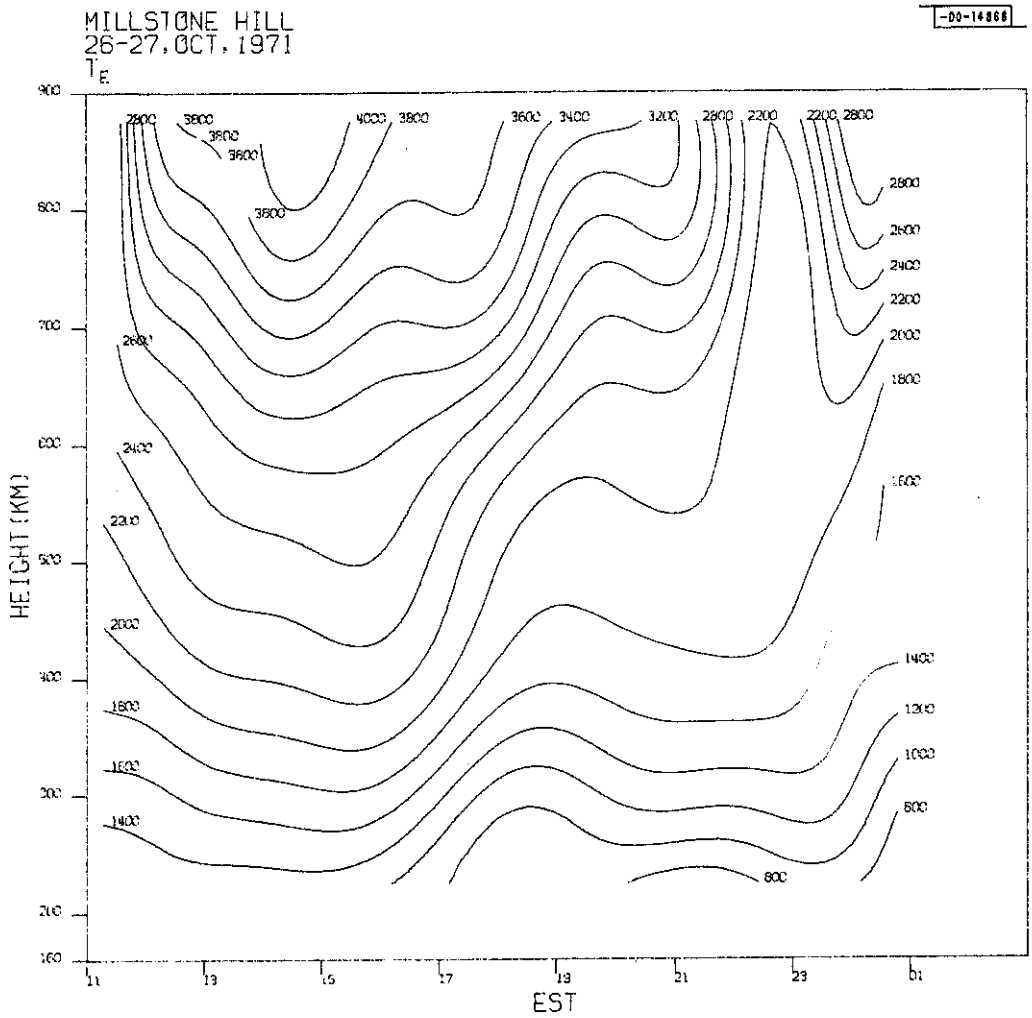

(b) T_e.

Fig. 24(a-d). Continued.

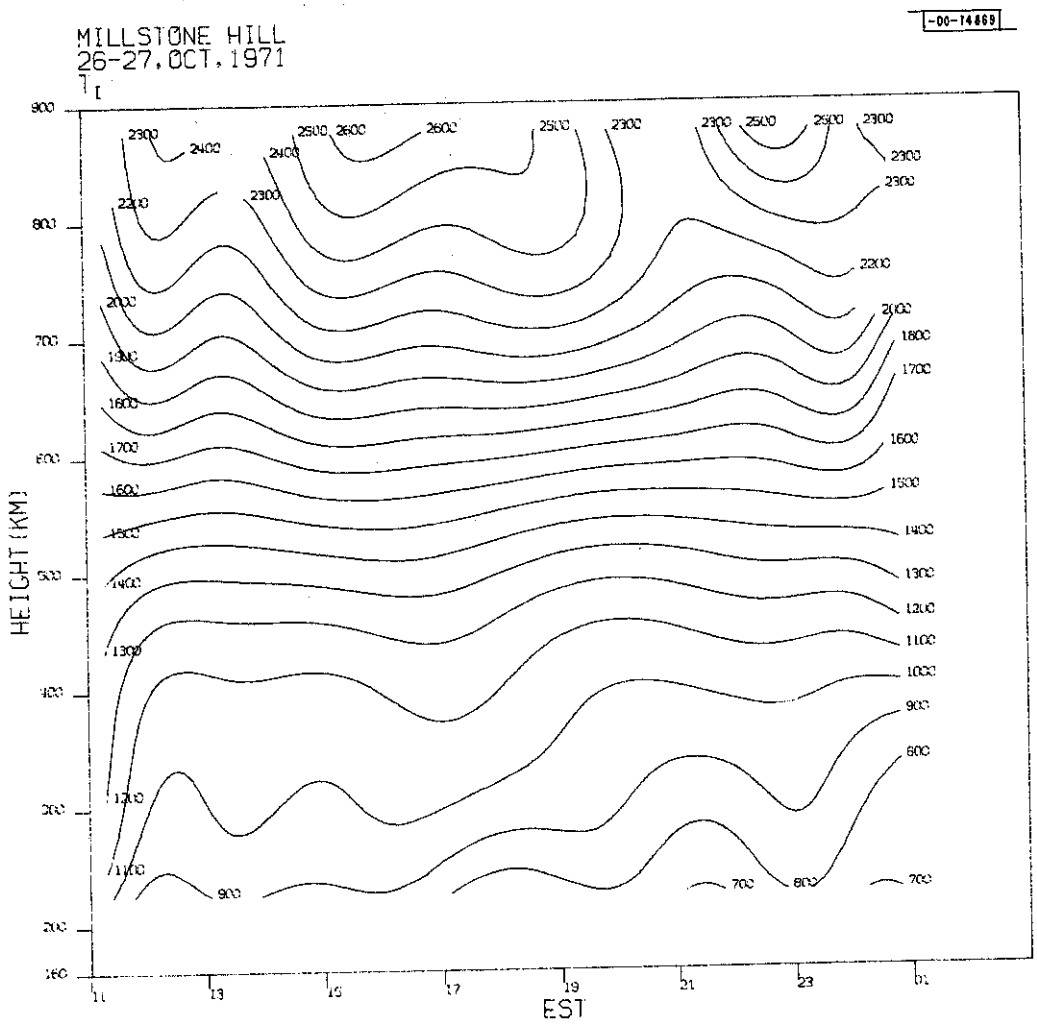

(c) T_i.

Fig. 24(a-d). Continued.

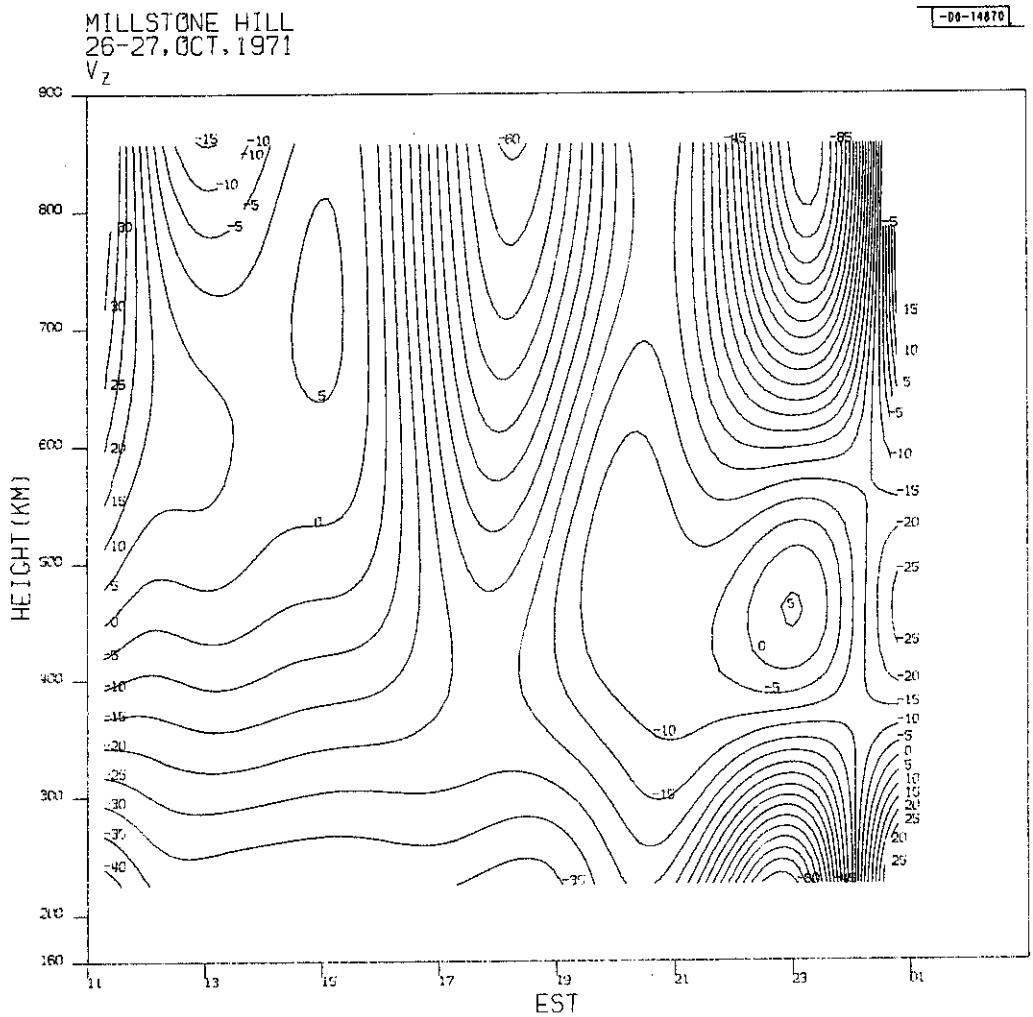

(d) V_z.

Fig. 24(a-d). Continued.

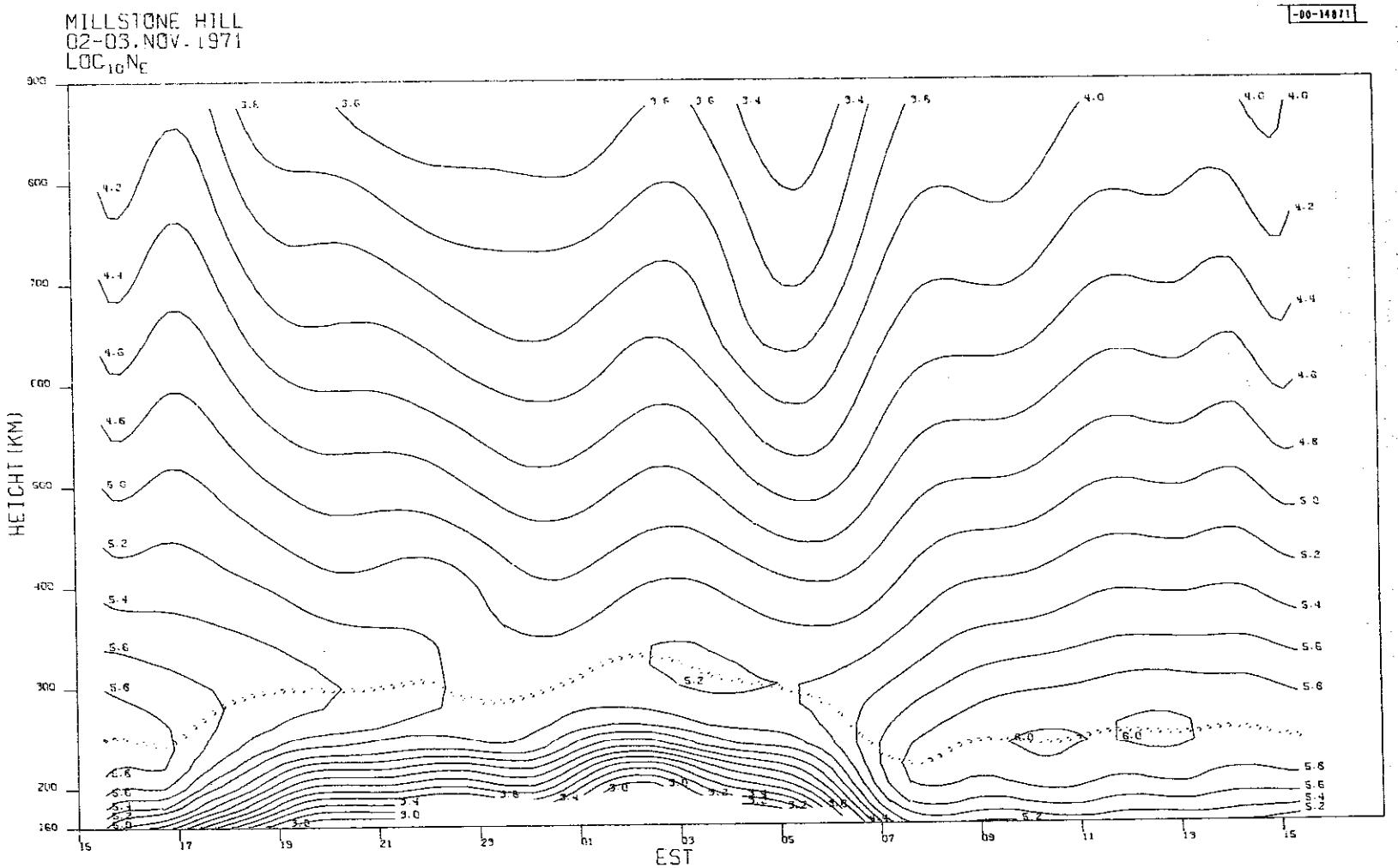

(a) $\text{Log}_{10} N_e$.

Fig. 25(a-d). Contours of density, temperature, and vertical velocity for 2-3 November 1971.

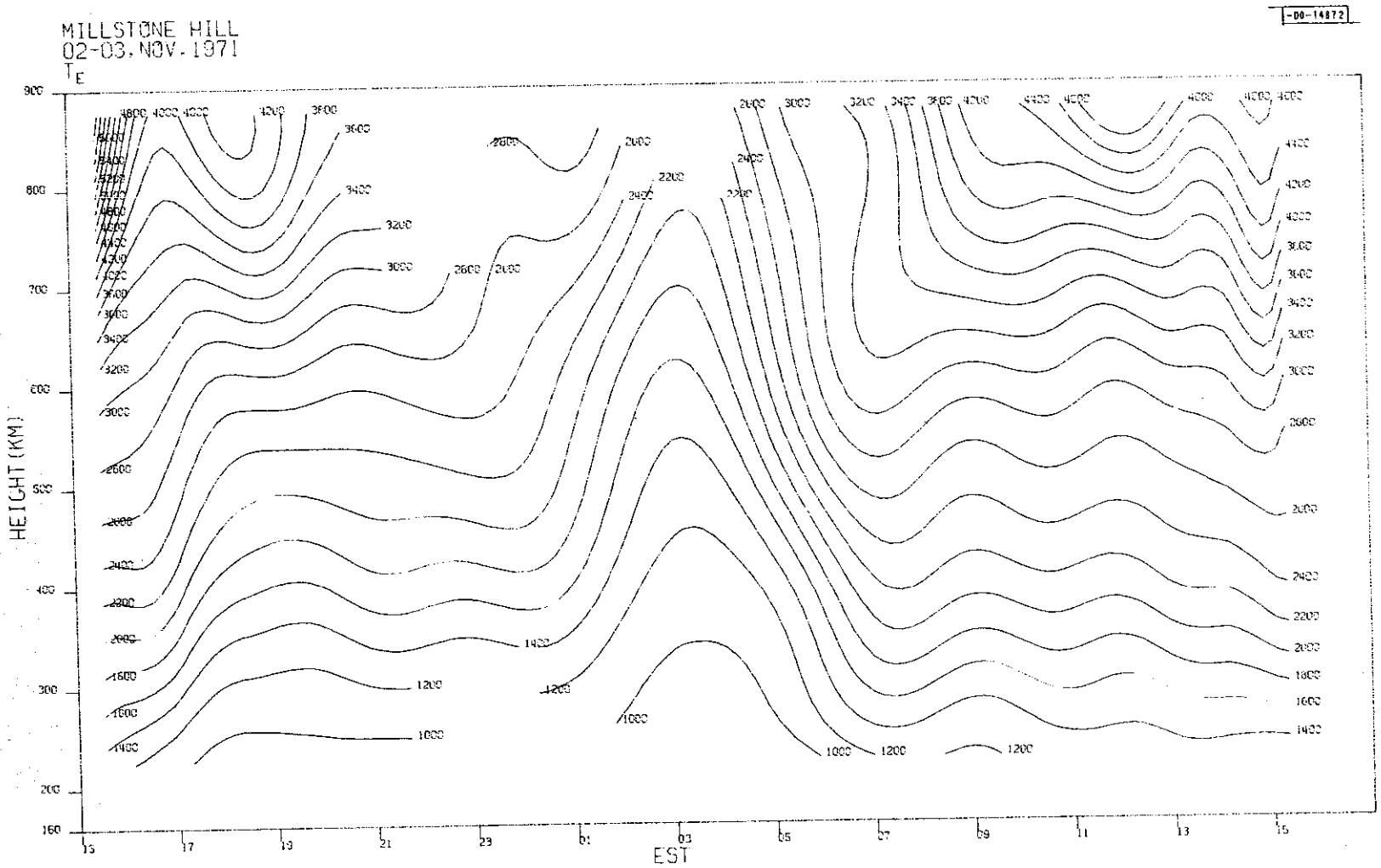

(b) T_e.

Fig. 25(a-d). Continued.

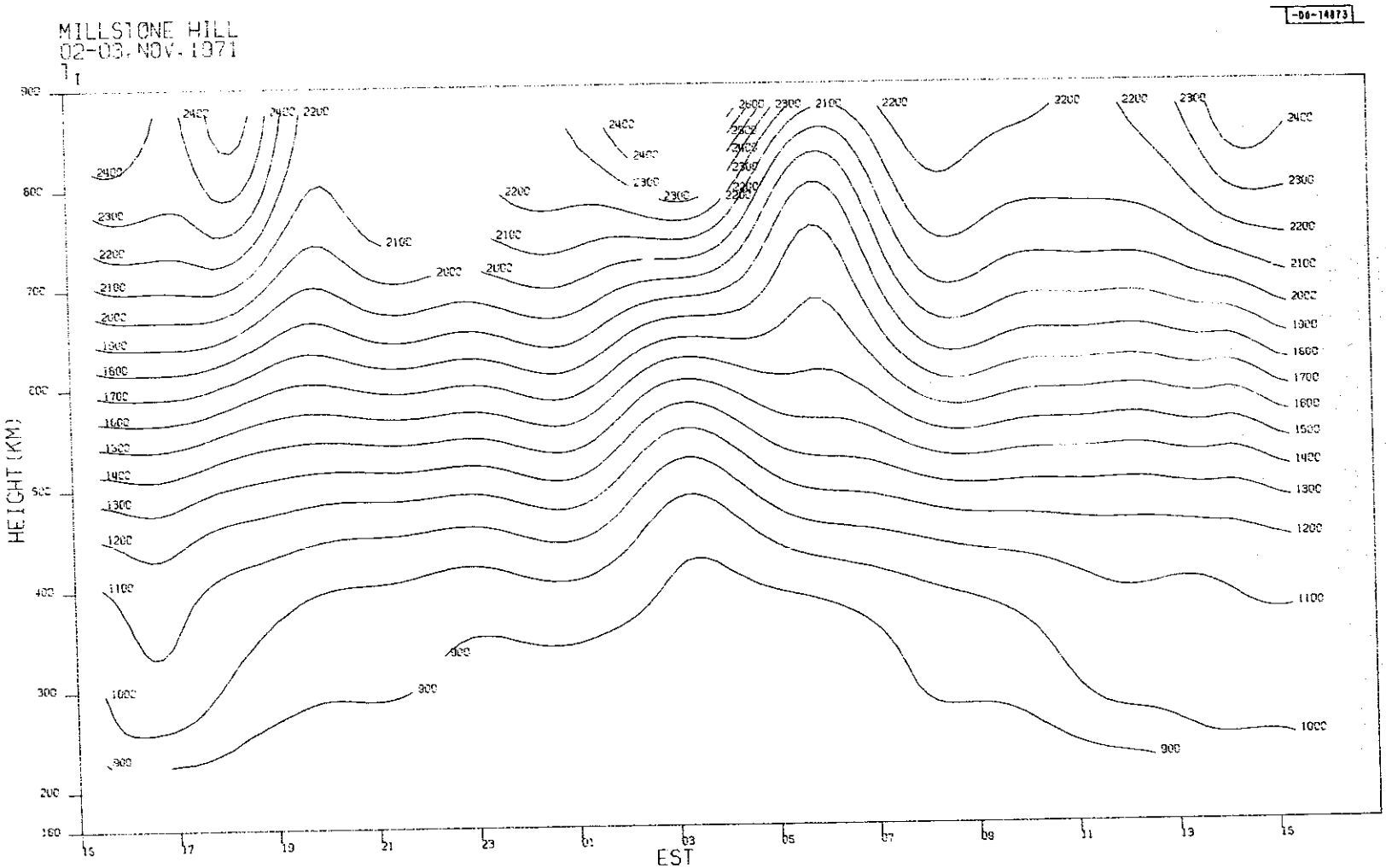

(c) T_i.

Fig. 25(a-d). Continued.

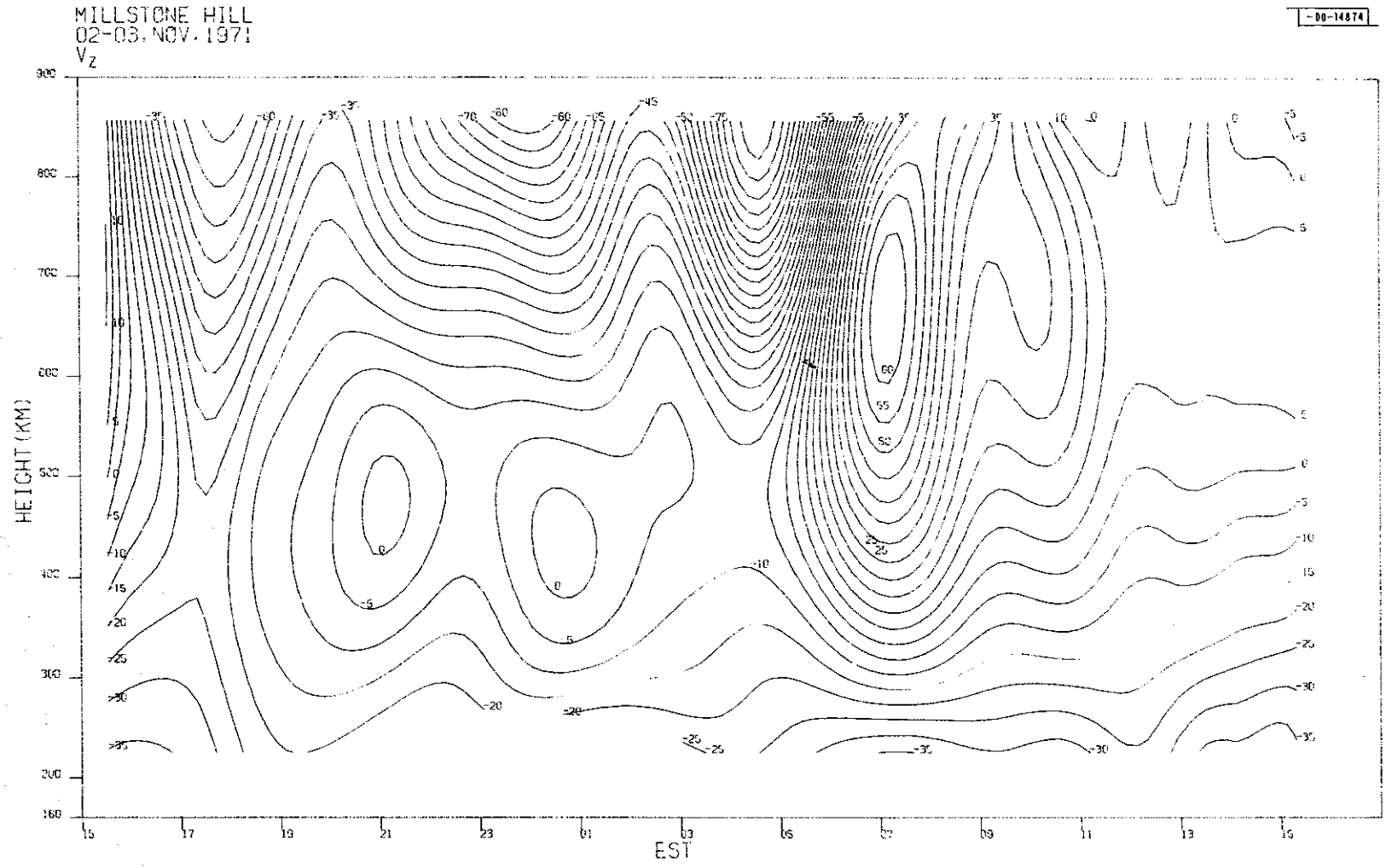

(d) V_z.

Fig. 25(a-d). Continued.

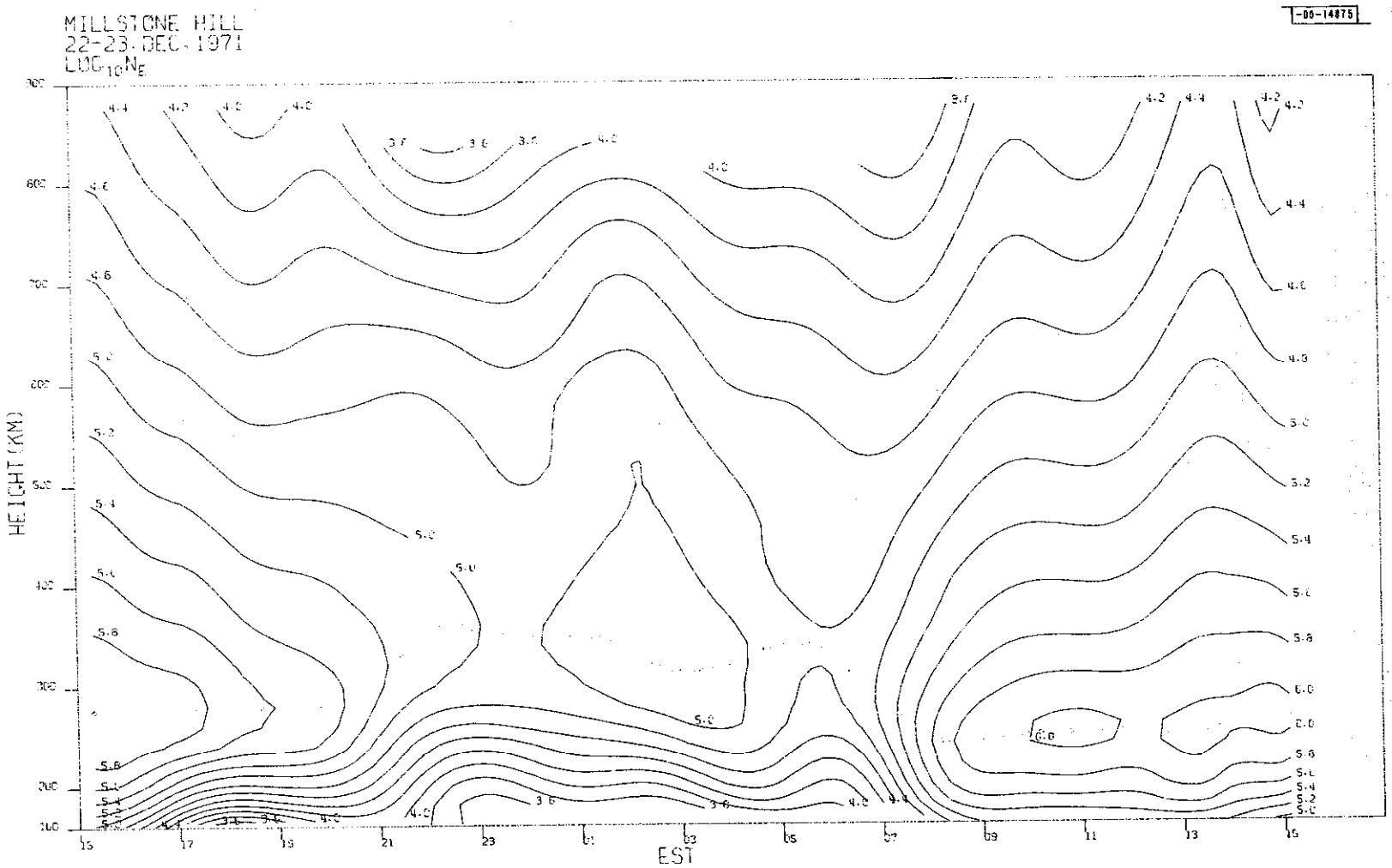

(a) $\text{Log}_{10} N_e$.

Fig. 26(a-d). Contours of density, temperature, and vertical velocity for 22-23 December 1971.

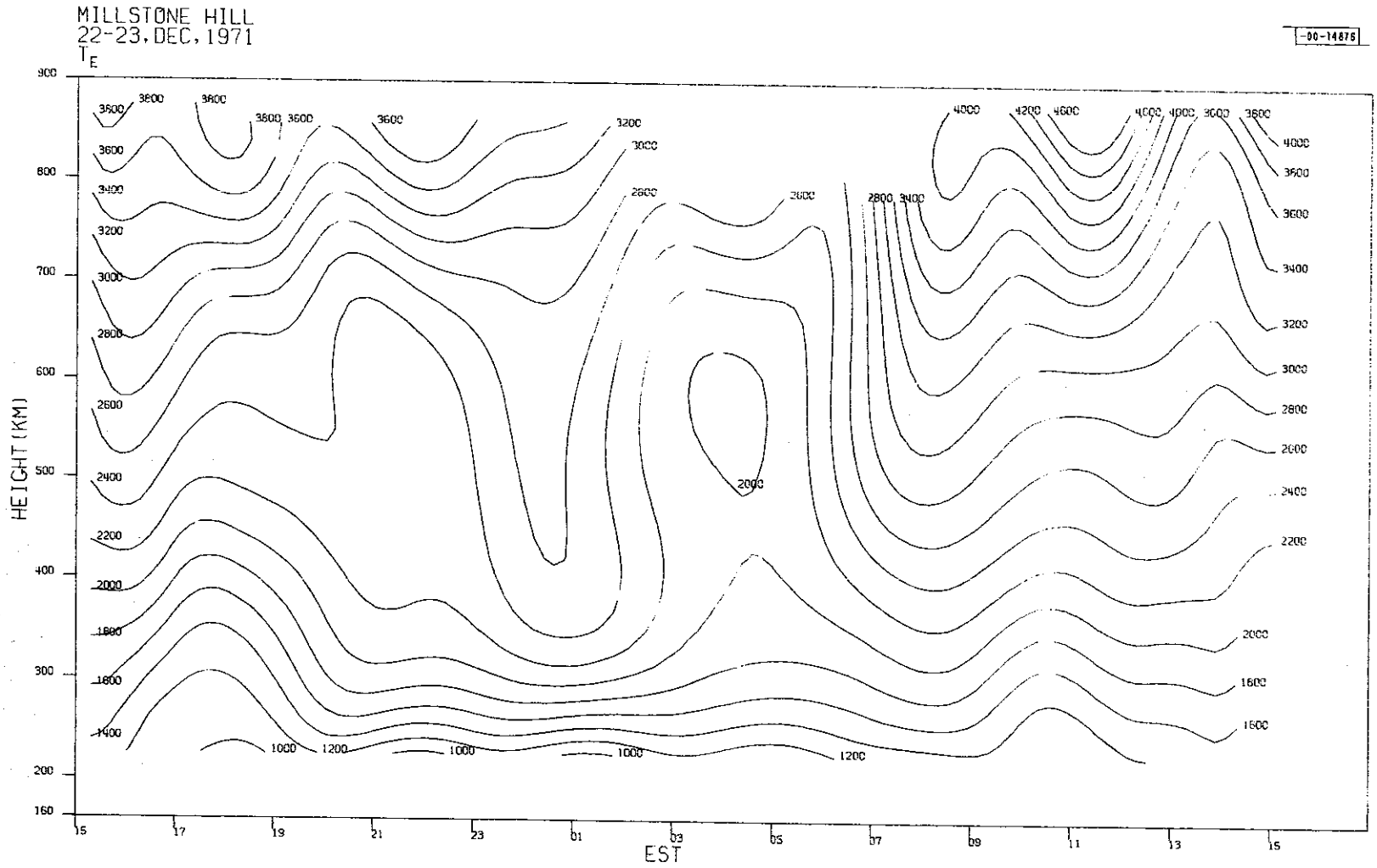

(b) T_e.

Fig. 26(a-d). Continued.

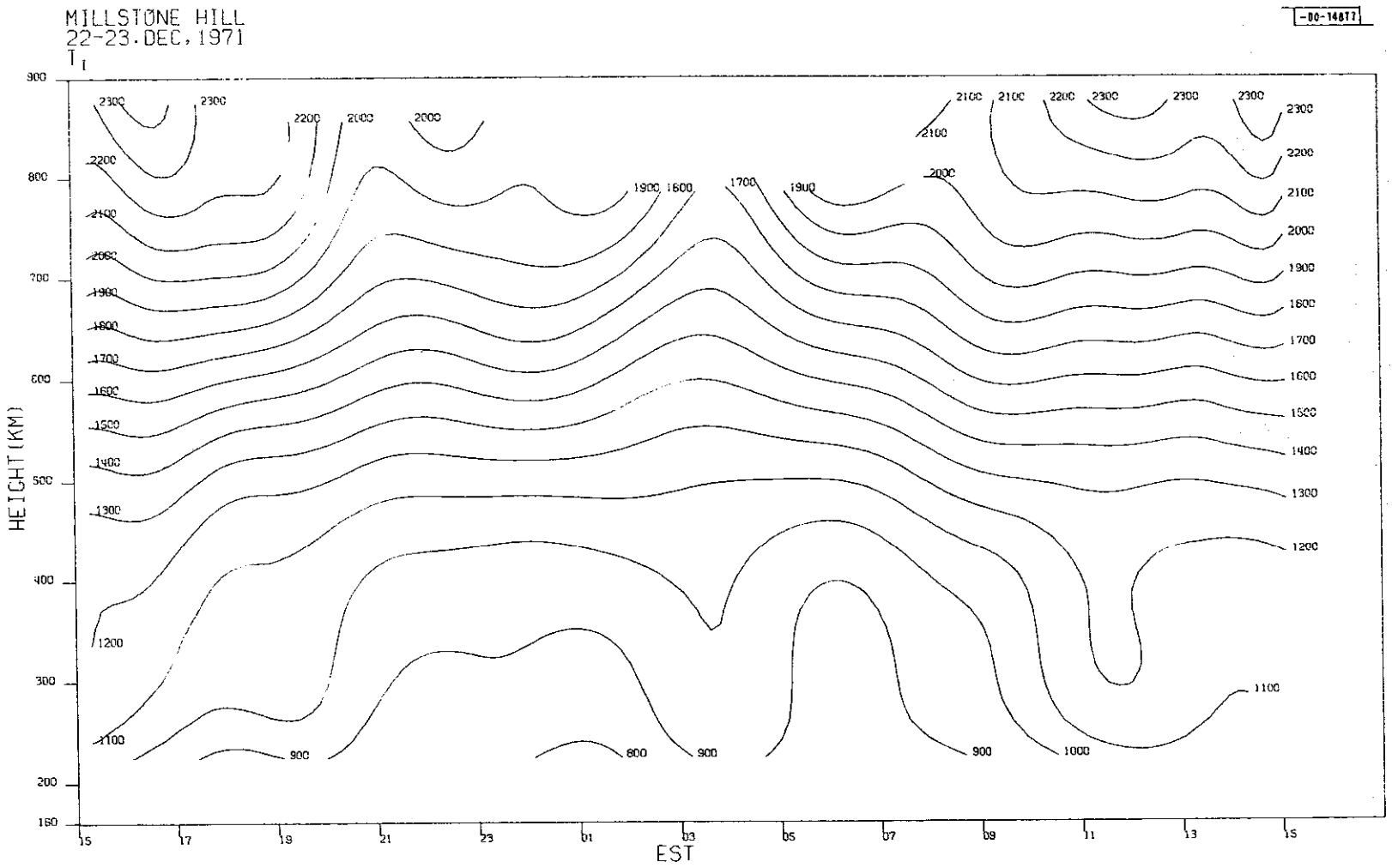

(c) T_i.

Fig. 26(a-d). Continued.

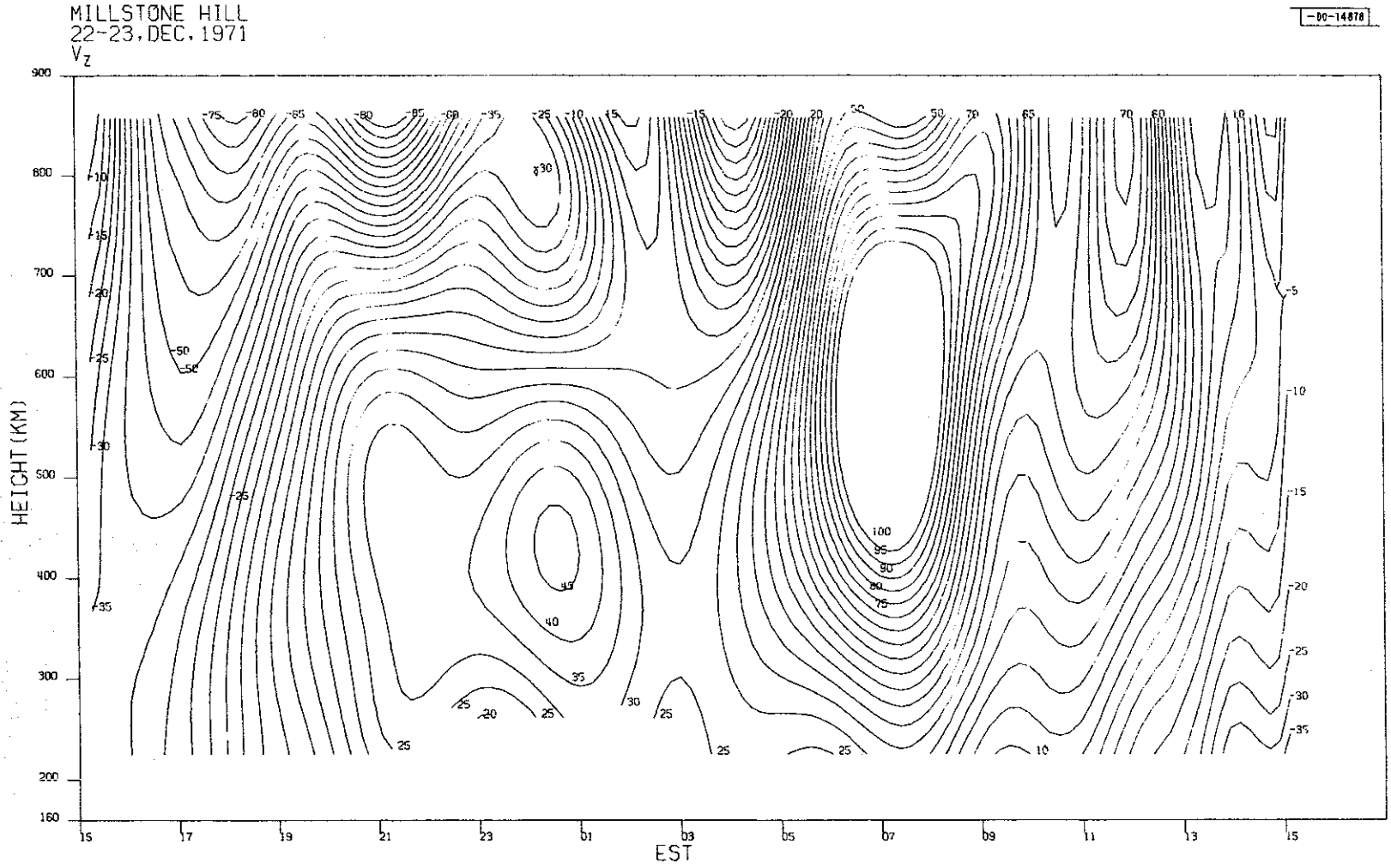

(d) V_z.

Fig. 26(a-d). Continued.

The evening increase is associated with a downward flux of ionization [see, for example, Figs. 13(a) and (d)] caused by the cooling of the layer at sunset. At sunrise, there are large upward vertical velocities caused by the growth and expansion of the layer.

By reanalyzing the spectra of the signals gathered at altitudes h > 450 km for some days between 1968 and 1973, we have been able to determine the H^+ concentration vs altitude. From these data we can infer that on summer nights the H^+ flux usually is upward even though the O^+ flux may be downward (as a consequence of the decay of the layer).[32] On some nights in 1971, however, (e.g., 27-28 May), the O^+ flux appears to be upward for a period near midnight, suggesting that the H^+ escape flux was then particularly large.

C. Magnetically Disturbed Summer Days

The days discussed above had average values of the Kp index (Table III) of $\leq 2-$. For larger average Kp values, a variety of disturbed behavior can be encountered depending upon when the observations are made in relation to the onset of the disturbance.

On four days in 1971 (30-31 March, 27-28 April, 14-15 July, and 28-29 July), very large, long-period traveling ionospheric disturbances were observed (Figs. 11, 12, 15, and 17). These waves (TIDs) are the ionospheric manifestation of acoustic-gravity waves in the neutral atmosphere. These waves cause an oscillation of the air horizontally, which drives the ions upward and downward along the magnetic field lines creating successive density increases and decreases and associated variations in T_e and T_i (Refs. 33 and 34). Long-period TIDs are thought to be generated in the auroral oval, possibly near the noon meridian and propagate to lower latitudes.

The days 30-31 March and 27-28 April both were magnetically disturbed and a TID appears to have been begun passing over the station shortly before the observations commenced. In both cases, the wave exhibited a period ~3 hours and persisted for at least 2 cycles. Significant perturbations in T_e, T_i, and V_z also were seen, especially on 30-31 March [Figs. 11(b-d)]. On 28 April, there is some evidence for a 2-hour oscillation commencing at about sunrise, but the corresponding oscillations in T_e, T_i, and V_z are absent or weak.

July 14-15 and 28-29 were relatively quiet days, yet both also showed evidence of large TIDs. On 14-15 July, oscillations in N_e appear to persist all day and are recognizable in V_z, but the daytime electron temperature shows little evidence of the wave. Some difficulty was experienced on this day in analyzing the ionosonde data owing to the large scatter in the points (possibly caused by off-vertical reflections). July 19-20 had the lowest average Kp value (1−) of the four and exhibits the weaker TID. Nevertheless, the associated oscillations of T_e, T_i, and V_z seem to be quite evident.

Extensive studies of long-period TIDs have been made at other incoherent scatter observatories, notably Arecibo[35,36] and St. Santin de Maurs.[37,38] The French group have proposed that successive large perturbations in electron density are not the manifestation of a very long period wave, but rather result from successive substorms at intervals of a few hours.[39]

The remaining disturbed summer days were 31 August – 1 September ($\overline{Kp} = 3$) and 7-9 September ($\overline{Kp} = 3-$). On 31 August – 1 September, the electron density in the F-region decayed rapidly near local sunset (i.e., much earlier than normal) to very low values that persisted until sunrise next day. This suggests that Millstone lay in the "trough" on this night. The nighttime data for the period 0200 to 0400 above 450 km were extremely poor as a consequence of the very low electron density (and hence echo power) prevailing. On the following day, the height and peak density of the F-layer were both depressed below their average monthly values –

a condition found usually on the second and (sometimes) third day of an ionospheric storm. This is believed to be caused by a reduction of the atomic oxygen abundance (relative to N_2) in the thermosphere brought about by equatorward winds.

A similar sequence of events was encountered on 7-8 September, though on this occasion there was a pronounced evening increase and the nighttime densities did not fall as low as those on 31 August – 1 September. On this night, the O^+/H^+ transition appears to have descended to a low altitude (~600 km) judging by the change in scale height apparent in Fig. 21(a). This suggests that the H^+ flux then was downward in contrast to the normal summer behavior. The behavior on these two days merits further study.

D. Magnetically Quiet Winter Behavior

In winter, the diurnal variation of the peak electron density is more pronounced. A maximum is reached usually a little after noon and there is a minimum just before sunrise. The difference between the maximum and minimum values increases markedly with increased sunspot activity. On many nights, there is a small secondary maximum after midnight around 0200 to 0400.

The variation of electron temperature is complicated by the fact that the conjugate point to Millstone remains sunlit throughout the night in winter. Fast photoelectrons created at the conjugate point escape into the protonosphere and lose much of their energy traversing the field tube to Millstone. The heat so generated is conducted downward, thereby heating the ionosphere at Millstone. Actually, following sunset, the temperature decays as the heat flux from the protonosphere is too low to maintain the local ionosphere at its daytime temperature. However, during the course of the evening, the electron density decays (reducing the local electron heat loss rate) and the temperature becomes constant or may even rise almost to its daytime value. The temperature falls again after midnight on those nights when the density is observed to increase. The temperature then rises again around sunset. A clear example of this type of behavior is evident on 2-3 November [Figs. 25(a-b)].

During winter nights, the electron density over Millstone frequently falls to such low values that the vertical velocity estimates become very unreliable. This tends to be obscured in the results presented here because the INSCON program still succeeds in generating contours. For this reason, data for V_z have not been included for the days 3-4 September, 10-11 September, and 23-24 September, when, through the use of the STATS program (Table III), the data sampling rate was reduced, and the uncertainty thereby increased further.

The days 11-12 January, 8-9 March, 26-27 October, and 2-3 November (Figs. 7, 10, 24, and 25) all appear to be quiet winter days, although there appears to be some evidence for TID activity on the last of these. During the night on the first three days listed, the peak density became roughly constant, suggesting that the lifting of the layer brought about by neutral winds combined with the H^+ flux from the protonosphere were able to balance the losses. On 2-3 November, there was a clear postmidnight density increase coinciding with a decrease in T_e. If the contours of V_z are to be trusted, they suggest that this increase was associated with an increased downward O^+ flux, suggesting that the arriving flux is particularly large at this time.

However, as we have noted elsewhere,[32] the variation of the H^+ abundance provides a more reliable guide to the protonospheric fluxes, and a detailed examination of this day must await a reanalysis of the spectra to obtain this information.

E. Magnetically Disturbed Winter Days

As noted above, no major magnetic storms occurred during any of the observing periods in 1971. The most disturbed day ($\overline{Kp} = 4$) was 30-31 March, which exhibited the effects of very large TIDs. However, 20-21 January, 18-19 February, and 22-23 December all appear somewhat abnormal and must be classed as disturbed. All had average Kp values >3−.

In winter, disturbed behavior is seen more readily during the long winter night when the density normally tends to remain constant, and the electron temperature provides a sensitive indicator of particle precipitation. January 20-21 at first sight appears to be a normal day [Fig. 8(a)], exhibiting a postmidnight increase in density. However, closer inspection reveals oscillations in h_{max}, T_e, and V_z during the 2000 to 0400 hours, suggesting the presence of a large-scale TID. The interpretation is complicated by the postmidnight increase which almost certainly caused the decrease in T_e seen after 0200 EST, and which may have a separate cause (i.e., protonospheric flux, whose onset is determined chiefly by the temporal variation of the densities of neutral atomic hydrogen and oxygen[32]).

An even more pronounced oscillation of layer height, electron temperature, and vertical velocity is evident on 18-19 February over the interval 2100 to 0600 EST. In this case, the lifting of the layer during the evening hours delayed the normal decay until 0000 to 0200 when the layer descended. The electron temperature increased rapidly during this period and then began to decrease to 0300 EST as the layer height and peak density began to rise again. For both days, these oscillations clearly are the result of changes in the vertical ion velocity. However, based on the evidence presented here, it is not possible to separate the effects of neutral air motions and electric-field induced drifts.

On 22-23 December, there was again a marked increase in the height of the F-layer during the evening associated with large positive drift values in the vicinity of $h_{max}F2$. After midnight, the density increased at all levels until about 0200 EST when the drift velocity decreased and the layer began to descend. After 0300 EST, the layer rose again as V_z began to increase and only descended at 0600 EST when sunrise occurred. Here again, cause and effect are clear, but the source of the vertical ion motion (neutral winds or electric fields) remains obscure.

As discussed previously,[7] there appears considerable evidence that substorm electric fields can penetrate to midlatitudes especially at night.[40-42] Prior to midnight, the layer is lifted by an eastward electric field and after midnight it usually is lowered by westward fields. However, it recently has been established that on disturbed nights, strong equatorward winds occur in the midnight sector[43] and these also can serve to raise the layer. A resolution of the contributions at the location of Millstone made by winds and electric fields to these nighttime perturbations must await the availability of the steerable antenna presently under construction.

IV. DERIVED QUANTITIES

A. Introduction

A number of parameters can be derived from the measurements presented here and some of these have been provided in earlier reports. Thus, for example, in Ref. 1, we examined the question of whether the observed scale height of the ionization above the F-region peak was equal to that calculated using the observed electron and ion temperatures and assuming only O^+ ions to be present. In Refs. 2 to 6, we computed average daytime (centered on midday) and nighttime (centered on midnight) temperature profiles. From these, the seasonal and sunspot

cycle variations of daytime and nighttime average electron temperature and average protonospheric heat flux were explored.[8] In Ref. 7, we examined the diurnal and seasonal variations of the vertical O^+ fluxes derived from the vertical velocity measurements. In this report, we present results obtained for the neutral exospheric temperature and thermospheric winds.

B. Exospheric Temperature – General

The neutral temperature of the exosphere can be derived from incoherent scatter measurements from thermal balance arguments.[28,44] Essentially, one equates the heat at any level in the region 300 to 500 km given from the electrons to the ions (which depends upon N_e, T_e, and T_i) to that given from the ions to the neutrals. This last depends upon N_e, T_i, T_n, and the abundance of neutral particles (principally atomic oxygen). If measurements are available at many altitudes, one may solve for N(O) by requiring that the neutral temperatures obtained follow the dependence given by Bates, viz:

$$T_n = T_\infty - (T_\infty - T_{120}) \exp[-s(h - 120)] \tag{3}$$

where T_∞ is the exospheric temperature, s is a constant (~0.02) and h is the height (km). The method has been described in a number of reviews[45,46] and will not be discussed further here.

The first significant use of the Millstone Hill data for this purpose was that of Salah and Evans,[20] who obtained T_∞ for 48 days, spanning a two-year period, March 1969 through March 1971. The daily average values T_∞, and the amplitudes of the 24-, 12-, and 8-hour components also were obtained and their dependence upon season and sunspot activity modeled.[20]

An independent model for approximately the same latitude was obtained by Alcayde[47] from the St. Santin data, which differed somewhat from that obtained at Millstone. A recent paper[48] has explored the contributions to the differences between models introduced by dissimilar reduction procedures, differences in the forms of the two models, and statistical effects of sampling. This paper[48] also provided results for the best combined model. Results from both stations contributed to the recent MSIS global model for the thermosphere.[49] The contribution of the incoherent scatter measurements has been to force the exospheric temperature to have the proper mean value and sunspot cycle dependence; these features were not modeled correctly in the earlier OGO VI mass spectrometer model.[50]

C. Exospheric Temperature – Results

As part of a study of the winds in the thermosphere (outlined in the following section) Emery[29] recalculated the exospheric temperature for the days of observation in 1970 and 1971. In these calculations, the following changes were introduced from the method employed by Salah and Evans:[20]

(1) The revised B-mode corrections (see Sec. II-D) were employed. These changed the values of T_e and T_i at low altitudes available to the INSCON smoothing program.

(2) Smoothed values of N_e, T_e, and T_i obtained from the INSCON program were used in place of the individual point values employed by Salah and Evans.[20]

(3) Estimates of the neutral density needed were taken from the MSIS model[49] instead of the Jacchia 1971 model that was the best available to Salah and Evans.[20]

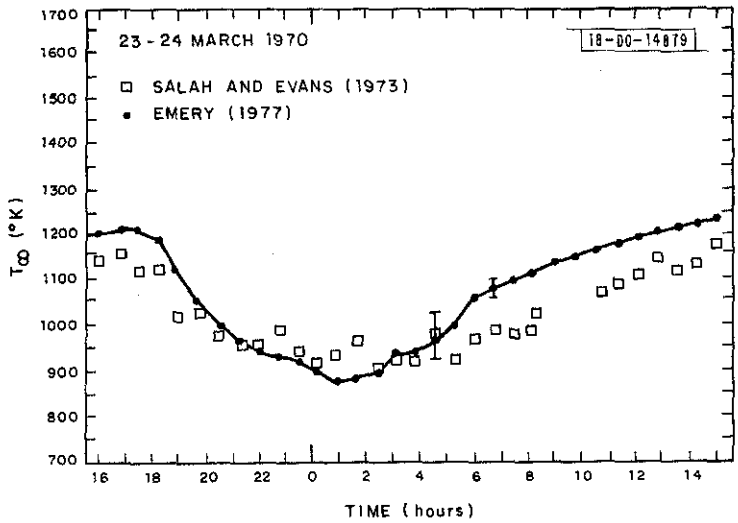

Fig. 27. Comparison of the exospheric temperature determined from the measurements on 23-24 March 1970 by Salah and Evans[20] and Emery.[29]

These changes are listed in order of their probable significance. Figure 27 provides a comparison of the results obtained for 23-24 March 1970 by the two methods. As can be seen, the new procedure has raised the daytime temperatures by almost 100°K (10 percent). The diurnal average $\overline{T}_\infty$ also has been increased from 1024° to 1077°K, i.e., by about 50°K (5 percent). Although no comparison has been undertaken, these changes are believed to bring the Millstone and St. Santin values into closer agreement for the most part. Previously, the St. Santin values of $\overline{T}_\infty$ were systematically higher than those from Millstone by an average amount of 24°K (Ref. 48). The revised reduction procedure does appear to provide closer agreement between the two data sets as can be seen in Fig. 28.

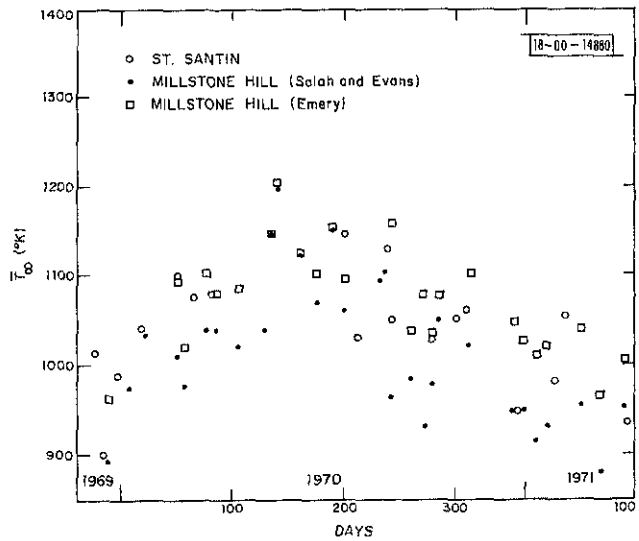

Fig. 28. Comparison of the values of the diurnally averaged exospheric temperature T_∞ common to the studies by Salah and Evans[20] and Emery[29] with results obtained in France.[47]

Data from which the exospheric temperature could be derived which is identical to that used for Figs. 27 and 28 were collected from August 1968 through January 1976. Analysis of these data to yield temperatures remains an outstanding task at this time.

D. Neutral Winds – General

In the F-region, the global variation of exospheric temperature causes global pressure variations which drive neutral winds. Attempts to compute the wind speeds have been made by a number of authors allowing for the influence of viscous, Coriolis, and ion drag forces.[51-56] These initial calculations showed that winds ~100 m/sec can be established, which should serve to drive the F-region (along magnetic field lines) to lower altitudes by day and raise it to higher altitudes by night, thereby having profound effects on the peak height and density.[57-60] This work has been reviewed by Rishbeth.[61]

In the first studies, the winds were computed using the Jacchia 1965 model atmosphere pressure variations, and a fixed profile for electron density distribution for all latitudes and time (or possibly separate profiles for day and night). Moreover, the calculations were based on solving the coupled momentum equations from which the nonlinear terms had been dropped. Recently, Blum and Harris[62] have calculated the full nonlinear solution taking as given the Jacchia 1965 pressure field and a global model for the ion densities.[63]

There are few direct methods of measuring neutral air motions at F-region heights. Some nighttime data have been obtained by observing the Doppler shift of the 6300-Å atomic oxygen line with Fabry-Perot interferometers,[64-66] and this technique has shown that the equatorward nighttime winds at midlatitudes are enhanced greatly during magnetic storms.[43]

The conclusion that horizontal neutral winds are capable of driving ionization along magnetic field lines opened the way for incoherent scatter to be used to determine the wind speed. If the horizontal wind speed in the magnetic meridian plane (approximately NS) is V_{Hn}, it will have a component $V_{Hn} \cos I$ along the magnetic field line where I is the magnetic inclination or dip angle (72° at Millstone). Through collisions, this component will attempt to drive the ions along the field line. In the absence of other effects, the ionization would be driven vertically at a speed of W_n where

$$W_n = -V_{Hn} \sin I \cos I \tag{4}$$

in which W_n is positive upward and V_{Hn} is positive poleward. Vertical motion of the ionization is opposed by downward diffusion resulting from pressure gradients in the plasma and the influence of gravity. This proceeds with a speed W_d, where

$$W_d = \frac{-2kT_i}{m_i \nu_{in}} \sin^2 I \left[\frac{(T_e + T_i)}{2T_i} \frac{\delta N_e}{N_e \delta z} + \frac{\delta (T_e + T_i)}{2T_i \delta z} + \frac{m_i g}{2kT_i} \right] \tag{5}$$

where m_i is the mass of the ions, k is Boltzmann's constant, and ν_{in} is the ion-neutral collision frequency for momentum transfer.

As a result of the competing influence of winds and diffusion, the ionization in the F-region will move with a vertical velocity V_z where

$$V_z = W_n + W_d \quad . \tag{6}$$

With the exception of ν_{in}, all the quantities in Eq. (5) can be measured by means of incoherent scatter radar and, if the collision frequency is taken from a model for the neutral atmosphere that matches the measured exospheric temperature, W_d can be calculated. Any difference between the observed value of V_z and the calculated value of W_d then gives W_n, from which the meridional neutral wind velocity V_{Hn} can be determined [via Eq. (4)].

While this technique permits only the component of the wind in the magnetic meridian to be determined, valuable results have been gathered in France[67-72] and the United States.[73-77] These observations appear to confirm the general wind pattern inferred from the static diffusion model atmospheres, but show additional features not reflected by such models, e.g., a seasonal variation in the winds at midlatitudes.

Recently Roble et al.[78] and Antoniadis[79] have developed methods of deducing zonal winds as well as the meridional component from incoherent scatter data. The method depends upon employing a three-dimensional dynamical model for the neutral atmosphere in which the latitudinal and longitudinal variations of pressure are specified by variations in the exospheric temperature T_∞. Since the incoherent scatter radar measures T_∞, the E-W variation is obtained directly; the N-S variation is obtained by adjusting the model to reproduce the observed meridional component of the winds in the presence of the observed ion densities (which control the ion drag). Roble et al.[80] have employed this approach to study 3 winter and 3 summer days data gathered at Millstone in 1969 and 1970. During summer, the daily mean zonal winds were found to be westward at about 15 m/sec and are eastward at about the same velocity in winter. The diurnally averaged meridional winds were southward with a value of ~50 m/sec in summer but weaker (~15 m/sec) and irregular in winter. These results tend to support the picture of the global thermospheric circulation presented by Dickinson et al.[81]

Employing this same approach, but using a somewhat different mathematical scheme and including curvature and other terms ignored previously, Emery[29] has obtained meridional and zonal winds over Millstone for 1970 and 1971, and these results are summarized below.

E. Neutral Winds – Analysis

The scheme outlined above for deducing winds from incoherent scatter data ignores the motion that can be imparted to the ions by electric fields. In the F-region, ions will move with a Hall drift in the presence of an imposed electric field, i.e., normal to both the electric field and the magnetic field direction.

By making measurements of the drift velocity parallel to the magnetic field line, one can isolate only the influence of winds and diffusion on the ion drift and this is the approach adopted in France.[67-72] At Arecibo, it has been the practice to measure several components of the drift velocity from which the effects due to electric fields and winds can be separated.[74,75,77] At Millstone, the observed vertical velocity V_z will comprise the sum of drifts due to winds, electric fields, and diffusion, i.e.,

$$V_z = W_n + W_d + W_E \tag{7}$$

in which

$$W_E = \frac{E_{EW}}{B} \sin I \tag{8}$$

where E_{EW} is the east-west component of the electric field and B is flux density of the earth's magnetic field. For Millstone, Eq. (8) becomes

$$W_E = 5.6\ E_{EW}\ \text{m/sec/mV} \tag{9}$$

when E_{EW} is measured in millivolts. From measurements with the L-band radar, it has been determined that typically by day $E_{EW} \leqslant 1$ mV (Ref. 73) and by night $E_{EW} \leqslant 2$ mV (Refs. 82, 83). Without introducing serious error, therefore, the effects of electric fields usually can be ignored in comparison to drifts W_n caused by neutral winds which tend to be larger. This approximation was made in the study described here.

The wind in the magnetic meridian V_{Hn} may be resolved into meridional and zonal components v (positive northward) and u (positive eastward), respectively, where

$$V_{Hn} = v \cos D + u \sin D \tag{10}$$

where D is the declination of the magnetic field (at Millstone $D = -14°$).

The meridional and zonal neutral winds are established by pressure gradients in the NS (y), EW (x) directions and coupled via Coriolis force. They are resisted by a frictional force introduced by collisions with the ions (which cannot be driven across magnetic field lines at F-region heights), and this causes the winds to blow directly from regions of high to low pressure (rather than circle them as at the earth's surface). The wind velocity can be computed from the momentum equations which, in spherical coordinates, can be written (neglecting vertical motions which are small) as[29]

$$\frac{\partial u}{\partial t} + u\frac{\partial v}{\partial x} + v\frac{\partial u}{\partial y} + \frac{-uv\tan\varphi}{r} = -\frac{1}{\rho}\frac{\partial p}{\partial x} + fv + F_x \tag{11}$$

$$\frac{\partial v}{\partial t} + u\frac{\partial v}{\partial x} + v\frac{\partial v}{\partial y} + \frac{u^2\tan\varphi}{r} = -\frac{1}{\rho}\frac{\partial p}{\partial y} - fu + F_y \tag{12}$$

where ρ and p are the neutral density and pressure; $f = 2\Omega \sin\varphi$ is the Coriolis parameter, where Ω is the earth's angular velocity and φ the latitude; r is the distance from the center of the earth; and F_x and F_y are the frictional forces in the x and y directions. Friction is provided by ion drag and molecular viscosity. Ion drag depends on the difference in the velocities of the neutral winds and the ions, e.g., $(u - u_{ions})$ at a rate

$$\text{ion drag} = \lambda(u_{ion} - u) \tag{13}$$

where $\lambda = n_i\mu_{in}\nu_{in}/\rho$ in which μ_{in} is the ion-neutral reduced particle mass and ν_{in} the ion-neutral collision frequency. For the study of winds at Millstone where electric fields were neglected, u_{ion} was set to zero, but calculations were carried out to determine the influence of the fields that are thought to exist at quiet times.[29]

The viscous force depends upon the gradient of the product of the molecular viscosity μ and the velocity gradient in each direction. Neglecting second-order terms, it can be written

$$\text{viscous force} = \frac{1}{\rho}\left[\mu\left(\frac{\partial^2 v}{\partial x^2} + \frac{\partial^2 v}{\partial y^2} + \frac{\partial^2 v}{\partial z^2}\right) + \frac{\partial\mu}{\partial z}\frac{\partial v}{\partial z}\right] \tag{14}$$

where z is in the vertical direction. The equations solved by Emery[29] were

$$0 = \frac{\partial u}{\partial t} + \frac{uv\tan\varphi}{r} - \frac{1}{\rho}\frac{\partial p}{\partial x} + fv + \frac{1}{\rho}\left(\mu\frac{\partial^2 u}{\partial z^2} + \frac{\partial\mu}{\partial z}\frac{\partial u}{\partial z}\right) - \lambda u \tag{15}$$

$$0 = -\frac{\partial v}{\partial t} - \frac{u^2 \tan\varphi}{r} - \frac{1}{\rho}\frac{\partial p}{\partial y} - fu + \frac{1}{\rho}\left(\mu \frac{\partial^2 v}{\partial z^2} + \frac{\partial \mu}{\partial z}\frac{\partial v}{\partial z}\right) - \lambda v \qquad (16)$$

where two nonlinear terms and two viscous terms have been dropped from each equation. The neglect of the horizontal viscous terms [Eq. (14)] was not thought to be serous, but dropping the nonlinear terms caused significant changes in the results and considerable effort was expended in determining the size of these.

Since the ion drag over Millstone (which depends upon the ion density $N_i = N_e$) is known from the observations, the momentum equations can be solved for u and v provided the zonal and meridional pressure gradients are known. To establish these, a simple static diffusion model of the atmosphere above Millstone was constructed in which the temperature varied vertically according to the Bates formula [Eq. (3)] and the density was established by values adopted for a lower boundary (120 km) taken as the annual mean of the MSIS model.[49] To reflect the variation in composition that is known to occur with season, a variation in the O/N_2 ratio at the lower boundary was introduced that matched that found by Cox and Evans[84] from previous incoherent scatter studies at Millstone. The zonal pressure variation now was set simply by the diurnal variation of the observed exospheric temperature T_∞. That is, the earth was assumed to rotate under a fixed pattern of pressure variation which is sampled by the radar as a function of time. Since the pattern must close, marked differences in T_∞ between the beginning and the end of a 24-hour run could not be tolerated and some days could not be analyzed on this account. To provide a continuous smooth variation of T_∞ (and hence well-behaved gradients), the actual values were replaced by a harmonic fit consisting of a mean, 24-, 12-, and 8-hour terms.

The remaining unknown is the NS pressure gradient and this was found by solving Eqs. (15) and (16) so as to produce winds u and v that together matched the measured component V_{Hn} in Eq. (10). The procedure employed was similar to that used by Antoniadis.[79] Each horizontal equation of motion was solved separately at one time step using a Crank-Nicholson iteration scheme until the derived meridional velocity V_{Hn} agreed with that measured to within 1 m/sec. The NS pressure gradients required to do this (represented as latitudinal gradients in exospheric temperature $\partial T_\infty/\partial\varphi$) were stored. These values subsequently were smoothed with a three-term harmonic fit and the momentum equations resolved to obtain final estimates of u and v.

By replacing the pressure gradients obtained from the incoherent scatter measurements with equivalent pressure gradients from the MSIS model and repeating this last step, the winds expected over Millstone on each day anticipated from the most recent model atmosphere could be calculated.

F. Neutral Winds – Diurnal Variation Results

Neutral wind results for one representative winter and summer day will be discussed here. Figures 29(a-d) present results for 20-21 January 1971. In Fig. 29(a), the final calculated value of the horizontal neutral wind in the magnetic meridian V_{Hn} is compared with that obtained directly from the smoothed measurements of V_z, N_e, T_e, and T_i. It can be seen that overall the fit is quite good. The experimental curve is compared with the winds predicted from the MSIS model in Fig. 29(b). Here the agreement in the daytime again is considered excellent, but the presence of the large nighttime TID (discussed in Sec. III-D) clearly is evident. This is thought to have given rise to the large southward surge of wind at 0200. Figures 20(c) and (d) show the zonal and meridional components u and v of the winds (as well as V_{Hn}) corresponding to these

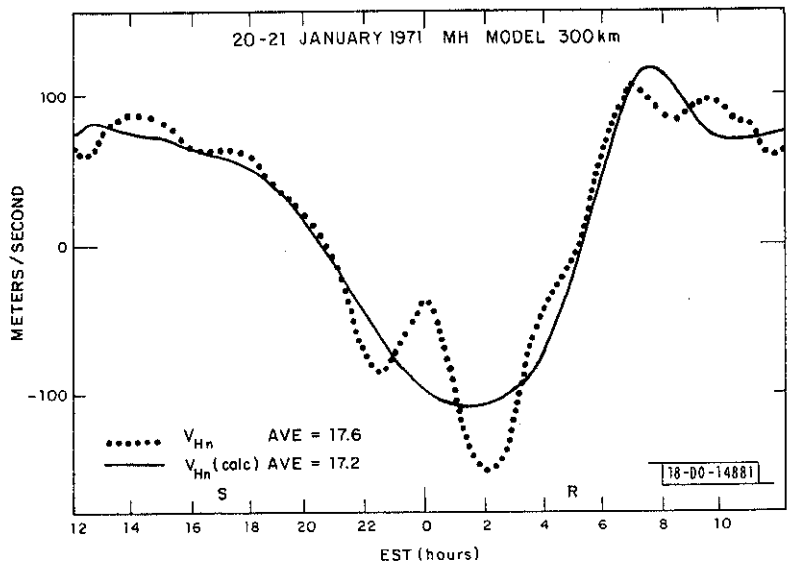

(a) V_{Hn} observed and calculated from the momentum equations.

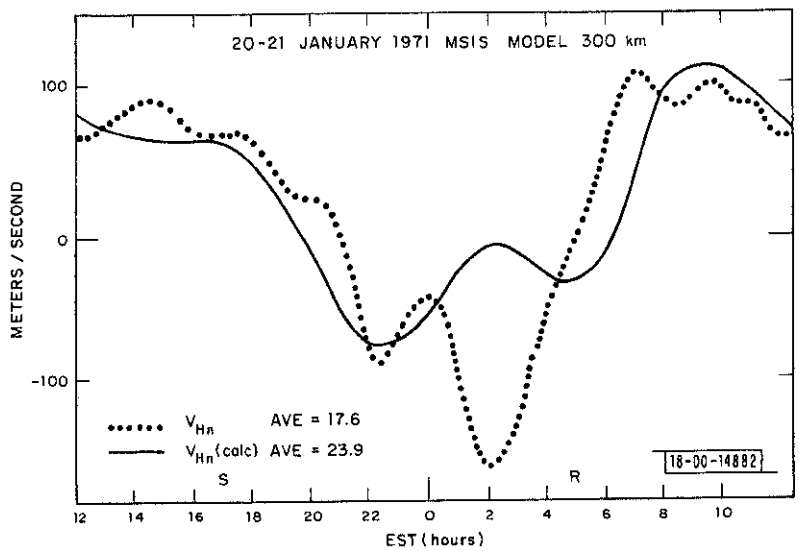

(b) V_{Hn} observed and expected from the MSIS model.

Fig. 29(a-d). Neutral wind results for 20-21 January 1971.

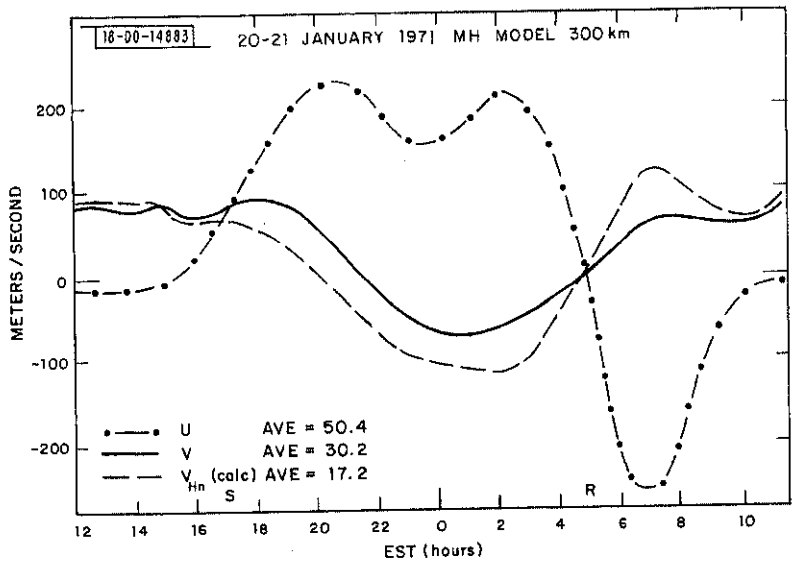

(c) U, V, and V_{Hn} calculated from the Millstone data.

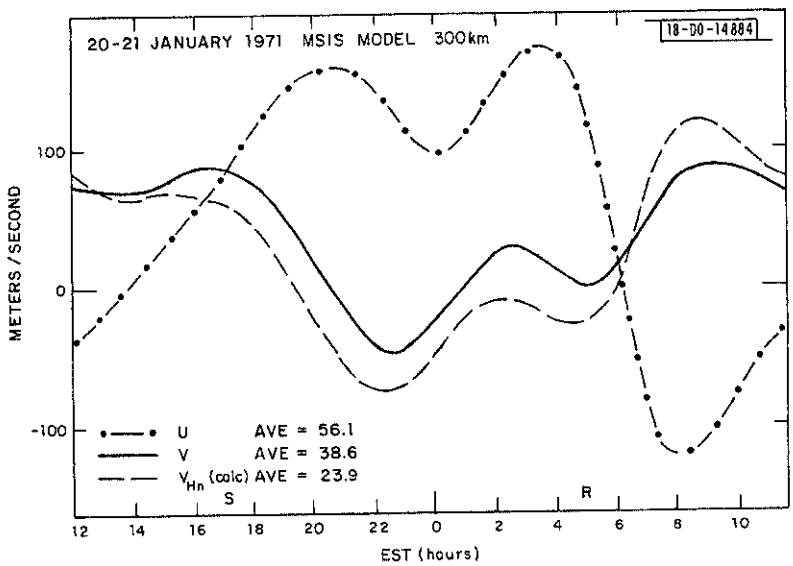

(d) U, V, and V_{Hn} calculated from the MSIS model.

Fig. 29(a-d). Continued.

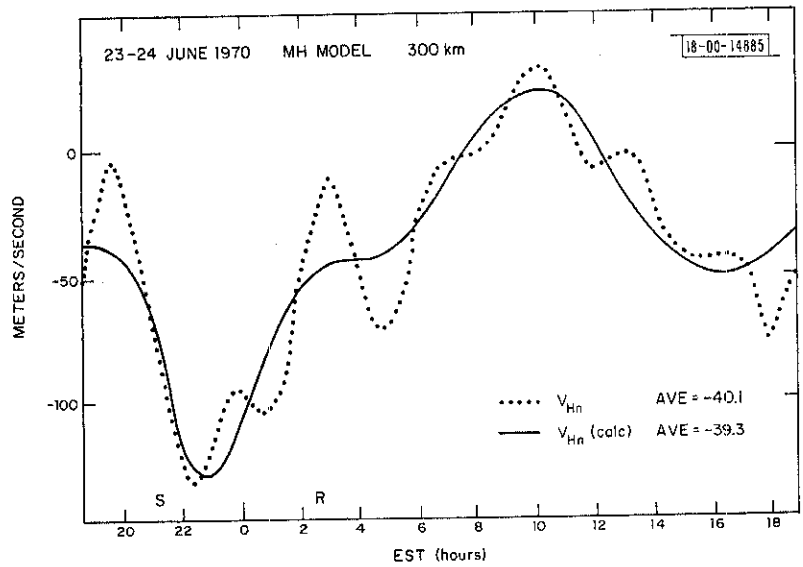

(a) V_{Hn} observed and calculated from the momentum equations.

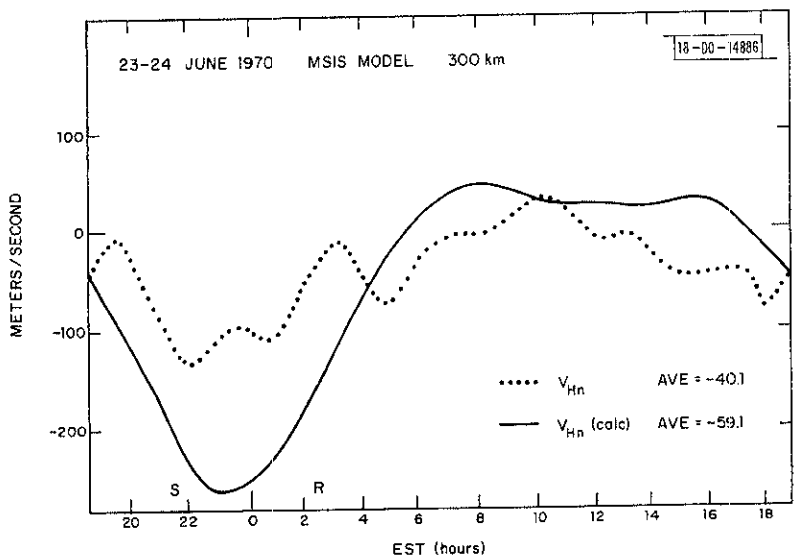

(b) V_{Hn} observed and expected from the MSIS model.

Fig. 30(a-d). Neutral wind results for 23-24 June 1970.

two cases. As anticipated, the meridional winds tend to be northward by day and southward at night. The zonal winds are eastward from about 1400 hours until around 0400, when they reverse and become westward.

Emery[29] has discussed at length the uncertainties in these results. Errors arise from experimental measurement accuracy limitations which combine to introduce uncertainties in T_∞ (and hence $\partial T_\infty/\partial t$), V_z, and W_d (and hence in V_{Hn}). The method of analysis, in particular the neglect of nonlinear terms and uncertainty in the form of the ion-neutral collision frequency introduce approximately equal amounts of error in the range 10 to 20 m/sec depending upon time of day.

The neglect of electric fields affects the interpretation of the drift observations [via Eq. (7)] as well as the ion drag parameter [Eq. (13)] employed in the solution of the momentum equations. Calculations performed with models for the ion motion suggest that the neutral winds obtained when electric fields are neglected (e.g., Fig. 29) are approximately correct for the rest frame of the ions.

Results for a summer day (23-24 June 1970) are presented in Figs. 30(a-d). This day appears to have been another one in which a large TID may have been present [Fig. 30(a)]. In this case, its effects can be traced in the electron density contours prior to about 0200 hours.[8] The three-harmonic fit to the calculated winds smooths out this variation.

The experimental estimates of V_{Hn} show significantly less variation than anticipated from the MSIS mode [Fig. 30(b)]. However, this is not typical and in part may be attributed to the influence of the TID which appears to have particularly influenced the velocities prior to 0200 hours when they are expected to be large and equatorward.

In Fig. 30(c), the zonal and meridional neutral winds that fit the Millstone data are presented. In this case, the zonal wind variations are very much larger than the meridional reaching 380 m/sec eastward just after sunset and 275 m/sec westward after sunrise. These large values are introduced chiefly by the large temperature gradients found around these times which in turn were caused by the presence of a deep temperature minimum centered on midnight. These large zonal velocities may not be real since they equal or exceed the angular speed of the earth at the latitude of Millstone (~340 m/sec). Moreover, such large values were not found in the MSIS model results [Fig. 30(d)]. These results were not unique. On 5 summer days examined for 1970 and 1971, the zonal velocity reached values >600 m/sec near dawn and in another 7 (mostly summer) days >400 m/sec. At such time the pressure gradient becomes balanced chiefly by the Coriolis force (rather than ion drag). This can introduce stability problems since the meridional wind is constrained by the measurements and is not completely free to respond. These large zonal winds appear to be associated with large temperature gradients near sunrise and in a complete solution of the problem (i.e., including all nonlinear terms) would probably be reduced considerably. Unfortunately, any attempts to test this prediction by including such terms as outside forcing functions could not be conducted since these large values meant that time and longitude were no longer interchangeable. In sum, Emery[29] concluded that the summer results probably were less reliable than the winter ones, especially around the times of sunrise and sunset.

G. Neutral Winds – Seasonal Variations

As noted above, seasonal variations in the thermospheric winds were found in previous studies.[78,80] A central objective of the present study was to determine the magnitude of any

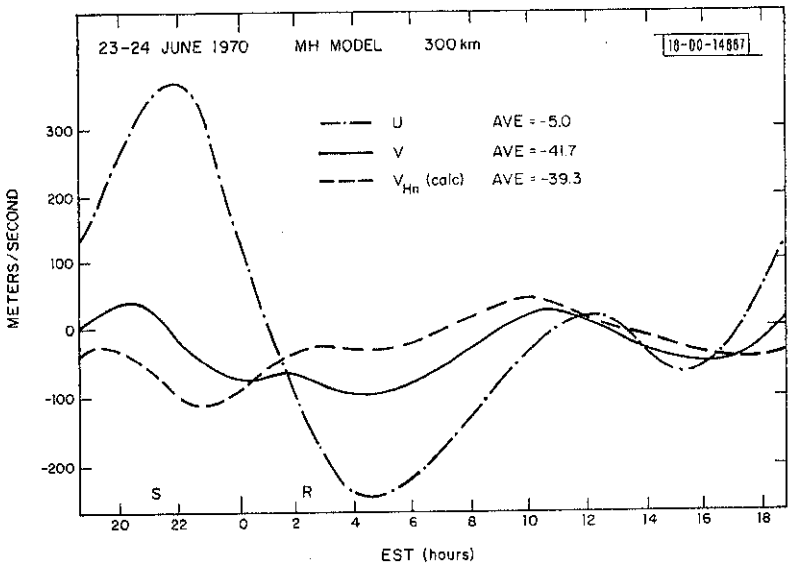

(c) U, V, and V_{Hn} calculated from the Millstone data.

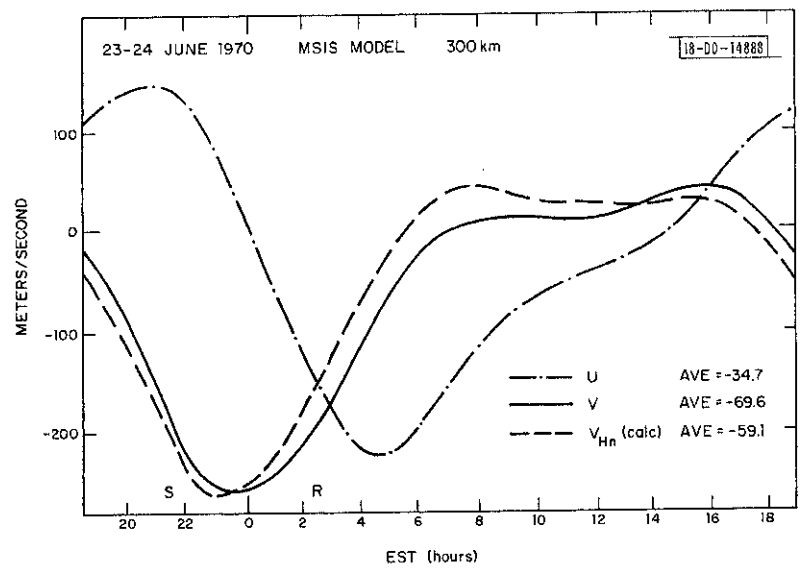

(d) U, V, and V_{Hn} calculated from the MSIS model.

Fig. 30(a-d). Continued.

variations in the diurnally averaged meridional and zonal winds. Figures 31(a-b) show the results obtained for the average meridional wind for 36 days in 1970 and 1971 for the Millstone Hill and MSIS results. Also shown is the best fitting curve that can be represented by a mean, annual, and semiannual variation. The trends are quite similar for both cases. In winter, the mean winds are poleward with a velocity of ~20 m/sec. In summer, the winds are equatorward

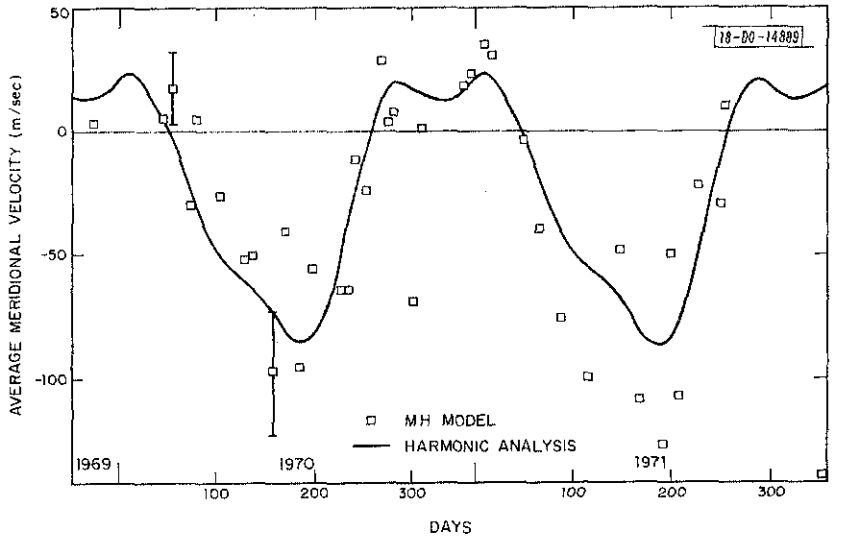

(a) Based on the Millstone Hill results.

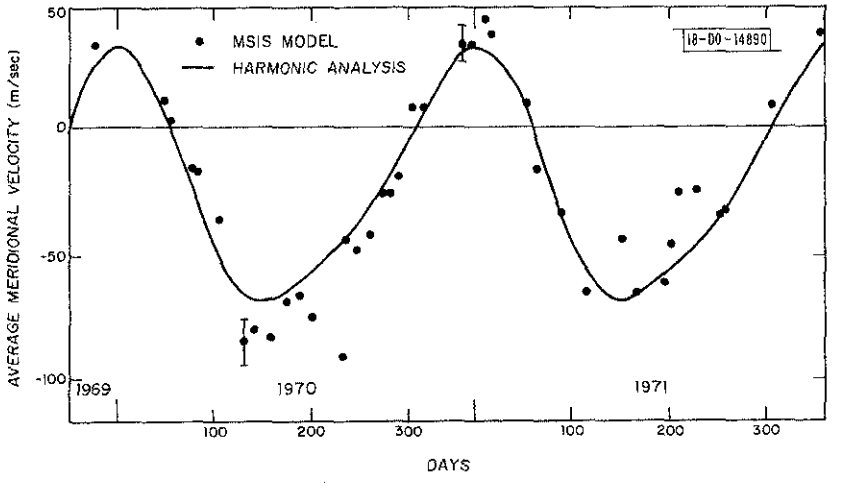

(b) Based on the MSIS model pressure variations.

Fig. 31(a-b). The seasonal variation of the diurnally averaged meridional wind V and best fitting curve that can be represented by a mean, annual, and semiannual variations.

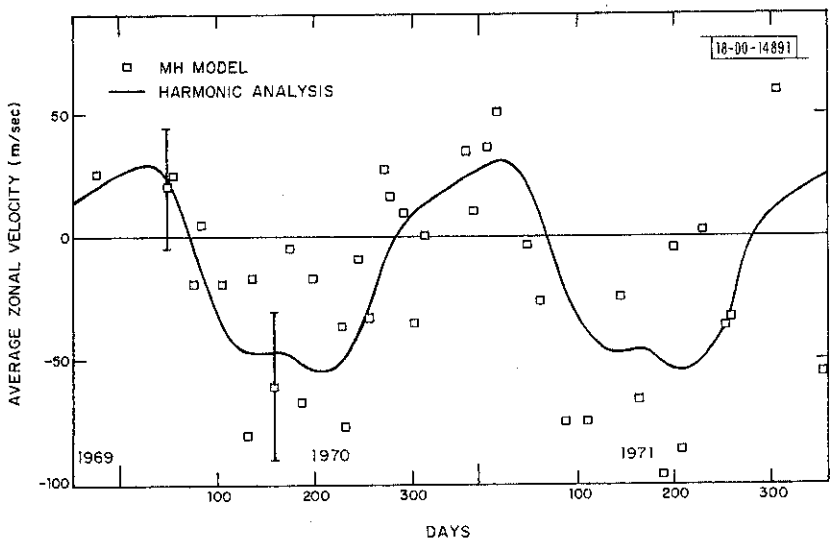

(a) Based on the Millstone Hill results.

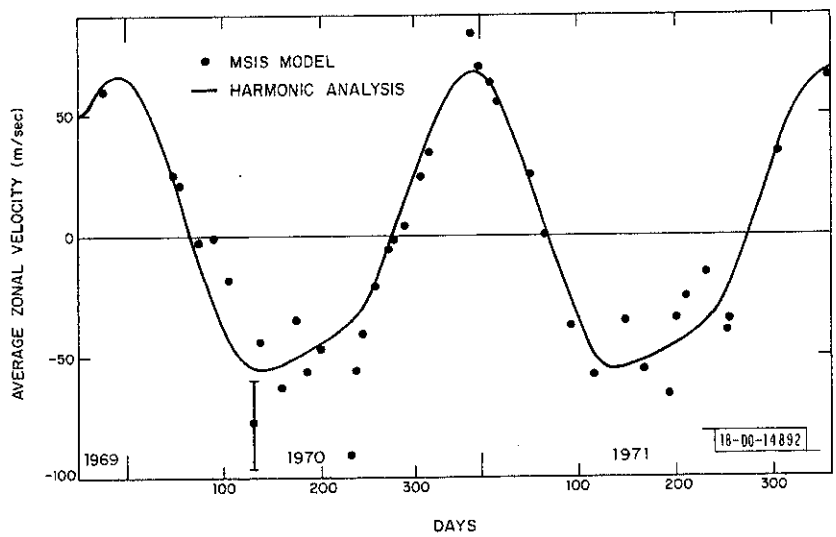

(b) Based on the MSIS model pressure variations.

Fig. 32(a-b). The seasonal variation of the diurnally averaged zonal wind u and best fitting curve that can be represented by a mean, annual, and semiannual variations.

with an average value of ~70 m/sec. The Millstone results suggest that the variation is more square wave than sinusoidal with a rapid variation around equinox, although the "winter" period appears shorter than "summer." This pattern is consistent with the characteristic "winter" and "summer" behavior for the electron density distribution discussed above and in previous papers.[4-8,12,15]

It is thought that the mean meridional winds transport atomic oxygen from the summer to winter hemisphere, thereby enriching the O/N_2 ratio in winter and decreasing it in the summer hemisphere.[85] This gives rise to the observed changes of neutral composition (e.g., Ref. 84) and accounts for the seasonal anomaly in the peak electron density. The very large differences in the diurnal behavior in summer and winter also reflect seasonal variations in the behavior of the neutral winds.[57,58]

According to Dickinson et al.,[81] this meridional circulation is driven by solar extreme ultraviolet (EUV) and auroral heating which, in the summer hemisphere, combine to create a Hadley cell that extends across the equator into the winter hemisphere. It is opposed at high latitudes in the winter hemisphere by the auroral heating in that hemisphere. The results presented here appear to support this picture.

The mean zonal winds are shown in Figs. 32(a-b). Here again, the Millstone results, though more scattered than those obtained using the MSIS model, appear to suggest a characteristic summer and winter behavior. However, in this case there appears to be no significant annual average (i.e., no superrotation); such an effect would not be anticipated from the analysis presented here.

Emery[29] searched for a dependence of the mean winds with a degree of magnetic disturbance and found a trend of increasing equatorward meridional winds for days with $A_p > 7$. However, this broke down for larger values of A_p and it seems that a more careful study, possibly allowing for the effects of electric fields would be needed. An attempt presently is under way to attempt to isolate changes in the winds associated with magnetically disturbed behavior.

ACKNOWLEDGMENTS

The authors are indebted to W. A. Reid, J. H. McNally, D. E. Olden, and others of the staff at Millstone Hill who assisted in operating and maintaining the equipment employed to gather the data reported here, and to Mrs. A. Freeman who contributed to the reduction of the results. During 1971, the incoherent scatter work at Millstone was supported by the U. S. Army as part of a program of radar propagation study. Preparation of this report was supported by the National Science Foundation under Grant ATM 75-22193.

REFERENCES

1. J. V. Evans, "Ionospheric Backscatter Observations at Millstone Hill," Technical Report 374, Lincoln Laboratory, M. I. T. (22 January 1965), DDC AD-616607.
2. _____, "Millstone Hill Thomson Scatter Results for 1964," Technical Report 430, Lincoln Laboratory, M. I. T. (15 November 1967), DDC AD-668436.
3. _____, "Millstone Hill Thomson Scatter Results for 1965," Technical Report 474, Lincoln Laboratory, M. I. T. (18 December 1969), DDC AD-707501.
4. _____, "Millstone Hill Thomson Scatter Results for 1966," Technical Report 481, Lincoln Laboratory, M. I. T. (15 December 1970), DDC AD-725742.
5. _____, "Millstone Hill Thomson Scatter Results for 1967," Technical Report 482, Lincoln Laboratory, M. I. T. (22 July 1971), DDC AD-735727.
6. _____, "Millstone Hill Thomson Scatter Results for 1968," Technical Report 499, Lincoln Laboratory, M. I. T. (23 January 1973), DDC AD-767251/2.
7. _____, "Millstone Hill Thomson Scatter Results for 1969," Technical Report 513, Lincoln Laboratory, M. I. T. (23 July 1974), DDC AD-A008505/0.
8. J. V. Evans and J. M. Holt, "Millstone Hill Thomson Scatter Results for 1970," Technical Report 522, Lincoln Laboratory, M. I. T. (11 May 1976).
9. J. V. Evans, Planet. Space Sci. 13, 1031 (1965), DDC AD-616607.
10. _____, J. Geophys. Res. 70, 1175 (1965), DDC AD-614310.
11. _____, Planet. Space Sci. 15, 1387 (1967).
12. _____, Planet. Space Sci. 18, 1225 (1970), DDC AD-716056.
13. _____, J. Atmos. Terr. Phys. 32, 1629 (1970), DDC AD-716057.
14. _____, J. Geophys. Res. 75, 4803 and 4815 (1970), DDC AD-714447 and DDC AD-714446, respectively.
15. _____, Planet. Space Sci. 21, 763 (1973), DDC AD-772137/6.
16. _____, J. Atmos. Terr. Phys. 35, 593 (1973), DDC AD-771877/8.
17. _____, Planet. Space Sci. 23, 1461 and 1611 (1975).
18. G. W. Armistead, J. V. Evans, and W. A. Reid, Radio Sci. 7, 153 (1972).
19. J. V. Evans and W. L. Oliver, Radio Sci. 1, 103 (1972).
20. J. E. Salah and J. V. Evans, Space Research XIII (Akademie-Verlag, Berlin, 1973), pp. 267-286.
21. J. E. Salah, J. Atmos. Terr. Phys. 36, 74 (1974).
22. J. E. Salah, R. H. Wand, and J. V. Evans, Radio Sci. 10, 347 (1975).
23. J. E. Salah, J. V. Evans, and R. H. Wand, Radio Sci. 9, 231 (1974).
24. R. J. Cicerone and S. A. Bowhill, Radio Sci. 6, 957 (1971).
25. J. V. Evans and I. J. Gastman, J. Geophys. Res. 75, 807 (1970).
26. R. J. Cicerone, Rev. Geophys. and Space Phys. 12, 259 (1974).
27. J. F. Noxon and J. V. Evans, Planet. Space Sci. 24, 425 (1976).
28. J. S. Nisbet, J. Atmos. Sci. 24, 586 (1967).
29. B. A. Emery, "Seasonal Wind Variations in the Mid-Latitude Neutral Thermosphere," Ph. D. Thesis, Meteorology Department, M. I. T. (May 1977).
30. J. V. Evans, R. F. Julian, and W. A. Reid, "Incoherent Scatter Measurements of F-Region Density, Temperatures, and Vertical Velocity at Millstone Hill," Technical Report 477, Lincoln Laboratory, M. I. T. (6 February 1970), DDC AD-706863.
31. J. V. Evans, editor, "Millstone Hill Radar Propagation Study: Scientific Results," Technical Report 509, Lincoln Laboratory, M. I. T. (13 November 1973), DDC AD-781179/7 (Part I), DDC AD-782748/8 (Part II), DDC AD-780519/5 (Part III).
32. J. V. Evans and J. M. Holt, "Nighttime Proton Fluxes at Millstone Hill," Trans. Am. Geophys. Union (EOS) 58, 453 (1977).

33. K. C. Yeh and C. H. Liu, Rev. Geophys. and Space Phys. 12, 193 (1974).
34. S. H. Francis, J. Atmos. Terr. Phys. 37, 1011 (1975).
35. G. Thome, J. Geophys. Res. 73, 6319 (1968).
36. R. M. Harper, J. Geophys. Res. 77, 1311 (1972).
37. J. Testud, J. Atmos. Terr. Phys. 32, 1793 (1970).
38. D. Alcayde, J. Testud, G. Vasseur, and P. Waldteufel, J. Atmos. Terr. Phys. 34, 1037 (1972).
39. J. M. Odoux, Ann. Geophys. 28, 287 (1972).
40. T. E. Van Zandt, V. L. Peterson, and A. R. Laird, J. Geophys. Res. 76, 278 (1971).
41. C. G. Park, J. Geophys. Res. 76, 4650 (1971).
42. C. G. Park and C. I. Meng, J. Geophys. Res. 76, 8326 (1971); also 78, 3828 (1973).
43. G. Hernandez and R. G. Roble, J. Geophys. Res. 81, 5173 (1976).
44. H. Carru, M. Petit, G. Vasseur, and P. Waldteufel, Ann. Geophys. 25, 485 (1967).
45. J. V. Evans, Proc. IEEE 57, 496 (1969).
46. _____, J. Atmos. Terr. Phys. 36, 2183 (1974).
47. D. Alcayde, Radio Sci. 9, 239 (1974).
48. J. E. Salah, J. V. Evans, D. Alcayde, and P. Bauer, Ann. Geophys. 32, 257 (1976).
49. A. E. Hedin, J. E. Salah, J. V. Evans, C. A. Reber, G. P. Newton, N. W. Spencer, D. C. Kayser, D. Alcayde, P. Bauer, L. Cogger, and J. P. McClure, J. Geophys. Res. 82, 2139 (1977).
50. A. E. Hedin, H. A. Mayr, C. A. Reber, N. W. Spencer, and G. R. Carignan, J. Geophys. Res. 79, 215 (1974).
51. G. J. Bailey, R. J. Moffett, and H. Rishbeth, J. Atmos. Terr. Phys. 31, 253 (1969).
52. J. E. Geisler, J. Atmos. Terr. Phys. 29, 1469 (1967).
53. H. Kohl and J. W. King, J. Atmos. Terr. Phys. 29, 1045 (1967).
54. J. E. Geisler, J. Atmos. Terr. Phys. 28, 703 (1966).
55. H. Rishbeth, R. J. Moffett, and G. J. Bailey, J. Atmos. Terr. Phys. 31, 1035 (1969).
56. P. Stubbe, J. Atmos. Terr. Phys. 32, 865 (1970).
57. H. Kohl, J. W. King, and D. Eccles, J. Atmos. Terr. Phys. 30, 1733 (1968).
58. H. Rishbeth, J. Atmos. Terr. Phys. 29, 225 (1967); also 30, 63 (1968).
59. M. F. K. Abur-Robb, Planet. Space Sci. 17, 1269 (1969).
60. D. L. Sterling, W. B. Hanson, R. J. Moffett, and R. G. Baxter, Radio Sci. 4, 1005 (1969).
61. H. Rishbeth, J. Atmos. Terr. Phys. 34, 1 (1972); also 36, 2309 (1974).
62. P. W. Blum and I. Harris, J. Geophys. Res. 37, 193 and 213 (1975).
63. J. S. Nisbet, Radio Sci. 6, 437 (1971).
64. P. B. Hays and R. G. Roble, J. Geophys. Res. 76, 5316 (1971).
65. J. W. Meriwether, J. P. Heppner, J. D. Stolarik, and E. M. Westcott, J. Geophys. Res. 78, 6643 (1973).
66. G. Hernandez and R. G. Roble, J. Geophys. Res. 81, 2065 (1976).
67. G. Vasseur, Ann. Geophys. 25, 517 (1969).
68. _____, J. Atmos. Terr. Phys. 31, 397 (1969).
69. P. Amayenc and C. Reddy, Planet. Space Sci. 20, 1269 (1972).
70. P. Amayenc and G. Vasseur, J. Atmos. Terr. Phys. 34, 351 (1972).
71. P. Amayenc, J. Fontanari, and D. Alcayde, J. Atmos. Terr. Phys. 35, 1499 (1973).
72. P. Amayenc, Radio Sci. 9, 281 (1974).

73. J. V. Evans, Radio Sci. 6, 609 (1971).

74. R. A. Behnke and R. M. Harper, J. Geophys. Res. 78, 8222 (1973).

75. R. M. Harper, J. Atmos. Terr. Phys. 35, 2023 (1973).

76. J. E. Salah and J. M. Holt, Radio Sci. 9, 310 (1974).

77. R. A. Behnke and H. Kohl, J. Atmos. Terr. Phys. 36, 325 (1974).

78. R. G. Roble, B. A. Emery, J. E. Salah, and P. B. Hays, J. Geophys. Res. 79, 2868 (1974).

79. D. A. Antoniadis, J. Atmos. Terr. Phys. 38, 187 (1976).

80. R. G. Roble, J. E. Salah, and B. A. Emery, "The Seasonal Variation of the Diurnal Thermospheric Winds over Millstone Hill," paper presented to the 16th General Assembly IUGG, Grenoble, France, 1975.

81. R. E. Dickinson, E. C. Ridley, and R. G. Roble, J. Atmos. Sci. 32, 1737 (1975).

82. J. V. Evans, J. Geophys. Res. 77, 2341 (1972).

83. V. W. J. H. Kirchhoff and L. A. Carpenter, J. Atmos. Terr. Phys. 37, 419 (1975).

84. L. P. Cox and J. V. Evans, J. Geophys. Res. 75, 159 (1970), DDC AD-703492.

85. H. G. Mayr and H. Volland, J. Geophys. Res. 77, 6774 (1972).

APPENDIX
INSCON SUMMARY – 6 OCTOBER 1977

DATE	TYPE		START (EST)	END (EST)	TEST VALUE	KDAT	FIT NO.
11-12,JAN,1971	DENSITY	RETIAS	1638	1631	.45849E 01	101	710110
11-12,JAN,1971	ELECTRON TEMPERATURE	RETIAS	1638	1631	-.77537E 03	203	710110
11-12,JAN,1971	ELECTRON TEMPERATURE	RETIAS	1638	1631	-.77670E 03	293	710110
11-12,JAN,1971	ION TEMPERATURE	RETIAS	1638	1631	-.69402E 03	303	710110
11-12,JAN,1971	ION TEMPERATURE	RETIAS	1638	1631	-.69404E 03	393	710110
11-12,JAN,1971	VERTICAL ION DRIFT	RETIAS	1638	1631	-.26238E 03	1001	710110
11-12,JAN,1971	VERTICAL ION DRIFT	RETIAS	1638	1631	-.26247E 03	1091	710110
20-21,JAN,1971	DENSITY	DRIFTS	1248	1218	.52372E 01	101	710200
20-21,JAN,1971	ELECTRON TEMPERATURE	DRIFTS	1248	1218	-.88985E 03	203	710200
20-21,JAN,1971	ELECTRON TEMPERATURE	DRIFTS	1248	1218	-.89024E 03	293	710200
20-21,JAN,1971	ION TEMPERATURE	DRIFTS	1248	1218	-.70507E 03	303	710200
20-21,JAN,1971	ION TEMPERATURE	DRIFTS	1248	1218	-.70514E 03	393	710200
20-21,JAN,1971	VERTICAL ION DRIFT	DRIFTS	1248	1218	-.26378E 03	1001	710200
20-21,JAN,1971	VERTICAL ION DRIFT	DRIFTS	1248	1218	-.26408E 03	1091	710200
16,FEB,1971	DENSITY	RETIAS	0052	0542	-.35715E 01	101	710470
16,FEB,1971	ELECTRON TEMPERATURE	RETIAS	0052	0542	-.74372E 03	203	710470
16,FEB,1971	ION TEMPERATURE	RETIAS	0052	0542	-.62468E 03	303	710470
16,FEB,1971	VERTICAL ION DRIFT	RETIAS	0052	0542	-.31888E 03	1001	710470
16,FEB,1971	ELECTRON TEMPERATURE	RETIAS	0052	0542	-.74010E 03	293	710470
16,FEB,1971	ION TEMPERATURE	RETIAS	0052	0542	-.62444E 03	393	710470
16,FEB,1971	VERTICAL ION DRIFT	RETIAS	0052	0542	-.31719E 03	1091	710470
18-19,FEB,1971	DENSITY	RETIAS	1939	1944	-.33513E 01	101	710490
18-19,FEB,1971	ELECTRON TEMPERATURE	RETIAS	1939	1944	-.74717E 03	203	710490
18-19,FEB,1971	ELECTRON TEMPERATURE	RETIAS	1939	1944	-.74714E 03	293	710490
18-19,FEB,1971	ION TEMPERATURE	RETIAS	1939	1944	-.64047E 03	303	710490
18-19,FEB,1971	ION TEMPERATURE	RETIAS	1939	1944	-.64050E 03	393	710490
18-19,FEB,1971	VERTICAL ION DRIFT	RETIAS	1939	1944	-.27873E 03	1001	710490
18-19,FEB,1971	VERTICAL ION DRIFT	RETIAS	1939	1944	-.27819E 03	1091	710490
08-09,MAR,1971	DENSITY	RETIAS	1548	1552	.50970E 01	101	710670
08-09,MAR,1971	ELECTRON TEMPERATURE	RETIAS	1548	1552	-.86460E 03	203	710670
08-09,MAR,1971	ELECTRON TEMPERATURE	RETIAS	1548	1552	-.86484E 03	293	710670
08-09,MAR,1971	ION TEMPERATURE	RETIAS	1548	1552	-.70547E 03	303	710670
08-09,MAR,1971	ION TEMPERATURE	RETIAS	1548	1552	-.70548E 03	393	710670
08-09,MAR,1971	VERTICAL ION DRIFT	RETIAS	1548	1552	-.28912E 03	1001	710670
08-09,MAR,1971	VERTICAL ION DRIFT	RETIAS	1548	1552	-.28887E 03	1091	710670
30-31,MAR,1971	DENSITY	L/UHF	1611	1541	.51417E 01	101	710890
30-31,MAR,1971	ELECTRON TEMPERATURE	L/UHF	1611	1541	-.94635E 03	203	710890
30-31,MAR,1971	ELECTRON TEMPERATURE	L/UHF	1611	1541	-.94604E 03	293	710890
30-31,MAR,1971	ION TEMPERATURE	L/UHF	1611	1541	-.74945E 03	303	710890

30-31,MAR,1971	ION TEMPERATURE	L/UHF	1611	1541	-.74953E 03	393	710890
30-31,MAR,1971	VERTICAL ION DRIFT	L/UHF	1611	1541	-.27994E 03	1001	710890
30-31,MAR,1971	VERTICAL ION DRIFT	L/UHF	1611	1541	-.27986E 03	1091	710890
27-28,APR,1971	DENSITY	RETIAS	1540	1558	.52246E 01	101	711170
27-28,APR,1971	ELECTRON TEMPERATURE	RETIAS	1540	1558	-.10630E 04	203	711170
27-28,APR,1971	ELECTRON TEMPERATURE	RETIAS	1540	1558	-.10632E 04	293	711170
27-28,APR,1971	ION TEMPERATURE	RETIAS	1540	1558	-.75885E 03	303	711170
27-28,APR,1971	ION TEMPERATURE	RETIAS	1540	1558	-.75886E 03	393	711170
27-28,APR,1971	VERTICAL ION DRIFT	RETIAS	1540	1558	-.29275E 03	1001	711170
27-28,APR,1971	VERTICAL ION DRIFT	RETIAS	1540	1558	-.29255E 03	1091	711170
27-28,MAY,1971	DENSITY	RETIAS	1536	1525	.52695E 01	101	711470
27-28,MAY,1971	ELECTRON TEMPERATURE	RETIAS	1536	1525	-.98158E 03	203	711470
27-28,MAY,1971	ELECTRON TEMPERATURE	RETIAS	1536	1525	-.98072E 03	293	711470
27-28,MAY,1971	ION TEMPERATURE	RETIAS	1536	1525	-.69369E 03	303	711470
27-28,MAY,1971	ION TEMPERATURE	RETIAS	1536	1525	-.69366E 03	393	711470
27-28,MAY,1971	VERTICAL ION DRIFT	RETIAS	1536	1525	-.28214E 03	1001	711470
27-28,MAY,1971	VERTICAL ION DRIFT	RETIAS	1536	1525	-.28198E 03	1091	711470
02-03,JUN,1971	DENSITY	RETIAS	1839	0747	-.46928E 01	101	711530
02-03,JUN,1971	ELECTRON TEMPERATURE	RETIAS	1839	0747	-.91537E 03	203	711530
02-03,JUN,1971	ION TEMPERATURE	RETIAS	1839	0747	-.75847E 03	303	711530
02-03,JUN,1971	VERTICAL ION DRIFT	RETIAS	1839	0747	-.34029E 03	1001	711530
02-03,JUN,1971	ELECTRON TEMPERATURE	RETIAS	1839	0747	-.91428E 03	293	711530
02-03,JUN,1971	ION TEMPERATURE	RETIAS	1839	0747	-.75793E 03	393	711530
02-03,JUN,1971	VERTICAL ION DRIFT	RETIAS	1839	0747	-.33991E 03	1091	711530
18-19,JUN,1971	DENSITY	RETIAS	0829	0756	-.53844E 01	101	711690
18-19,JUN,1971	ELECTRON TEMPERATURE	RETIAS	0829	0756	-.11123E 04	203	711690
18-19,JUN,1971	ELECTRON TEMPERATURE	RETIAS	0829	0756	-.11116E 04	293	711690
18-19,JUN,1971	ION TEMPERATURE	RETIAS	0829	0756	-.74320E 03	303	711690
18-19,JUN,1971	ION TEMPERATURE	RETIAS	0829	0756	-.74316E 03	393	711690
18-19,JUN,1971	VERTICAL ION DRIFT	RETIAS	0829	0756	-.29969E 03	1001	711690
18-19,JUN,1971	VERTICAL ION DRIFT	RETIAS	0829	0756	-.29964E 03	1091	711690
14-16,JUL,1971	DENSITY	RETIAS	1558	2032	-.52679E 01	101	711950
14-16,JUL,1971	ELECTRON TEMPERATURE	RETIAS	1558	2032	-.10975E 04	203	711950
14-16,JUL,1971	ELECTRON TEMPERATURE	RETIAS	1558	2032	-.10968E 04	293	711950
14-16,JUL,1971	ION TEMPERATURE	RETIAS	1558	2032	-.72874E 03	303	711950
14-16,JUL,1971	ION TEMPERATURE	RETIAS	1558	2032	-.72880E 03	393	711950
14-16,JUL,1971	VERTICAL ION DRIFT	RETIAS	1558	2032	-.29041E 03	1001	711950
14-16,JUL,1971	VERTICAL ION DRIFT	RETIAS	1558	2032	-.29041E 03	1091	711950
19-20,JUL,1971	DENSITY	L/UHF	1911	1912	-.45169E 01	101	712000
19-20,JUL,1971	ELECTRON TEMPERATURE	L/UHF	1911	1912	-.87385E 03	203	712000
19-20,JUL,1971	ELECTRON TEMPERATURE	L/UHF	1911	1912	-.87357E 03	293	712000
19-20,JUL,1971	ION TEMPERATURE	L/UHF	1911	1912	-.70644E 03	303	712000
19-20,JUL,1971	ION TEMPERATURE	L/UHF	1911	1912	-.70648E 03	393	712000
19-20,JUL,1971	VERTICAL ION DRIFT	L/UHF	1911	1912	-.27998E 03	1001	712000
19-20,JUL,1971	VERTICAL ION DRIFT	L/UHF	1911	1912	-.87022E 03	1091	712000

28-29,JUL,1971	DENSITY	RETIAS	1058	1008	-.53713E 01	101	712090
28-29,JUL,1971	ELECTRON TEMPERATURE	RETIAS	1058	1008	-.11398E 04	203	712090
28-29,JUL,1971	ELECTRON TEMPERATURE	RETIAS	1058	1008	-.11396E 04	293	712090
28-29,JUL,1971	ION TEMPERATURE	RETIAS	1058	1008	-.73033E 03	303	712090
28-29,JUL,1971	ION TEMPERATURE	RETIAS	1058	1008	-.73047E 03	393	712090
28-29,JUL,1971	VERTICAL ION DRIFT	RETIAS	1058	1008	-.26887E 03	1001	712090
28-29,JUL,1971	VERTICAL ION DRIFT	RETIAS	1058	1008	-.26898E 03	1091	712090
19-20,AUG,1971	DENSITY	RETIAS	1504	1414	.53204E 01	101	712310
19-20,AUG,1971	ELECTRON TEMPERATURE	RETIAS	1504	1414	-.10794E 04	203	712310
19-20,AUG,1971	ELECTRON TEMPERATURE	RETIAS	1504	1414	-.10791E 04	293	712310
19-20,AUG,1971	ION TEMPERATURE	RETIAS	1504	1414	-.69780E 03	303	712310
19-20,AUG,1971	ION TEMPERATURE	RETIAS	1504	1414	-.69784E 03	393	712310
19-20,AUG,1971	VERTICAL ION DRIFT	RETIAS	1504	1414	-.27370E 03	1001	712310
19-20,AUG,1971	VERTICAL ION DRIFT	RETIAS	1504	1414	-.27375E 03	1091	712310
27-28,AUG,1971	DENSITY	STATS	1008	2045	.55156E 01	101	712390
27-28,AUG,1971	ELECTRON TEMPERATURE	STATS	1008	2045	-.10845E 04	203	712390
27-28,AUG,1971	ION TEMPERATURE	STATS	1008	2045	-.69703E 03	303	712390
27-28,AUG,1971	VERTICAL ION DRIFT	STATS	1008	2045	-.25462E 03	1001	712390
27-28,AUG,1971	ELECTRON TEMPERATURE	STATS	1008	2045	-.10858E 04	293	712390
27-28,AUG,1971	ION TEMPERATURE	STATS	1008	2045	-.69729E 03	393	712390
27-28,AUG,1971	VERTICAL ION DRIFT	STATS	1008	2045	-.25472E 03	1091	712390
31AUG-01SEP,1971	DENSITY	STATS	1754	1513	-.48143E 01	101	712430
31AUG-01SEP,1971	ELECTRON TEMPERATURE	STATS	1754	1513	-.96902E 03	203	712430
31AUG-01SEP,1971	ELECTRON TEMPERATURE	STATS	1754	1513	-.96908E 03	293	712430
31AUG-01SEP,1971	ION TEMPERATURE	STATS	1754	1513	-.71975E 03	303	712430
31AUG-01SEP,1971	ION TEMPERATURE	STATS	1754	1513	-.71987E 03	393	712430
31AUG-01SEP,1971	VERTICAL ION DRIFT	STATS	1754	1513	-.21663E 03	1001	712430
31AUG-01SEP,1971	VERTICAL ION DRIFT	STATS	1754	1513	-.21676E 03	1091	712430
03-04,SEP,1971	DENSITY	STATS	0942	0513	-.54833E 01	101	712460
03-04,SEP,1971	ELECTRON TEMPERATURE	STATS	0942	0513	-.11574E 04	203	712460
03-04,SEP,1971	ION TEMPERATURE	STATS	0942	0513	-.72353E 03	303	712460
03-04,SEP,1971	VERTICAL ION DRIFT	STATS	0942	0513	-.30096E 03	1001	712460
03-04,SEP,1971	ELECTRON TEMPERATURE	STATS	0942	0513	-.11562E 04	293	712460
03-04,SEP,1971	ION TEMPERATURE	STATS	0942	0513	-.72243E 03	393	712460
03-04,SEP,1971	VERTICAL ION DRIFT	STATS	0942	0513	-.29971E 03	1091	712460
07-08,SEP,1971	DENSITY	RETIAS	1645	1625	-.50411E 01	101	712500
07-08,SEP,1971	ELECTRON TEMPERATURE	RETIAS	1645	1625	-.10896E 04	203	712500
07-08,SEP,1971	ELECTRON TEMPERATURE	RETIAS	1645	1625	-.10893E 04	293	712500
07-08,SEP,1971	ION TEMPERATURE	RETIAS	1645	1625	-.69407E 03	303	712500
07-08,SEP,1971	ION TEMPERATURE	RETIAS	1645	1625	-.69410E 03	393	712500
07-08,SEP,1971	VERTICAL ION DRIFT	RETIAS	1645	1625	-.29161E 03	1001	712500
07-08,SEP,1971	VERTICAL ION DRIFT	RETIAS	1645	1625	-.29210E 03	1091	712500
10-11,SEP,1971	DENSITY	STATS	0939	0432	-.54058E 01	101	712530
10-11,SEP,1971	ELECTRON TEMPERATURE	STATS	0939	0432	-.10203E 04	203	712530
10-11,SEP,1971	ELECTRON TEMPERATURE	STATS	0939	0432	-.10203E 04	293	712530

10-11,SEP,1971	ION TEMPERATURE	STATS	0939	0432	-.64369E 03	303	712530
10-11,SEP,1971	ION TEMPERATURE	STATS	0939	0432	-.64367E 03	393	712530
10-11,SEP,1971	VERTICAL ION DRIFT	STATS	0939	0432	-.26372E 03	1001	712530
10-11,SEP,1971	VERTICAL ION DRIFT	STATS	0939	0432	-.26371E 03	1091	712530
23-24,SEP,1971	DENSITY	STATS	1240	0536	.53522E 01	101	712660
23-24,SEP,1971	ELECTRON TEMPERATURE	STATS	1240	0536	-.10065E 04	203	712660
23-24,SEP,1971	ELECTRON TEMPERATURE	STATS	1240	0536	-.66321E 03	303	712660
23-24,SEP,1971	ION TEMPERATURE	STATS	1240	0536	-.25684E 03	1001	712660
23-24,SEP,1971	ION TEMPERATURE	STATS	1240	0536	-.10064E 04	293	712660
23-24,SEP,1971	VERTICAL ION DRIFT	STATS	1240	0536	-.66319E 03	393	712660
23-24,SEP,1971	VERTICAL ION DRIFT	STATS	1240	0536	-.25707E 03	1091	712660
30SEP-01OCT1971	DENSITY	STATS	1540	2240	-.51419E 01	101	712730
30SEP-01OCT1971	ELECTRON TEMPERATURE	STATS	1540	2240	-.96681E 03	203	712730
30SEP-01OCT1971	ION TEMPERATURE	STATS	1540	2240	-.68627E 03	303	712730
30SEP-01OCT1971	VERTICAL ION DRIFT	STATS	1540	2240	-.28357E 03	1001	712730
30SEP-01OCT1971	ELECTRON TEMPERATURE	STATS	1540	2240	-.95586E 03	293	712730
30SEP-01OCT1971	ION TEMPERATURE	STATS	1540	2240	-.68260E 03	393	712730
30SEP-01OCT1971	VERTICAL ION DRIFT	STATS	1540	2240	-.28399E 03	1091	712730
05-06,OCT,1971	DENSITY	RETIAS	1646	2329	-.48444E 01	101	712780
05-06,OCT,1971	ELECTRON TEMPERATURE	RETIAS	1646	2329	-.82861E 03	203	712780
05-06,OCT,1971	ION TEMPERATURE	RETIAS	1646	2329	-.64860E 03	303	712780
05-06,OCT,1971	VERTICAL ION DRIFT	RETIAS	1646	2329	-.24294E 03	1001	712780
05-06,OCT,1971	ELECTRON TEMPERATURE	RETIAS	1646	2329	-.82980E 03	293	712780
05-06,OCT,1971	ION TEMPERATURE	RETIAS	1646	2329	-.64800E 03	393	712780
05-06,OCT,1971	VERTICAL ION DRIFT	RETIAS	1646	2329	-.24097E 03	1091	712780
26-27,OCT,1971	DENSITY	RETIAS	1117	0047	.53564E 01	101	712990
26-27,OCT,1971	ELECTRON TEMPERATURE	RETIAS	1117	0047	-.81923E 03	203	712990
26-27,OCT,1971	ION TEMPERATURE	RETIAS	1117	0047	-.71337E 03	303	712990
26-27,OCT,1971	VERTICAL ION DRIFT	RETIAS	1117	0047	-.24964E 03	1001	712990
26-27,OCT,1971	ELECTRON TEMPERATURE	RETIAS	1117	0047	-.82019E 03	293	712990
26-27,OCT,1971	ION TEMPERATURE	RETIAS	1117	0047	-.71155E 03	393	712990
26-27,OCT,1971	VERTICAL ION DRIFT	RETIAS	1117	0047	-.24942E 03	1091	712990
02-03,NOV,1971	DENSITY	RETIAS	1532	1519	.49875E 01	101	713060
02-03,NOV,1971	ELECTRON TEMPERATURE	RETIAS	1532	1519	-.89433E 03	203	713060
02-03,NOV,1971	ELECTRON TEMPERATURE	RETIAS	1532	1519	-.89361E 03	293	713060
02-03,NOV,1971	ION TEMPERATURE	RETIAS	1532	1519	-.63744E 03	303	713060
02-03,NOV,1971	ION TEMPERATURE	RETIAS	1532	1519	-.63749E 03	393	713060
02-03,NOV,1971	VERTICAL ION DRIFT	RETIAS	1532	1519	-.26027E 03	1001	713060
02-03,NOV,1971	VERTICAL ION DRIFT	RETIAS	1532	1519	-.26054E 03	1091	713060
22-23,DEC,1971	DENSITY	RETIAS	1518	1506	.49870E 01	101	713560
22-23,DEC,1971	ELECTRON TEMPERATURE	RETIAS	1518	1506	-.90410E 03	203	713560
22-23,DEC,1971	ELECTRON TEMPERATURE	RETIAS	1518	1506	-.90373E 03	293	713560
22-23,DEC,1971	ION TEMPERATURE	RETIAS	1518	1506	-.72539E 03	303	713560
22-23,DEC,1971	ION TEMPERATURE	RETIAS	1518	1506	-.72540E 03	393	713560
22-23,DEC,1971	VERTICAL ION DRIFT	RETIAS	1518	1506	-.26518E 03	1001	713560
22-23,DEC,1971	VERTICAL ION DRIFT	RETIAS	1518	1506	-.26510E 03	1091	713560

BIBLIOGRAPHIC DATA SHEET 1. Report No.	3. Recipient's Accession No.
4. Title and Subtitle Millstone Hill Thomson Scatter Results for 1971	5. Report Date 24 March 1978 6.
7. Author(s) John V. Evans Barbara A. Emery John M. Holt	8. Performing Organization Rept. No. Technical Report 528
9. Performing Organization Name and Address Lincoln Laboratory, M. I. T. P.O. Box 73 Lexington, MA 02173	10. Project/Task/Work Unit No. 11. Contract/Grant No. ATM 75-22193
12. Sponsoring Organization Name and Address National Science Foundation Atmospheric Science Section Washington, DC 20550	13. Type of Report & Period Covered Technical Report 14.

15. Supplementary Notes

16. Abstracts

During 1971, the incoherent scatter radar at Millstone Hill (42.6°N, 71.5°W) was employed to measure the electron density, electron and ion temperatures, and the vertical velocity of the O^+ ions in the F-region over periods of 24 hours on 20 days. The observations spanned the height interval 200 to 900 km, approximately, and achieved a time resolution of about 30 minutes. This report presents these results, after smoothing, as a set of machine-drawn contour plots.

The report discusses the behavior observed in 1971 in light of that seen in previous years. A significant number of days appear to have been disturbed by large traveling ionospheric disturbances. Results for the average exospheric temperature, the mean meridional, and zonal winds for 1970 and 1971 derived from these incoherent scatter measurements in a separate study by B.A. Emery are summarized here for completeness. The results appear to confirm the mean wind behavior that would be predicted by the recent Mass-Spectrometer, Incoherent-Scatter (MSIS) global model for the thermosphere and support the view that interhemispheric transport of light neutral constituents (e.g., atomic oxygen) gives rise to the anomalous seasonal behavior of the ionosphere at midlatitudes.

17. Key Words and Document Analysis. 17a. Descriptors

Millstone radar
F-region
diurnal variations
electron density
ionospheric scatter
seasonal variations
temperature effects
spectrum analyzers

17b. Identifiers/Open-Ended Terms

17c. COSATI Field/Group

18. Availability Statement	19. Security Class (This Report) UNCLASSIFIED	21. No. of Pages 124
	20. Security Page UNC	